ANALYSIS OF THE THERMAL RESPONSE OF PARACHUTE FABRICS IN CRASH-FIRE ENVIRONMENTS

B. Laub, et al

Acurex Corporation

Prepared for:

Aeronautical Systems Division

February 1974

NOTICE

When Government drawings, specifications, or other data are used for any purpose other than in connection with a definitely related Government procurement operation, the United States Government thereby incurs no responsibility nor any obligation whatsoever; and the fact that the government may have formulated, furnished, or in any way supplied the said drawings, specifications, or other data, is not to be regarded by implication or otherwise as in any manner licensing the holder or any other person or corporation, or conveying any rights or permission to manufacture, use, or sell any patented invention that may in any way be related thereto.

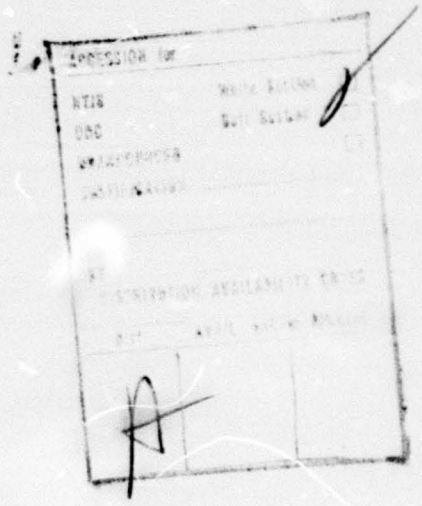

Copies of this report should not be returned unless return is required by security considerations, contractual obligations, or notice on a specific document.

AIR FORCE/56780/2 December 1974 — 100

Unclassified
Security Classification

AD/A004133

DOCUMENT CONTROL DATA - R & D

(Security classification of title, body of abstract and indexing annotation must be entered when the overall report is classified)

1. ORIGINATING ACTIVITY (Corporate author)
Aerotherm Division/Acurex Corporation
485 Clyde Ave.
Mountain View CA 94042

2a. REPORT SECURITY CLASSIFICATION
Unclassified

2b. GROUP

3. REPORT TITLE
Analysis of the Thermal Response of Parachute Fabrics in Crash-Fire Environments

4. DESCRIPTIVE NOTES (Type of report and inclusive dates)

5. AUTHOR(S) (First name, middle initial, last name)
B. Laub, K. J. Clark, and K. A. Green

6. REPORT DATE	7a. TOTAL NO. OF PAGES	7b. NO. OF REFS
February 1974	~~119~~ 135	28

8a. CONTRACT OR GRANT NO.	9a. ORIGINATOR'S REPORT NUMBER(S)
F33657-73-C-0815	Aerotherm Final Report 74-96
b. PROJECT NO.	
c.	9b. OTHER REPORT NO(S) (Any other numbers that may be assigned this report)
d.	

10. DISTRIBUTION STATEMENT
Approved for Public Release, Disbribution Unlimited

11. SUPPLEMENTARY NOTES

12. SPONSORING MILITARY ACTIVITY
Life Support System Program Office
Wright-Patterson Air Force Base
Ohio 45433

13. ABSTRACT

A theoretical study was performed to evaluate the thermal performance of the Air Force C-9 personnel parachute and various parachute materials during encounters with JP-4 aircraft crash fires. The objectives of this study were to

- Develop an analytical model of a parachute encounter with a fire
- Determine what parameters are critical to thermal response
- Provide a relative measure of thermal performance of Nylon, Nomex and PBI
- Assess the range of failure conditions

These were accomplished by developing a computer model of the crash fire, the parachute material and configuration, and the trajectory simulating the heating and thermal response of a parachute during descent. Values of the fire, trajectory, parachute, and material properties used in this study were obtained from the literature. In cases where specific data were not available, extrapolations from applicable data were made; no new data were generated in this study.

Principal findings were that the canopy is the most vulnerable component due to the low thermal capacitance per unit surface area and the high heat fluxes in the fire resulting in a thermal time constant of less than one second. The convective heat transfer mode is dominant in the C-9 parachute canopy due to the high permeability. Effectively, only trajectories which go through the fire result in failure because of the convective cooling in ambient air. In determining threshold failure altitudes, knowledge of the fire temperature at entry, and thus the vertical fire temperature profile, is critical since the canopy temperature quickly equilibrates with the local environment.

With regard to the three fabrics considered, both Nomex and PBI exhibit improved thermal tolerance over Nylon, retaining strength to several hundred degrees (°F) above Nylon. The forms of Nomex and PBI studied both shrink significantly (30 to 40 percent) which may lead to failure before loss of strength. In this event PBI is superior to Nomex while both remain superior to Nylon. The amount of improved performance in terms of difference in altitude of threshold failure is dependent upon fabric type, fire diameter, and failure mode.

DD FORM 1 NOV 68 1473 REPLACES DD FORM 1473, 1 JAN 64, WHICH IS OBSOLETE FOR ARMY USE.

Unclassified
Security Classification

(125)

14 KEY WORDS	LINK A		LINK B		LINK C	
	ROLE	WT	ROLE	WT	ROLE	WT
Parachutes						
Parachute Fabrics						
Aircraft Crash Fires						
Fabric Thermal Model						
Fire Modeling						
Trajectories						
Laboratory Test Apparatus						

FOREWORD

This report was prepared by the Aerotherm Division of Acurex Corporation under Contract F33657-73-C-0815. Dr. Howard Morse was program manager and Mr. Bernard Laub was program engineer. The work was administered under the direction of Mr. Ken Troup of the Life Support SPO, Aeronautical Systems Division, Air Force Systems Command, Wright-Patterson Air Force Base, Ohio, with Mr. Stanley Schulman and Mr. Robert Stanton of the Air Force Materials Laboratory acting as Technical Monitors.

The authors wish to express their gratitude to Mr. Kurt Suchsland and Mr. Ken Lambson for their technical assistance during this program and to Dr. Howard Morse and Mr. James Thompson for the invaluable guidance they provided.

This report covers work conducted from June 1973 through January 1974, and was released by the authors for publication in May 1974.

This technical report has been reviewed and is approved for publication.

William M. Quinn

WILLIAM M. QUINN, Colonel, USAF
System Program Director
Life Support System Program Office
Deputy for Subsystems

TABLE OF CONTENTS

TABLE OF CONTENTS (concluded)

LIST OF ILLUSTRATIONS

LIST OF ILLUSTRATIONS (concluded)

LIST OF TABLES

SUMMARY

OBJECTIVES

An analytical study has been made of the thermal response of personnel parachutes on exposure to aircraft crash fires during descent in order to evaluate, on the basis of available data, whether improvements in the thermal survivability of parachutes can be made. The objectives of this study were

- To develop an analytical model of a parachute encounter with a fire
- To determine which properties of the fire, parachute configuration, and fabrics are most critical to the thermal response
- To provide a relative measure of the thermal performance of three specific fabrics, Nylon, Nomex, and PBI
- To assess the range of fire and descent trajectory conditions in which parachutes of these three fabrics may be expected to fail.

APPROACH

The approach of this study was to model analytically the crash fire, the descent trajectory, and the fabrics and configurations used in personnel parachutes. This model was developed into a computer code, called AFPARTS, which calculates the transient thermal response of a parachute as it descends on various trajectories near and through a crash fire. This new code provides an integrated analysis capability never before available. Data used to model each part of this problem were collected primarily form the literature. No new property data were generated as a result of this program.

The scope of the study was defined to consider

- A fully inflated canopy in steady descent
- Design specifications for the Air Force C-9 personnel parachute. Note, this fixes canopy permeability, dimensions, pressure distribution, and fabric weight
- Three materials; standard Nylon as used in the present C-9 parachute, and Nomex and PBI assuming these fabrics to be constructed to the permeability and weight specifications of the C-9 parachute

- Use of available fabric property data including thermal (specific heat, conductivity), optical (absorptance), thermochemical, strength, and shrinkage. Where specific data were not available for the configuration being considered, data were extrapolated or inferred from existing, relevant sources
- Fully developed JP-4 crash fires from 50 to 200 feet in base diameter at sea level and wind velocities from 0 to 30 knots
- A range of initial trajectory altitudes and lateral offsets from the fire centerline sufficient to define a failure envelope

Possible failure criteria were considered to include:

- Mechanical - due to load exceeding fabric strength at elevated temperature
- Configuration instability - due to excessive shrinkage
- Thermochemical - burning

No established failure criteria exist for any of these modes. For the purposes of this study the temperature range and amount of shrinkage are noted to indicate potential failure; loss of strength below the steady-state descent loads (i.e., no safety factor) is considered mechanical failure; and, any evidence of melting or burning is considered a failure.

- Failure temperatures for each of the failure modes for Nylon, Nomex, and PBI are indicated below:

Material	Shrinkage (maximum amount)	Mechanical Strength	Burning
Nylon	not determined	450°F	488°F (melts)
Nomex	590 - 710°F (30% linear)	835°F	935°F
PBI	750 - 790°F (40% linear)	890°F	not observed

Note that Nylon loses strength at a temperature well below any form of failure for Nomex and PBI. Both Nomex and PBI undergo significant amounts of shrinkage at temperatures well below those for mechanical failure. Whereas the latter mode represents certain failure, no data were found or generated which equate the shrinkage with failure. Burning or melting does not occur at temperatures below the mechanical failure temperatures for any of these materials, and thus is not a failure mode of concern.

RESULTS

Key results of this study are summarized below with the aid of Table S-1 and Figure S-1. Table S-1 lists all the parameters considered in this study and indicates their level of criticality. Column 1 lists parameters which were not critical to this study and are not likely to be in any nominal parachute configuration. Column 2 includes those which were not critical to this study, but may be for other configurations or defined conditions. Parameters in Column 3 were of moderate criticality and those in Column 4 were of primary criticality in this study, and therefore, would be in the general case as well.

A primary observation to come from this study is that upon entry into the fire or hot gas plume, the canopy temperature reaches near equilibrium with the local environment in approximately one second. Therefore, it is concluded that

- The canopy fabric is the most critical component in the parachute system due to its very low thermal capacity (thin and lightweight) and its high permeability.

Since the thermal time constant is so short, the temperature of the fire upon entry can be directly related to the various temperature dependent failure mechanisms. Consequently,

- The vertical temperature variation of the fire is of primary importance in determining thresholds of failure for various materials.

A number of other conclusions follow from the basic observation stated above.

- Permeability is a key property since the C-9 requirement results in a high blow-through convective heat transfer which dominates other modes of heat transfer.
- All other fabric thermal properties (specific heat, thermal conductivity, etc.) are not critical for C-9 canopy fabrics due to 1) the dominance of permeability, and 2) the small variability of these properties among the candidate materials. Optical properties, which are not critical for C-9 canopy fabrics, might be significant for other configurations.
- Other components in a parachute are not critical to failure since they are at least an order of magnitude slower in thermal response compared to the permeable canopy
- Mechanical failure of Nomex and PBI fabrics is predicted only for through-the-fire trajectories. Nylon is predicted to fail under windless conditions for descent within one fire base radius of the periphery of large fires.

TABLE S-1

	Not Critical In General	Not Critical For This Study	Moderately Critical For This Study	Critical in This Study
FIRE RELATED				
Vertical Temperature Profile				X
Composition	X			
Wind Velocity	X			
Base Diameter			X	
Fire Geometry		X		
Fire Velocities		X		
Optical Properties		X		
TRAJECTORY RELATED				
Initial Altitude	X			
Entry Altitude				X
Wind Velocity	X			
Bypass Distance from Fire ℄				X
Vertical Velocity		X		
PARACHUTE RELATED				
Component				
Canopy				X
Cord	X			
Webbing	X			
Thermal Properties				
Specific Heat		X		
Conductivity	X			
Optical Properties				
Absorptance		X		
Configuration				
Permeability				X
Weight		X		
Mechanical				
Strength				X
Shrinkage				X
Thermochemical				
Burning-Decomposition		X		
FAILURE CRITERIA				
Structural Failure				X
Dimensional Stability				X
Burning		X		

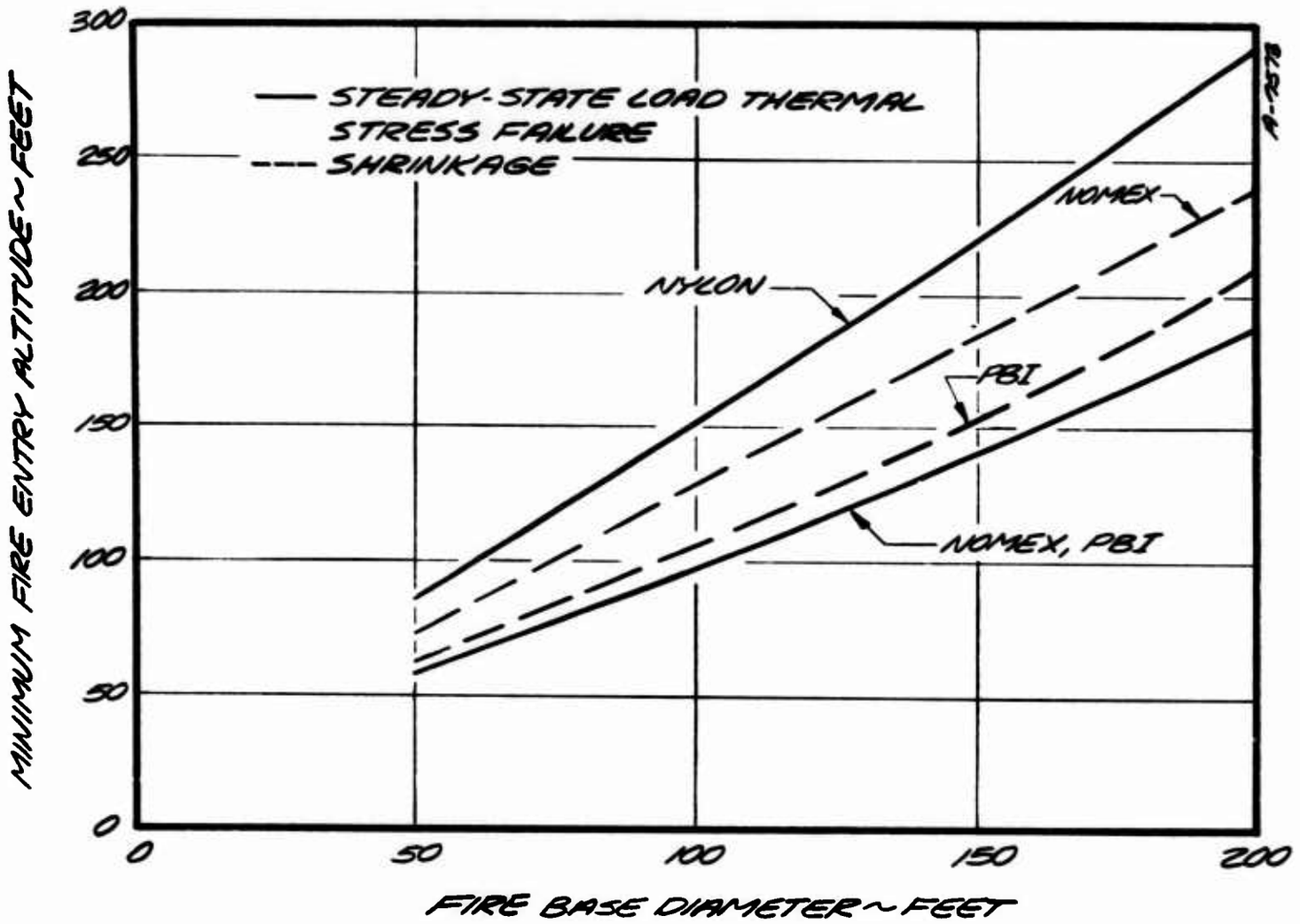

Figure S-1. Minimum survival altitudes of candidate canopy fabrics for through-the-fire trajectories.

With regard to the results for the three materials considered (Nylon, Nomex, and PBI) Figure S-1 shows the minimum fire entry altitude, below which the canopy is predicted to fail, as a function of fire base diameter. Two failure modes are shown; shrinkage (i.e. resultant dimensional instability) which represents a possible failure mode and the ultimate failure mode of tensile stress failure under a steady state descent load. These results are based upon:

- Worst case fully-developed fires
- Worst case trajectories - passing directly through the fire/plume center
- Failure temperatures - criteria as shown above

The difference between Nomex and PBI is negligible based on thermal stress, but favors PBI based on shrinkage (based on its higher shrinkage onset temperature; not the amount of shrinkage). In both cases PBI and Nomex are superior to Nylon. It must be noted that the predicted threshold altitudes of failure are strongly dependent upon the calculated vertical temperature profiles in the fire, (no data exist to verify the fire model presented in this study), and the assumed failure temperatures of the candidate materials. Consequently, while the relative ranking of the three materials studied is clearly indicated, both the relative and absolute magnitude of improvements in survivability are subject to uncertainties which have not been evaluated. The results clearly indicate that

- The use of alternate materials in canopy fabrics shows potential for improved survivability in encounters with JP-4 crash fires.

The need for experimental data in a simulated fire environment was addressed in this study. A laboratory test apparatus which can provide end-use simulation is shown to be feasible and a preliminary design concept is presented. Such an apparatus can be used to verify the analytical results and to screen candidate fabrics.

RECOMMENDATIONS

This study has shown that improvements in the thermal survivability of personnel parachutes on exposure to aircraft crash fires is attainable through the use of improved fabrics for the parachute canopy. In addition, the vertical temperature profile in the fire, the temperature dependence of possible failure modes and, in particular, the permeability requirements of the C-9 configuration have been identified as the most critical parameters influencing parachute thermal survivability. It must be recognized that the uncertainties associated with the first two parameters and the limited scope of this study (which did not consider alternate configurations, other improved fabrics, and only addressed worst

case conditions) does not allow an accurate evaluation of the ultimate improvements in parachute thermal survivability that can be realized. The following recommendations are provided to define additional tasks that should be performed in order to improve the developed capabilities and permit an evaluation of the achievable improvements in parachute thermal performance.

- Consider configurations other than the C-9.
- Consider other improved fabrics.
- Obtain additional property data on actual candidate fabrics under conditions simulating actual use conditions.
- Evaluate and improve definition of failure criteria.
- Construct a laboratory test apparatus for accurate end-use simulation testing of candidate materials.
- Obtain a better understanding of the fire environment to define and reduce the uncertainties in failure altitude predictions.

SECTION 1

INTRODUCTION

The following report describes the results of an analytical study designed to understand and achieve a means for predicting the thermal response of personnel parachute materials when exposed to a fully developed JP-4 fueled aircraft crash fire. The study has two primary objectives: first, to evaluate the fire-fabric system in order to determine those properties or qualities of a parachute which are most critical to system survivability. The goal of this objective is to provide guidance in the design of fabrics and parachutes such that improvements in system survivability upon fire environment exposures can be realized. The second primary objective is to evaluate three candidate materials being used or considered by the Air Force as materials for parachutes. These include Nomex, PBI (polybenzimidazole), and Nylon.

In order to pursue these objectives, a representative analytical thermal model of the fire-fabric system has been developed which considers the primary mechanisms that determine the thermal response of parachute fabrics. This includes:

1. Radiative exchange of energy with the environment.
2. Convective exchange of energy with the environment due to "blow-by" of ambient gases.
3. Convective exchange of energy with the environment due to "blow-through" of ambient gases.
4. Decomposition (mass loss) of the fabric by pyrolysis at elevated temperatures.
5. Variation of fabric properties with temperature.

A new computer code has been developed for solution of this problem. This code is a one-dimensional, time-dependent, finite-difference implicit solution of the energy balance equations written for one isothermal node describing the fabric. The code accounts for all the above factors by including models for typical wind-blown JP-4 fuel fires and the effects on parachute descent trajectories.

A major portion of this study is directed toward defining the fire and parachute fabric systems. Section 2 describes the characteristics of a crash fire and its influence on a parachute descending in its vicinity. Included in this work is the development of an analytical model for the prediction of nominal JP-4 crash fires which considers air entrainment, updrafts, air/fuel chemistry, and flame-bending due to wind. Also described is a model for calculating the radiant thermal energy emanating from the fire that is incident to a parachute descending in near proximity which accounts for the altitude variations of fire temperature. This section concludes with a description of the modeling of parachute descent trajectories which accounts for the influence of wind and velocity fields in the fire.

Details of the fabric thermal model are presented in Section 3. Included are descriptions of the analytical formulations for convective heat transfer between the fabric and its environs and fabric decomposition at elevated temperatures. Parachute survivability is based on the decay of the mechanical strength of a fabric with temperature. The failure criterion and the fabric material thermal properties selected are the result of a detailed review of the literature.

Section 4 describes the results of the analytical study for which a parametric analysis was performed. The effects of variations in fire, trajectory, and fabric characteristics are evaluated. Predicted performance is correlated for the candidate materials to ascertain their failure thresholds.

The lack of applicable data on the thermal response of parachute fabrics in fuel fire environments suggests the desirability of simulating such encounters in the laboratory. Section 5 describes a feasibility and preliminary design study of an apparatus for simulating such encounters in a laboratory environment.

Conclusions and recommendations for future study are presented in Section 6.

In this report all quantities, except as noted, are reported in two sets of units. In general, the quantity is first reported in the English (engineering) unit and is then followed by the appropriate metric conversion in parentheses. Conversion of data and scales to metric units has been added where possible.

SECTION 2

CRASH-FIRE ENVIRONMENT

Definition of the thermochemical and geometric characteristics of large open pool fires is required before the thermal response of fabrics heated by such fires can be predicted. This section describes the analytical models formulated to define the characteristics of a JP-4 crash fire, the radiant energy emitted by the fire and incident to a descending parachute, and the influence of the fire upon parachute descent trajectories.

2.1 FIRE DEFINITION

2.1.1 Overview

In order to properly assess the response of parachute fabrics to typical crash fire heating environments, the principal aspects of the associated fuel fire must be quantified with an appropriate mathematical model. The crash fire influences the parachute in two ways: radiative and convective heat fluxes generated by the hot combustion gases impinge upon the parachute fabric; and the convective motions of the plume gases, associated both with the lateral motion of entrained air and the upward motion of combustion products due to buoyancy forces, act to alter the parachute's descent trajectory. The nature of these heating and convection influences depends strongly on the location of the parachute relative to the fire plume, e.g., whether the chute is actually in the plume or at some distance outside the plume.

In the present study, the mathematical model of the fuel fire must have the following features:

a. The model must be capable of predicting fire temperature, convective velocities, chemical composition, and plume radius as functions of altitude above the ground.

b. The model must permit the specification of arbitrary base diameter and wind velocity vector.

c. The computer code formulation of the model should require a minimum execution time, in order to facilitate economical parametric studies of parachute response under a wide range of conditions.

A fundamental assumption made in this work is that the actual crash fire can be represented by a circular pool of burning liquid fuel. The actual crash fire scenario has been considered in detail in Reference 4. It is pointed out there that during the crash, the fuel can be released in one or more of the following three forms: carbureted fuel vapor-air mixture, mist, liquid. The first two forms occur in relatively small amounts and, therefore, are important only in the ignition phase of the fire, the duration of which is typically twenty seconds. The nature of the crash fire beyond this initial transient is largely dependent on the manner in which the spilled fuel burns. Important factors in this phase of the fire are

1. Location of the fuel source.
2. Distribution of the fuel spillage prior to initiation of the fire.
3. Wind magnitude and direction.
4. Terrain topology.
5. Nature of the soil and/or foliage in the vicinity of the fire.

All of these parameters behave essentially randomly under real crash conditions and, hence, are impossible to include rigorously in a mathematical model. Nevertheless, the large open pool fire is felt to provide an adequate representation of the actual crash fire with respect to heating levels and convective motions.

A number of models for free-burning fires have been presented in the literature. However, with respect to this study, each of these available models has at least one significant deficiency. In many cases, the authors choose to concentrate on the plume above the combustion zone and, hence, ignore combustion entirely. This was done by Taylor[1], who concentrated on an accurate treatment of the turbulence field and stratification effects while ignoring combustion and radiation; by Smith[2], who developed an accurate treatment of the radiation field and assumed frozen chemistry; and by Morton[3], who again concerned himself mainly with the fluid mechanics and radiation transport in a frozen plume. Other models available have attempted a more thorough treatment of combustion processes in the combustion zone close to the fuel source, but have oversimplified their treatments of the plume above the combustion zone. Thus, Albright, et al.[4], assumed the combustion zone to be characterized by a single temperature, density, and chemical composition, but failed to include a momentum equation for the proper treatment of buoyancy effects. Similarly, Morse, et al.[5], developed and solved a more complete model of a thermochemically uniform combustion zone, but again ignored the details of the plume

at greater distances above the fuel source by assuming a constant temperature/velocity field for this region.

The most complete model available in the literature is that of Nielsen and Tao[6], who account for turbulent entrainment, buoyancy forces, combustion, radiation, and vertical variations in all of these quantities. However, their fuel chemistry was that associated with wood, rather than JP-4 fuel, and they assumed windless ambient conditions at all times.

The approach taken in the study was to develop a model which accounts for vertical variations in the fire properties, but assumes these properties to be constant in planes parallel to the ground. This idealization is valid in view of the fact that, globally, the characteristic length of the entire fire zone (combustion zone plus plume) in the vertical or fire axis direction is much greater than its characteristic transverse width. The model described below treats the evolution of the fire from its origin at the fuel surface, through the combustion zone, and into the plume where temperatures eventually decay to ambient levels and the convective motions are essentially dispersed. In addition, arbitrary base diameter, fuel chemical composition, and wind velocity are permissible. Hence, the model incorporates and extends many of the features of the aforementioned models currently available in the literature.

2.1.2 Modeling

Two different fire models were developed in the present study. The first treats the entire fire region, including both combustion zone and plume, assuming chemical equilibrium applies. Hence, the fuel vapors are allowed to combust in equilibrium with entrained oxygen, and the equilibrium combustion products become more fuel-lean with increasing distance above the fuel source. At the stoichiometric air/fuel ratio, peak temperatures are reached in the fire column. The elevation at which this occurs is assumed to define the tip of the combustion zone. The combustion products are further diluted with entrained air as they continue rising above this combustion zone, with the result that, because of this mixing and radiation losses, their average temperature decays. Chemical equilibrium is assumed to hold in the dilution process. Eventually, the combustion gases thermally decay to ambient temperature. The entire region of the fire from the tip of the combustion zone to the point where fire temperature has decayed to near-ambient values is called the fire plume.

The second fire model developed here treats only the fire plume, that is, the portion of the fire above the combustion zone. In this model, air is allowed to entrain and mix with the combustion products flowing upwards out

of the combustion zone, but no chemical reactions are permitted. Hence, the plume is assumed to be chemically "frozen." It is shown below that, for identical starting conditions (conditions at the top of the combustion zone), the frozen and equilibrium models predict very nearly identical fire profiles. The advantage of the frozen model is computational speed, which is one of the prerequisites called out in the introduction to this section.

2.1.3 Results

Consistent with the desire for minimum computational time, only the frozen plume routine has been incorporated into the composite AFPARTS code which is used to determine the parachute fabric response. However, the frozen plume routine requires input data on the conditions at the top of the combustion zone. The chemical equilibrium code described above was used to calculate these conditions for 50, 100, 150, and 200 foot (15.2, 30.4, 45.7, and 61 meters) base-diameter fires. These data were then built into the AFPARTS code, in DATA-statement format, so that conditions at the top of the combustion zone for a fire with arbitrary base diameter can be determined from linear interpolation.

In carrying out the calculations for the combustion zone, utilizing the chemical equilibrium code, it was found that an augmented fire emissivity greater than unity was required in order to obtain energy losses from the fire column of sufficient magnitude. Without the augmented emissivity, the maximum value of the mean temperature T_p was significantly overpredicted. Use of an augmented emissivity can be rationalized via the "radiation burst" concept[2]. According to this concept, the actual temperature at the fire periphery is the average temperature T_{cp} plus a time-varying component, for example

$$T(t) = T_{cp}\left[1 + q \sin^2\left(\frac{\pi t}{\tau}\right)\right] \qquad (1)$$

where

$$q = \frac{T_m - T_{cp}}{T_{cp}} \qquad (2)$$

The temperature T_m is the maximum temperature attained at the fire periphery at any instant in time. The oscillating component is associated with the motion of the large-scale eddies in the fire. These eddies carry "cells" of hot gases at the fire core to the fire periphery where they are free to radiate to the environment. Since the fire is relatively black (optically thick) due to the presence of large amounts of soot and relatively long path lengths, the

"cells" at the core of the fire column are essentially insulated and, therefore, unable to lose energy to the surroundings. If these cells are assumed to be adiabatic, then the maximum instantaneous temperature they can attain is the flame temperature of the fuel (adiabatic, stoichiometric combustion). For JP-4 fuel, flame temperatures of 4000 - 5000°F (2200 - 2760°C) have been reported[4]. In contrast, average temperatures in nominally thirty-foot JP-4 fires have been measured and found to be approximately 1850°F (1010°C)[4,7,11].

The average radiative loss at the fire periphery is given by (assuming blackbody radiation)

$$\left\{\sigma\left[T(t)\right]^4\right\}_{ave} = \tau^{-1}\int_o^t \sigma T_{cp}\left[1 + q\sin^2\left(\frac{\pi t}{\tau}\right)\right]dt = \sigma\varepsilon_{cp}(q)T_{cp}^4 \qquad (3)$$

where

$$\varepsilon_{cp}(q) = 1 + 2q + 9q^2/4 + 3q^3/4 + 35q^4/128 \qquad (4)$$

To illustrate typical magnitudes for $\varepsilon_{cp}(q)$, assume T_{cp} = 2310°R (1010°C) and T_m = 5460°R (2760°C). Then q = 1.36 and $\varepsilon_{cp}(q)$ = 12.

Figure 1 presents profiles of V_{cp}, T_{cp} and r_{cp} for a 30 ft (9.144 meters) JP-4 fuel fire with no wind, as computed with the chemical-equilibrium model. An effective emissivity of twelve was used, and ninety chemical species were considered, including many hydrocarbons and condensed-phase carbon (soot). The peak average temperature is 2450°R (1088°C) which agrees well with availablve experimental data[4,7,11]. In addition, this peak value occurs at an elevation for which air/fuel ratio $\dot{m}_a/\dot{m}_f$ is 14.0 - 15.0, the approximate stoichiometric ratio for JP-4 fuel. Note that in the fuel-rich region extending from the fuel surface to an altitude of sixteen feet (4.87 m), soot is predicted to form under the constraint of chemical equilibrium. At greater altitudes, chemical equilibrium requires that the soot concentration goes to zero. However, chemical kinetics most likely comes into play, with the result that the carbon particles are frozen and therefore appear throughout the fire column.

Figure 1 also illustrates a comparison between frozen and chemical equilibrium solutions for the plume. The frozen solution was initiated at the top of the combustion zone, where the peak average temperature and stoichiometric air/fuel ratio occurred. The agreement between the two solutions is seen to be quite satisfactory and justifies use of the more expedient frozen routine in the AFPARTS computer code.

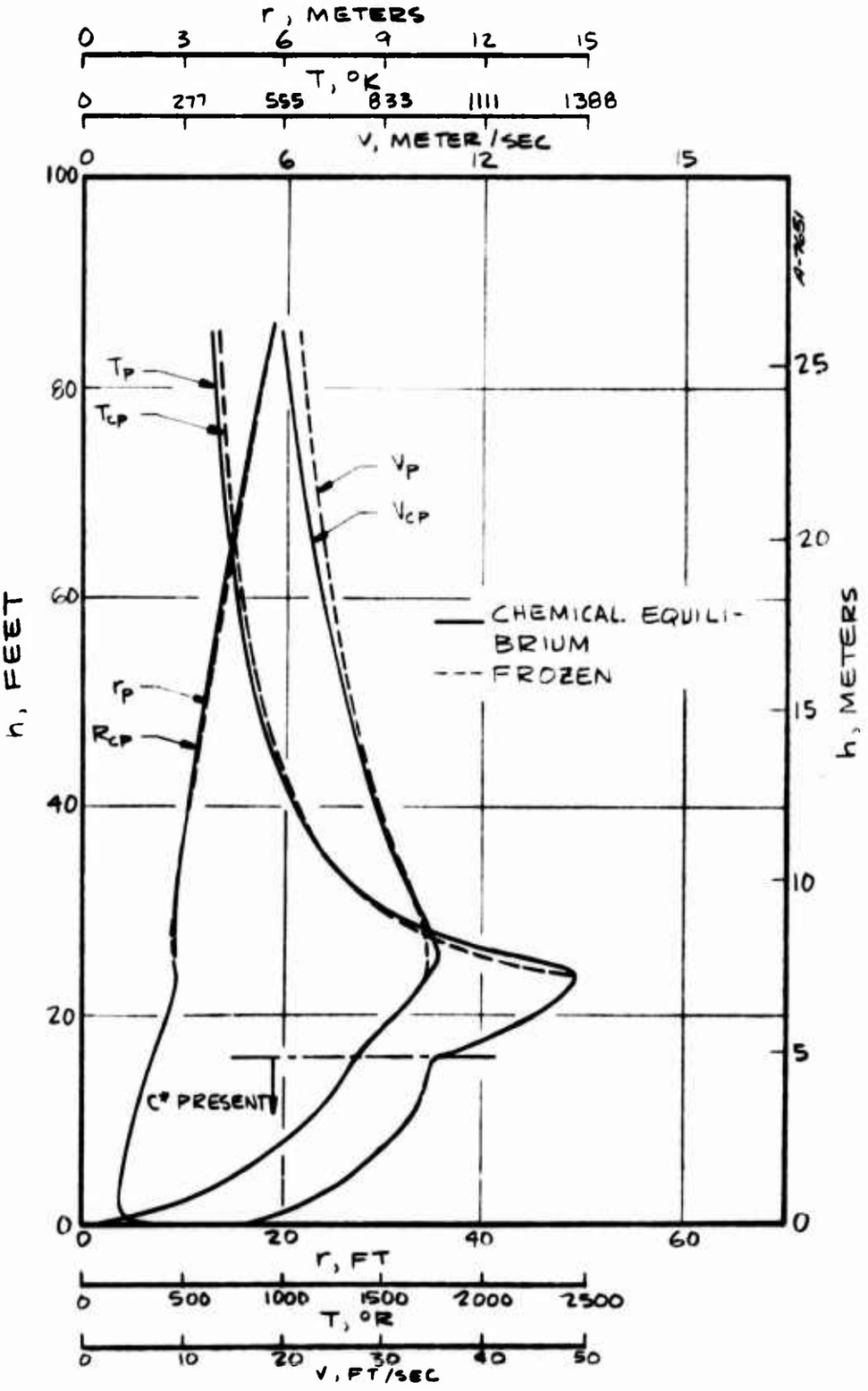

Figure 1. Vertical profiles in a 30-foot (9 meter) base diameter JP-4 fuel fire.

Use of an effective fire emissivity of twelve to obtain energy losses of the proper magnitude implies that the heat flux impinging upon the parachute fabric will be inordinately high. To avoid this, an emissivity of unity was used, in conjunction with the local mean temperature, to compute the actual radiative heat fluxes to the fabric. Thus, for a maximum mean fire temperature of 2000°F (1093°C), the blackbody radiation flux is 17.4 Btu/ft^{2}sec (1.97×10^5 watts/meter^2). Comparing this value with maximum instantaneous heat fluxes measured in JP-4 fuel pool fires, 30 - 35 Btu/ft^{2}sec (3.4×10^5 - 4.0×10^5 watts/meter^2), it appears that the actual effect of the radiation burst phenomena is to give an effective emissivity of something less than two (but greater than unity), rather than twelve. For this reason the use of the higher value for effective emissivity must be viewed as an artifice, although radiation bursts are in fact real phenomena which are commonly observed.

Since the artifice of an effective emissivity of twelve is required to give fire energy losses of the appropriate magnitude, it is probable that the assumption of equilibrium combustion leads to unrealistically high levels of energy release in the combustion zone. As mentioned earlier, a certain portion of the condensed-phase carbon (soot) created in the combustion zone never undergoes further combustion, which would result in additional energy release since the reaction is exothermic. The assumption of chemical equilibrium ignores the fact that some soot is "frozen," which explains how this assumption could lead to an overestimate of the chemical energy release in the fire. Further pursuit of this question was beyond the scope of this effort.

2.2 FIRE RADIANT ENVIRONMENT

Thermal radiation to a parachute in proximity to a fuel fire is one of the major contributors to the total thermal environment experienced by the parachute fabric. When the parachute is outside of the hot gas region (plume) the radiation field is calculated accounting for the vertical temperature profile in the plume, the variation in geometric configuration factor with wind-blown tilt angle, the distance from source to target, plume geometry, i.e., height and radius, and the orientation of the target with respect to the source.

The calculation of the incident radiant intensity to the target is subject to a few basic assumptions. The fire (combustion zone and plume) is considered to be essentially a "solid source" with radius and temperature varying with altitude. It is assumed that the surface of this "solid" emits energy as a blackbody radiator, and that the ambient air between the fire and the parachute is perfectly transparent such that it does not absorb or scatter any

of the emitted energy. The "target" is considered to be a differential area element of arbitrary location on a parachute canopy. A right-hand cartesian coordinate system is selected with the origin centered in the fire base, the x-axis aligned with the wind vector, the z-axis taken normal to the ground and pointing in the direction of increasing altitude, with the y-axis completing the right-hand system. The requirement for a reference coordinate system arises from the continually changing orientation and displacement of the "target" with respect to the "source" during the parachute descent. The calculation of the radiant environment from the fire to a differential parachute element is discussed in Appendix B.

The AFPARTS code calculates the incident radiant flux to both sides of a differential area element arbitrarily located on a parachute canopy. The fire (combustion zone and plume) is subdivided into N isothermal zones. The combustion zone is taken as an isothermal cylinder of radius $(d_b + d_{cp})/4$ and temperature T_{cp}. The plume is divided into N-1 isothermal cylinders with cuts taken every 200°F (111°C). Each of these isothermal cylindrical zones are further subdivided dependent upon the standoff to radius ratio, $(r/R)_j$, where r is the distance from the fire centerline at altitude Z_j to the target and R is the mean zone radius. If $(r/R)_j$ is greater than 2 the zone is subdivided into 5 disks; if $(r/R)_j$ is less than 2 the zone is subdivided into 10 disks of equal radius. The cylindrical surface of each disk is further subdivided into 36 equal angular sections.

If the parachute enters the hot gas region the calculation of a configuration factor is not required. Since the fire is assumed to behave as a blackbody, the radiant flux to each side of the fabric is simply taken to be the blackbody intensity at temperature T_p, corresponding to altitude Z within the plume.

2.3 PARACHUTE TRAJECTORIES

The calculation of parachute descent trajectories can be complex if stability and glide considerations are included. Parameters such as load, suspension line length, uninflated configuration, porosity, fabric permeability, apex hole size, and diameter all affect gore shape and the fully inflated configuration of a parachute in steady descent. The baseline configuration for this study is defined as the A/F C-9 canopy. Since the primary objective is to evaluate the thermal response of parachute materials exposed to a crash-fire thermal environment, the simplification of the trajectory calculation is considered appropriate. To effect this simplification the following assumptions were made:

- The uninflated configuration is a 28 foot (8.5 meters) diameter flat circular.

- The fully inflated canopy profile is hemispherical.
- Canopy oscillations (due to spilling) are neglected.
- Canopy spin is neglected.
- The canopy is in a fully inflated, steady-descent mode.

2.3.1 Steady Descent Velocity

The drag coefficient of flat circular canopies is based upon the total surface area of the canopy, i.e.,

$$A = \frac{\pi}{4} D_o^2 \tag{5}$$

where

D_o = diameter of flat circular canopy (uninflated)

In steady descent, equilibrium is established between the load and the drag, i.e.,

$$W = \frac{1}{2} \rho_\infty V_o^2 C_D A \tag{6}$$

where

W = load (man and equipment)

ρ_∞ = ambient air density

V_o = steady descent velocity

C_D = drag coefficient

A = drag area

Using a nominal drag coefficient of 0.75 given in Reference 12 and a nominal load of 200 lbs (890 newtons) allows the steady descent velocity to be calculated from Equation (6).

$$V_o = 19 \text{ ft/sec} = 5.8 \text{ m/sec} \tag{7}$$

2.3.2 Influence of the Fire

The trajectory of a parachute in proximity to a large fuel fire is influenced by the convective flows in and around the fire. In calculating descent trajectories for this study no attempt was made to model the dynamics associated with the flow field and their effect upon parachute motion. Instead, the parachute is assumed to act as a point mass that instantaneously assumes the velocities associated with the local flow field.

When the parachute is outside of the fire, i.e., when the magnitude of the instantaneous position vector (measured from the fire centerline to the parachute in a plane parallel to the ground at the same altitude as the parachute) is larger than the fire radius at the parachute altitude the influence is only due to wind and air entrainment by the fire (Figure 2). The velocity field due to air entrainment is radially symmetric about the fire centerline and varies with altitude and distance from the fire centerline. Since the fire model defines the entrainment velocity at the plume boundary the entrainment velocity at any position is defined as

$$V_e(x_p, y_p, z_p) = V_{e_{plume}}(z_p) \cdot \frac{R_f}{R_p} \qquad (R_p > R_f) \qquad (8)$$

where

$V_{e_{plume}}(z_p)$ = air entrainment velocity at the plume boundary at altitude of parachute, z_p

R_f = plume radius at altitude z_p

R_p = Radius from fire centerline to parachute at altitude z_p

Thus, outside of the fire the parachute velocity components are taken as

$$V_x = V_{wind} - V_e(x_p, y_p, z_p) \cos\theta \qquad (9)$$

$$V_y = -V_e(x_p, y_p, z_p) \sin\theta \qquad (10)$$

$$V_z = -V_o \qquad (11)$$

where

V_{wind} = wind velocity defined to be coincident with the x-axis

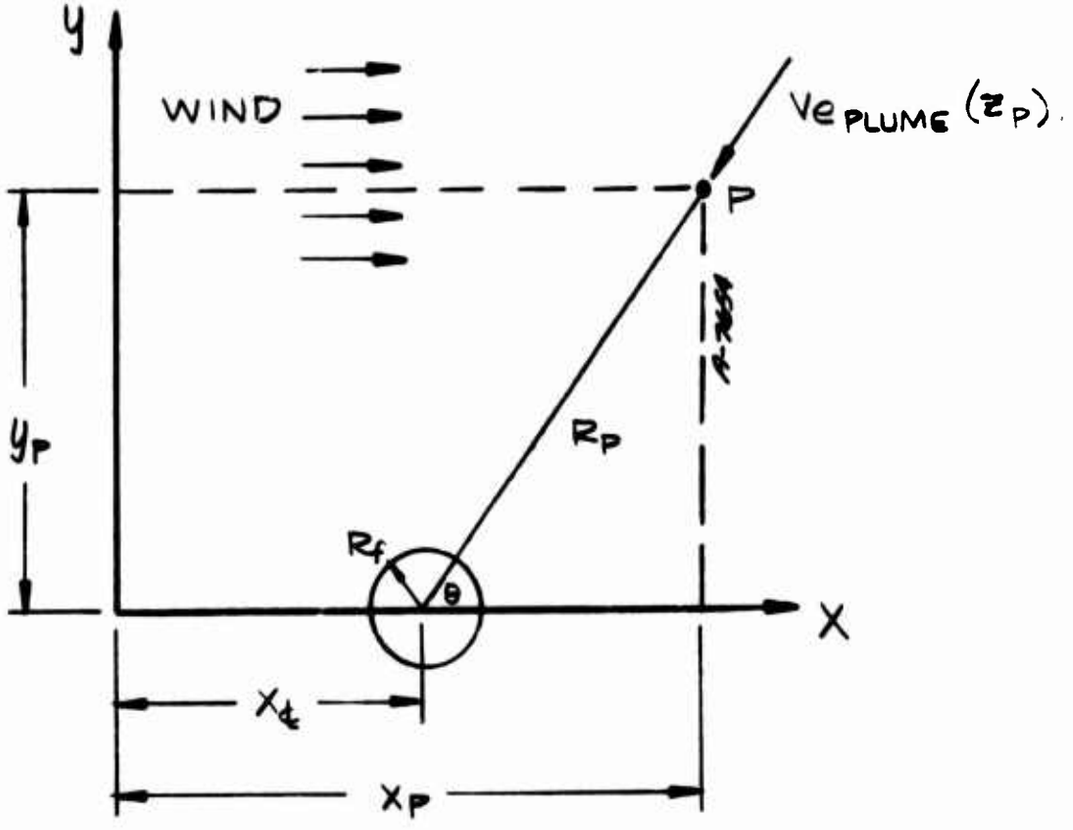

Figure 2. Top view of velocity fields influencing parachute trajectory when outside of fire.

θ = angle between the x-axis and the position vector from the fire centerline to the parachute at altitude z_p.

If the parachute enters the plume (Figure 3), i.e., $R_p < R_f$, the direct influence of wind and entrainment are assumed to vanish. The effect of air entrainment appears in the updrafts (which are parallel to the fire centerline) and the effect of wind is to cause the fire to tilt giving rise to both horizontal and vertical components of the updraft velocity field.

Thus, inside the plume the parachute velocity components are taken as

$$V_x = V_{plume}\ (z_p)\ \sin\ \phi \tag{12}$$

$$V_y = 0 \tag{13}$$

$$V_z = V_{plume}(z_p)\ \cos\ \phi - V_o \tag{14}$$

where

$V_{plume}(z_p)$ = updraft velocity within the plume at altitude z_p

ϕ = wind-blown plume tilt angle, between the z-axis and the fire centerline.

2.3.3 Position Coordinates

A simple predictor-corrector technique is used to calculate the instantaneous position coordinates of the parachute. At any instant of time, t_i, the parachute has position coordinates x_{p_i}, y_{p_i}, z_{p_i}. Associated with this location are velocity components V_{x_i}, V_{y_i}, V_{z_i}. These velocity components are used to project the position of the parachute at the next time, t_{i+1}, by assuming that the velocities are invariant, i.e.,

$$x'_{p_{i+1}} = x_{p_i} + V_{x_i}\ \Delta t \tag{15}$$

$$y'_{p_{i+1}} = y_{p_i} + V_{y_i}\ \Delta t \tag{16}$$

$$z'_{p_{i+1}} = z_{p_i} + V_{z_i}\ \Delta t \tag{17}$$

where the primes denote projected values.

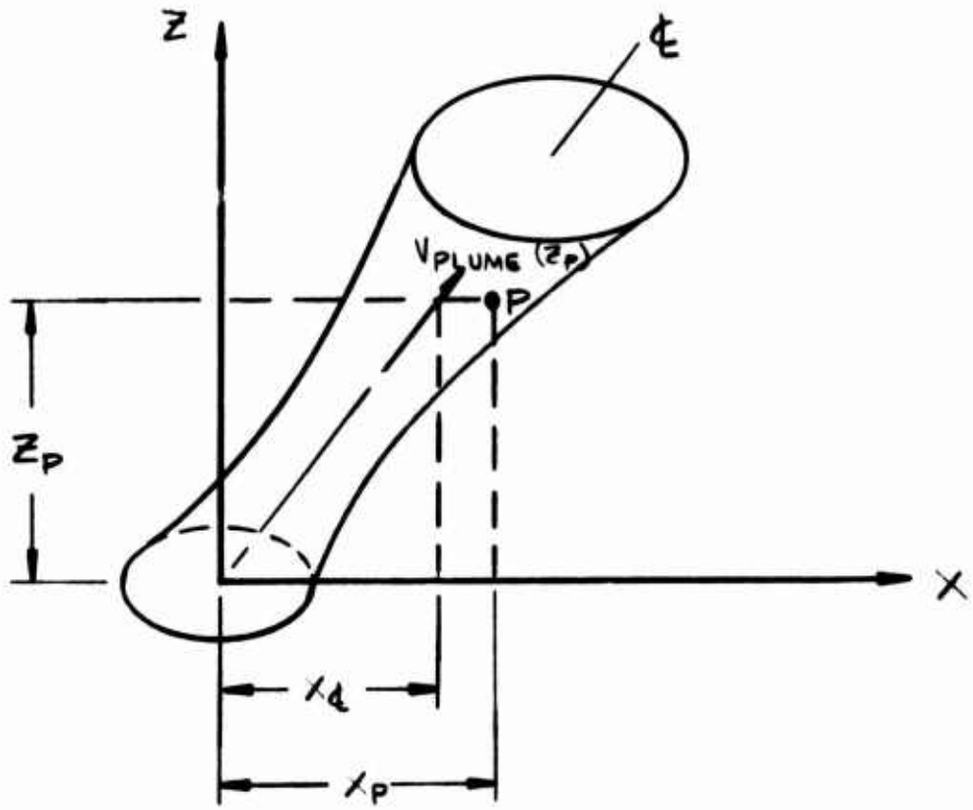

Figure 3. Side view of velocity fields influencing parachute trajectory when inside of fire.

New velocity components are calculated at the projected position; $V'_{x_{i+1}}$, $V'_{y_{i+1}}$, $V'_{z_{i+1}}$. The velocities at time t_i are taken as the mean of the velocities at location $(x_p, y_p, z_p)_i$ and $(x'_p, y'_p, z'_p)_{i+1}$; i.e.,

$$\left(\bar{V}_x\right)_i = \frac{1}{2}\left(V_{x_i} + V'_{x_{i+1}}\right) \tag{18}$$

$$\left(\bar{V}_y\right)_i = \frac{1}{2}\left(V_{y_i} + V'_{y_{i+1}}\right) \tag{19}$$

$$\left(\bar{V}_z\right)_i = \frac{1}{2}\left(V_{z_i} + V'_{z_{i+1}}\right) \tag{20}$$

and the actual position at time t_{i+1} is calculated from

$$x_{p_{i+1}} = x_{p_i} + \left(\bar{V}_x\right)_i \Delta t \tag{21}$$

$$y_{p_{i+1}} = y_{p_i} + \left(\bar{V}_y\right)_i \Delta t \tag{22}$$

$$z_{p_{i+1}} = z_{p_i} + \left(\bar{V}_z\right)_i \Delta t \tag{23}$$

SECTION 3

FABRIC THERMAL MODEL

The analytical modeling of the energy transfer and the prediction of the transient temperature of parachute components requires the idealization of the parachute-fire system into an equivalent heat transfer system. The previous section described the analytical models that were developed to define a nominal fuel fire, the radiation field emitted by the fire, and the influence of the fire on the trajectory of a parachute in its proximity. This section will describe the analytical models developed to define the thermal interaction between a parachute material and its environment. Included in the following paragraphs are discussions of the analytical models formulated to describe the blow-by and blow-through of ambient air, the heat transfer associated with these convective environments, the decomposition kinetics of heated fabrics, the energy equation describing the thermal response of thin parachute fabrics, the material properties utilized for the baseline materials investigated in this study (Nylon, Nomex, PBI), and a discussion of how all of these models are incorporated in the APPARTS computer code.

3.1 CONVECTIVE ENVIRONMENT

In defining the flow field about a parachute canopy a few basic assumptions were made, namely

- The flow is incompressible (ρ = constant, locally)
- The environs behaves as a perfect gas ($P = \rho RT$)
- The flow is isentropic

The velocity distribution tangential to the outside of a parachute canopy is determined from knowledge of the pressure distribution with Bernoulli's equation:

$$P - P_\infty = \frac{1}{2}\rho_\infty V_\infty^2 - \frac{1}{2}\rho_\infty V^2 \qquad (\rho = \rho_\infty = \text{constant}) \qquad (24)$$

or

$$V = \sqrt{\frac{2(P_\infty - P)}{\rho_\infty} + V_\infty^2} \tag{25}$$

The pressure distribution, in terms of coefficient of pressure, over a fully inflated flat circular canopy is taken from Reference 12 and is given in Table 1 as a function of geometric parameters illustrated in Figure 4. The coefficient of pressure over the outside of the canopy is defined as

$$CP_{out} = \frac{P_\infty - P_{out}}{\frac{1}{2}\rho_\infty V_\infty^2} \tag{26}$$

and on the inside of the canopy as

$$CP_{in} = \frac{P_{in} - P_\infty}{\frac{1}{2}\rho_\infty V_\infty^2} \tag{27}$$

where

P = local pressure

P_∞ = ambient pressure (1 atm)

ρ_∞ = ambient density

V_∞ = freestream velocity relative to the fabric

If the canopy is descending outside of the hot gas region the ambient gas is assumed to be air at standard temperature and pressure (70°F and 1 atm), and the freestream velocity relative to the fabric is taken to be the steady descent velocity, i.e.,

$$V_\infty = V_o \tag{28}$$

If the canopy is within the bounds of the plume, the ambient gas is a mixture of air and combustion products and has the properties associated with the plume at the instantaneous parachute altitude, namely

$$\rho_\infty = \rho_{plume}(z_p) \tag{29}$$

$$T_\infty = T_{plume}(z_p) \tag{30}$$

TABLE 1. PRESSURE DISTRIBUTION OVER FLAT CIRCULAR CANOPY

S*	δ (degrees)	CP_{in}	CP_{out}
0.0	0.0	1.01	0.50
0.2	18.0	0.95	0.50
0.4	36.0	0.88	0.50
0.6	54.0	0.82	0.50
0.8	72.0	0.76	0.50
1.0	90.0	0.70	0.50

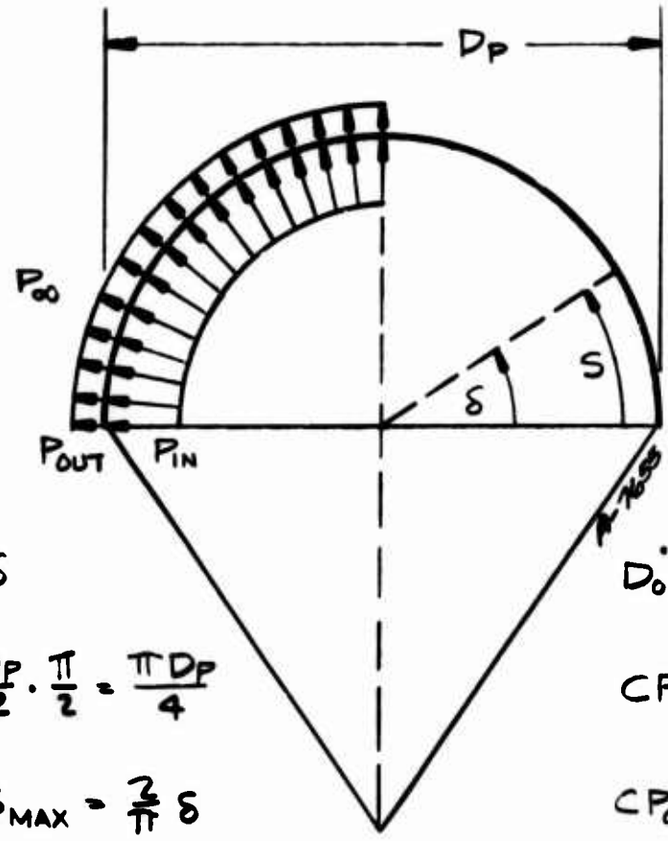

$$S = \frac{D_P}{2} \cdot \delta$$

$$S_{MAX} = \frac{D_P}{2} \cdot \frac{\pi}{2} = \frac{\pi D_P}{4}$$

$$S^* = S/S_{MAX} = \frac{2}{\pi}\delta$$

$$D_0^* = 2 \cdot S_{MAX} = \frac{\pi}{2} D_P$$

$$C_{P_{IN}} = \frac{P_{IN} - P_\infty}{\frac{1}{2}\rho_\infty V_\infty^2}$$

$$C_{P_{OUT}} = \frac{P_\infty - P_{OUT}}{\frac{1}{2}\rho_\infty V_\infty^2}$$

Figure 4. Geometry of fully inflated canopy.

and the freestream velocity relative to the fabric is the steady descent velocity.

$$V_\infty = V_o$$

It is further assumed that the boundary layer along the inside surface of the canopy disappears due to suction induced by the positive pressure gradient across the permeable fabric. The velocity through the fabric (blow-through) is determined from solution of a Darcy's Law expression[5] for flow through porous media:

$$\frac{\Delta P}{L} = \frac{\alpha \mu_\infty V_w}{g_c} + \frac{\beta \rho_\infty V_w^2}{g_c} \tag{32}$$

where

$\Delta P = P_{in} - P_{out}$ = pressure gradient across the fabric

L = fabric thickness

μ_∞ = ambient gas viscosity

ρ_∞ = ambient gas density

V_w = blow-through velocity

α, β = permeability coefficients associated with a given fabric

At any selected location on a canopy knowlege of the local tangential velocity, V_{out}, and local gas properties allows the calculation of heat transfer between the ambient gas and the fabric. The tangential flow is analogous to a boundary layer over a flat plate for which the Stanton number can be determined from[20]

$$(St_o)_{lam} = 0.332/\sqrt{Re}_x \tag{33}$$

for laminar flow, and

$$(St_o)_{turb} = 0.0296/(Re_x)^{0.2} \tag{34}$$

for turbulent flow, where

St_o = Stanton number in the absence of blowing

Re_x = local Reynolds number = $V_{out} S/\nu_\infty$

S = streamwise length from leading edge of canopy

ν_∞ = ambient gas kinematic viscosity

The transition from laminar to turbulent flow is assumed to occur at a local Reynolds number of 200,000. Since the boundary layer on the outside of the canopy is being blown due to the flow through the permeable fabric, the Stanton number must be modified accordingly with a correction of the form[20]

$$\frac{St}{St_o} = \frac{1}{(1 + \eta B')^3} \tag{35}$$

where

St = Stanton number in the presence of blowing

B' = dimensionless blowing parameter = $\dfrac{V_w}{V_{out} St_o}$

η = blowing coefficient = $\begin{cases} 0.90 \text{ for laminar flow} \\ 0.17 \text{ for turbulent flow} \end{cases}$

Heat transfer to the fabric is calculated from

$$\dot{q} = h_c (T_r - T_w) \tag{36}$$

where

$\dot{q}$ = heat flux to the fabric

h_c = local heat transfer coefficient

T_r = local recovery temperature $\approx T_\infty$

T_w = local fabric temperature

and the heat transfer coefficient is obtained from the definition of Stanton number as:

$$h_c = \rho_\infty V_{out} C_{p_\infty} St \tag{37}$$

The leading edge (S = 0) is treated as a stagnation point with nose radius taken as half the fabric thickness. The stagnation point Stanton number is taken from Kays[21] as

$$(St_o) = \frac{0.81}{Re^{0.5} Pr^{0.6}} \tag{38}$$

where

Re = stagnation point Reynolds number = $\frac{V_{out}\ L/2}{\nu_\infty}$

Pr = Prandtl number of ambient gas (Pr = 0.7 assumed)

The stagnation point Stanton number is modified for blowing using Equation (35) and the heat transfer coefficient is obtained from Equation (37).

In passing through the fabric the ambient gases exchange energy with the fabric. If an equilibrium state is achieved between the fabric and the blow-through gas the heat flux can be expressed as

$$\dot{q} = \rho_\infty V_w C_{p_\infty} (T_\infty - T_w) \tag{39}$$

and the heat transfer coefficient (using the definition of Equation (36)) as

$$h_c = \rho_\infty V_w C_{p_\infty} \frac{(T_\infty - T_w)}{(T_r - T_w)} \tag{40}$$

However, it is possible that the residence time of the gas within the fabric is so short that equilibrium cannot be established and that the total energy content of the gas is not transferred to the fabric. If it is assumed that the fabric temperature change is small, in comparison to the temperature change of the gas in its passage through the fabric, an estimate of the gas temperature within the fabric can be evaluated from[5]

$$\frac{\left(T_{\infty_x} - T_w\right)}{\left(T_{\infty_o} - T_w\right)} = \exp\left[-\frac{4h_c}{\rho_\infty C_{p_\infty} V_w}\left(\frac{x}{D}\right)\right] \tag{41}$$

where

T_{∞_x} = gas temperature at depth x in the fabric

T_{∞_o} = initial gas temperature on entering the fabric

T_w = fabric temperature

x = depth in fabric

D = fabric effective flow passage diameter

h_c = convective heat transfer coefficient to fabric

If we define equilibrium as the condition where the temperature difference between the gas and fabric is less than five percent of its initial value, Equation (41) can be used to calculate the passage distance required to attain this condition.

$$x \simeq \frac{3\rho_\infty C_{p_\infty} V_w}{4h_c} \tag{42}$$

The quantities which have not been evaluated in Equation (42) are h_c and D. The effective flow passage diameter, D, is related to fabric permeability and a good approximation is[5]

$$D = \frac{1}{\sqrt{\alpha}} \tag{43}$$

If a nominal heat transfer coefficient of 1.0 Btu/ft^{2}hr°F (5.67 watts/meter^2°C) is assumed between the gas and the fabric the passage distance required for equilibrium is simply

$$x = \frac{3}{4} \rho_\infty C_{p_\infty} V_w D \tag{44}$$

If x is greater than the fabric thickness, L, all of the available energy is not transferred to the fabric, and the heat transfer coefficient is modified accordingly, i.e.,

$$h_c = \rho_\infty C_{p_\infty} V_w \left(\frac{L}{x}\right) \frac{(T_\infty - T_w)}{(T_r - T_w)} \tag{45}$$

where

$$\frac{L}{x} \leq 1.0 \tag{46}$$

3.2 DECOMPOSITION KINETICS

As fabrics are heated to elevated temperatures their thermal response can be influenced by pyrolysis phenomena. Therefore, it is essential to know how mass is lost as a function of time and temperature. Dr. Ivan Goldfarb of the Air Force Materials Laboratory at Wright-Patterson AFB, Ohio, has formulated a relationship describing the mass loss of polymers undergoing N identifiable pyrolysis reactions. In this model it is assumed that each reaction obeys an Arrhenius relation of the form

$$-\frac{dw_i}{dt} = A_i \exp(-Ei/RT) w_i^{n_i} \tag{47}$$

where

A_i = rate constant for reaction i

E_i = activation energy for reaction i

R = gas constant

n_i = reaction order for reaction i

and

$w_i = \frac{\rho_i - \rho_{r_i}}{\rho_{o_i} - \rho_{r_i}}$ = weight fraction remaining of the reactable portion of reactant i

ρ_{o_i} = initial density associated with reactant i

ρ_{r_i} = fully reacted (final) density associated with reactant i

ρ_i = instantaneous density associated with reactant i

$\frac{dw_i}{dt}$ = time rate of change of instantaneous reactable fraction of reactant i

If the total reactable fraction of the material is defined as

$$F = \frac{\rho_o - \rho_r}{\rho_o} \tag{48}$$

where

ρ_o = virgin material density

ρ_r = fully decomposed material density

and the fraction of total reactant attributable to reactant i is defined as

$$\lambda_i = \frac{\rho_{o_i} - \rho_{r_i}}{\rho_o - \rho_r} \tag{49}$$

it can be shown that the instantaneous weight fraction of total reactant is:

$$W_T = \frac{\rho - \rho_r}{\rho_o} = F \sum_{i=1}^{N} \lambda_i w_i \tag{50}$$

Differentiating Equation (50) with respect to time yields the expression utilized to calculate the time rate of change of density.

$$\dot{\rho} = F\rho_o \sum_{i=1}^{N} \lambda_i A_i \exp(-E_i/RT) w_i^{n_i} \tag{51}$$

3.3 FABRIC THERMAL RESPONSE

Included among the components comprising a personnel parachute are the suspension lines, canopy, webbing, risers, and pack. Since the canopy fabric is extremely thin it has the smallest thermal capacitance among the parachute components and, as such, is the critical component in the parachute system. The analytical model developed in this study is directed at an accurate simulation of the thermal response of canopy fabrics, although the model can be used to assess the performance of suspension lines, risers, and webbing. The basic assumptions inherent in the model allow irradiation from both sides, reradiation from both sides, and neglect in-depth conduction. The ASTER[19] code is better suited for the analysis of fabrics where in-depth temperature gradients might be significant and more complex boundary conditions are required for an accurate description.

As indicated above, canopy fabrics are so thin that in-depth temperature gradients can be neglected. Therefore, the fabric is idealized as one isothermal node as shown in Figure 5. An overall energy balance is written for the fabric at a selected location on the canopy as:

$$q_{conv_{ext}} + q_{conv_{int}} + q_{rad_{in_{ext}}} + q_{rad_{in_{int}}} - 2q_{rad_{out}} - q_{rxn} - q_{sens} = 0 \tag{52}$$

The terms in Equation (52) are defined below.

- q_{sens} = time rate of increase in sensible enthalpy
- q_{rxn} = energy absorbed due to fabric decomposition
- $q_{conv_{ext}}$ = energy convected to fabric surface due to boundary layer flow over exterior surface
- $q_{conv_{int}}$ = energy convected to fabric due to ambient gas permeating through the fabric
- $q_{rad_{in_{ext}}}$ = radiation absorbed from exterior direction

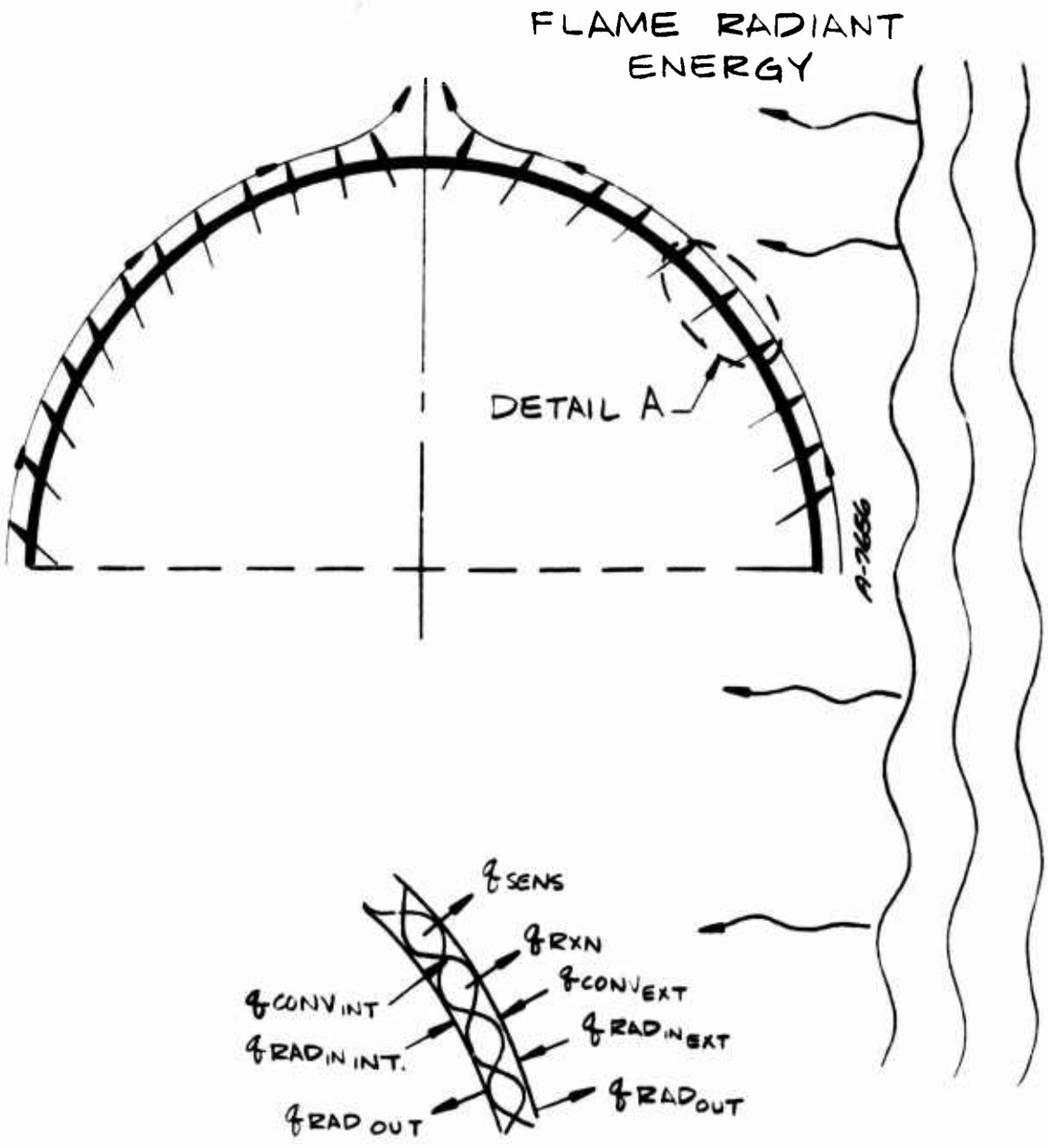

DETAIL A

Figure 5. Schematic of energy balance on canopy area element.

- $q_{rad_{in_{int}}}$ = radiation absorbed from interior direction
- $q_{rad_{out}}$ = radiation emitted from each surface

As shown in Section 3.2, the convective terms are expressed as

$$q_{conv_{ext}} = h_{c_{out}} (T_r - T_w) \tag{53}$$

and

$$q_{conv_{int}} = h_{c_{in}} (T_r - T_w) \tag{54}$$

where T_r is the recovery temperature of the ambient gas, T_w is the instantaneous fabric temperature, and $h_{c_{out}}$ and $h_{c_{in}}$ are local heat transfer coefficients between the ambient gas and the fabric.

The absorbed radiant fluxes are expressed as

$$q_{rad_{in_{ext}}} = \alpha q_{rad_{ext}} \tag{55}$$

and

$$q_{rad_{in_{int}}} = \alpha q_{rad_{int}} \tag{56}$$

where $q_{rad_{ext}}$ and $q_{rad_{int}}$ are the incident radiant fluxes to the exterior and interior surfaces of the canopy element, respectively, and α is the absorptivity of the fabric.

Radiation by the fabric is emitted to the environs from both the interior and exterior surfaces; therefore, the reradiation term is expressed as

$$2q_{rad_{out}} = 2\sigma\epsilon T_w^4 \tag{57}$$

where ϵ is the emissivity of the fabric and σ is the Stefan-Boltzmann constant.

The time rate of increase in fabric sensible enthalpy is given by

$$q_{sens} = \rho C_p L \frac{dT}{dt} \tag{58}$$

where ρ is the fabric density, C_p is the fabric specific heat, L is the fabric thickness and dT/dt is the time rate of temperature rise.

The energy absorbed due to decomposition is expressed as

$$q_{rxn} = L\Delta H_{rxn} \frac{d\rho}{dt} \tag{59}$$

where $d\rho/dt$ is the overall decomposition rate and ΔH_{rxn} is the enthalpy change associated with pyrolysis reactions, and is given by

$$\Delta H_{rxn} = rH_{char} + (1 - r)\, H_{pgas} - H_{virgin} \tag{60}$$

where r is the residual weight fraction of char after decomposition and H_{char}, H_{pgas}, and H_{virgin} are the enthalpies of the charred fabric, pyrolysis gas, and virgin fabric, respectively.

The instantaneous fabric temperature is determined by a Newton - Raphson iteration procedure. The iteration temperature is accepted when the error in Equation (52) is within 0.01 percent of the summation of the absolute value of each term in the equation.

3.4 FABRIC PROPERTIES

The initial objectives of this study were to assess the relative performance of the components of a personnel parachute system and to evaluate the survivability potential of selected candidate materials. The primary parachute configuration is the standard AF C-9 canopy. The detailed specifications for each of the components are defined in the existing Mil Specs[22-27]:

- Cloth, parachute, nylon (Type I) MIL-C-7020F
- Cord, nylon, (Type III) MIL-C-5040E
- Webbing, textile, woven nylon (Type XXII) MIL-W-4088G
- Cloth, duck, nylon (Type III) MIL-C-7219D

As discussed previously, the thermal capacitance of canopy fabric is so small that it is the most critical component of the system in terms of thermal survivability. Therefore, the following discussion is limited to the properties associated with canopy materials, consistent with the Mil-Spec defined above. The materials considered in this study include, and are limited to, Nylon, Nomex, and PBI.

3.4.1 Thermophysical Properties

The specifications defined in MIL-C-7020F that are pertinent to this study are summarized in Table 2.

TABLE 2. CANOPY FABRIC SPECIFICATIONS

Property	Specification
Weight (max)	1.1 oz./sq.yd. ripstop
Thickness (max)	0.003 inches
Air Permeability (max)	100 ± 20 CFM/sq.ft.

The weight and thickness specification defines the virgin density of canopy fabrics as

$$\rho_o = \frac{\text{weight}}{\text{thickness}} = \frac{1.1 \text{ oz./sq.yd.}}{0.003 \text{ inches}} = 30.55 \text{ lbs}_m/\text{cu.ft.} \quad (0.4896 \text{ gm/cc}) \qquad (61)$$

The char density is defined as

$$\rho_c = (1 - F)\ \rho_o \qquad (62)$$

where F is the reactive fraction.

The specific heat of all polymeric fibers are of the same order of magnitude. The values for nylon, Nomex and PBI[5] are summarized in Table 3.

TABLE 3. FABRIC SPECIFIC HEAT

Temperature	C_p(Btu/lbm - °F) or (cal/gm - °C)			Temperature
(°F)	Nylon 6-6	Nomex	PBI	(°C)
40	0.360	0.300	0.300	4.
200	0.418	0.360	0.350	94.
450	0.515	0.450	0.422	232.
600		0.500	0.470	316.
835		0.575	0.540	446.
890			0.565	477.

3.4.2 Decomposition Properties

The pyrolysis model described in Section 3.2 is consistent with Goldfarb's reducted TGA data for Nomex and PBI as given in Appendix II of Reference 5 and more accurately represents the sensitivity of fabric thermal response to pyrolysis events. Detailed data of this form for Nylon was not available for this study. Existing data taken from Reference 13 was utilized. The decomposition kinetic constants used in this study are summarized in Table 4.

TABLE 4. DECOMPOSITION KINETIC CONSTANTS

Fabric	Nomex	PBI	Nylon
F	0.615555	0.29095	0.930
E_1, cal/mole	93158.0	10279.01	52666.0
E_2, cal/mole	76882.0	88363.91	---
E_3, cal/mole	107645.0	85497.54	---
E_4, cal/mole	---	104182.9	---
E_5, cal/mole	---	64223.09	---
$\log_{10}A_1$	29.0	3.25431	13.267
$\log_{10}A_2$	20.4393	20.23019	---
$\log_{10}A_3$	23.8207	21.21431	---
$\log_{10}A_4$	---	24.46445	---
$\log_{10}A_5$	---	13.27577	---
N_1	4.1670	1.6064	1.0
N_2	3.1690	5.8249	---
N_3	2.7059	1.3620	---
N_4	---	3.0148	---
N_5	---	1.6269	---
λ_1	0.649437	0.0702877	1.0
λ_2	0.251007	0.257945	---
λ_3	0.099557	0.301164	---
λ_4	---	0.081481	---
λ_5	---	0.2891223	---

3.4.3 Thermochemical Properties

The variation of enthalpy with temperature, of virgin and fully charred fabric, is determined from the heat of formation and specific heat as:

$$H = \Delta H_{f_{298°K}} + \int_{298°K}^{T} C_p dT \qquad (63)$$

The heats of formation of Nomex and PBI fabrics are not derived from heat of combustion data but rather are values that were determined from analytical correlation of experimental data as reported in Reference 5. The heat of formation of Nylon 6-6 was taken from Reference 14. Table 5 summarizes the heat of formation values used for virgin and charred fabrics considered in this study.

TABLE 5. FABRIC HEAT OF FORMATION

State	Heat of Formation (cal/gm)		
	Nomex	PBI	Nylon
Virgin	-472.	0.0	-844.
Char	0.0	0.0	0.0

The pyrolysis gas elemental composition was assumed to be uniform during pyrolysis. Table 6 summarizes the pyrolysis gas compositions which were calculated from the virgin material composition and the char residual weight fraction of each fabric. The values for Nomex and PBI were taken from Reference 5 and Nylon from Reference 14. Pyrolysis gas enthalpies were calculated by the ACE[9] code. The values are the equilibrium enthalpy of a gas mixture at 1.0 atm and are summarized in Table 7.

3.4.4 Optical Properties

The optical properties of a fabric determine how much of the radiant heat flux from the fire is reflected, absorbed, transmitted and reradiated. The parameters of interest in this study are the absorptivity and emissivity of the candidate canopy fabrics. As discussed in Section 3.2, the radiant

TABLE 6. PYROLYSIS GAS ELEMENTAL COMPOSITION BY MASS FRACTION

Element	Nomex	PBI	Nylon 6-6
H	0.069	0.134	0.09798
C	0.522	0.242	0.63684
N	0.191	0.624	0.12378
O	0.218	0.0	0.14139

TABLE 7. PYROLYSIS GAS ENTHALPY

Temperature	Enthalpy (cal/gm)		
(°C)	Nomex	PBI	Nylon 6-6
25.	-664.	-513.	-449.
100.	-661.	-429.	-468.
200.	-658.	-327.	-480.
232.	-652.	-303.	-496.
300.	-583.	-254.	--
400.	-482.	-161.	--
446.	-436.	-138.	--
476.	--	- 99.	--

energy incident on an area element of a parachute canopy is the total of partial contributions emitted from the fire over a range of temperatures. The correct formulation for radiant energy absorbed by a fabric is

$$q_{rad_{in}} = \int_0^\infty \alpha_\lambda (T_w)\ H_{b_\lambda} (T_p)\, d\lambda \qquad (64)$$

where α_λ is the spectral absorptivity of the fabric at temperature T_w, and $H_{b_\lambda} (T_p)$ is the spectral irradiation from a blackbody at temperature T_p incident to the fabric element. Utilization of the formulation given in Equation (64) would require integrations of this type over the N isothermal zones used to characterize the fire radiation field. This additional complexity was considered beyond the intended scope of this effort.

The optical properties obtained under a previous study [5] are representative of an 1800°F (982°C) source and a thicker fabric (dimensions typical of flight suits). Optical property data for parachute fabrics were not available for this study. Inaccuracies in optical properties will not seriously affect the results since it was found that radiative absorption is not the primary source of fabric thermal response. Therefore, for simplicity, the fabrics were assumed to behave as gray bodies, i.e.,

$$\alpha = \varepsilon \neq f(\lambda) \qquad (65)$$

and the optical properties for Nomex and PBI from Reference 5 and for Nylon from Reference 15 were adopted. These values are summarized in Table 8.

TABLE 8. FABRIC OPTICAL PROPERTIES

Fabric	Absorptivity, α		
	Nomex	PBI	Nylon
Virgin	0.57	0.62	0.60
Char	0.72	0.76	0.75

The optical properties are linearly weighted by the degree of decomposition according to:

$$\alpha = \varepsilon = x \cdot \alpha_{virgin} + (1 - x) \cdot \alpha_{char} \tag{66}$$

where x is the fraction of uncharred fabric.

3.4.5 Fluid Mechanical Properties

The flow of ambient gases through the fabric is controlled by the pressure gradient across the fabric and the permeability. The nominal permeability of 1.1 oz/yd^2 ripstop weave canopy fabric is 100 CFM/ft^2 at a pressure gradient of 0.5 inches of water (2.6 psf). This specification essentially states that the velocity of sea level air through a 0.003 inch thick fabric is 100 ft/sec for a pressure gradient of 2.6 psf. Utilizing the correlation between α and β given in Reference 5, the permeability coefficients appearing in Equation (32) are found to be:

$$\alpha = 7.358 \times 10^9 \text{ ft}^{-2} \quad (7.92 \times 10^{10} \text{ m}^{-2})$$

$$\beta = 8.829 \times 10^5 \text{ ft}^{-1} \quad (2.896 \times 10^6 \text{m}^{-1}) \tag{67}$$

3.4.6 Mechanical Properties

Included among the potential failure mechanisms of a parachute component are melting, burning, shrinking, and loss of tensile strength. Tensile properties of fabrics have been measured at temperature for materials of various thicknesses and constructions but data is not currently available for Nomex and PBI fabricated in a 1.1 oz/sq.yd. ripstop fabric. This data deficiency required the use of the available tensile data for heavier and thicker fabrics to form the data base. In utilizing this data an attempt was made to develop a universal common indicator of the relative strength of fabrics which accounts for the variations in density and thickness of the test specimens. The common factor should be mass, i.e., variations in cross-sectional area and density can be normalized by a mass/unit length parameter. This suggests that tensile strength data for a variety of fabrics can be correlated on the basis of a form of strength-to-weight ratio.

Tensile data[16-18] were correlated in the form of strength per unit mass per unit length as a function of temperature. The actual data base and reduction is discussed in Appendix C. The data suggest that the decay of mechanical strength with temperature is a stronger function of the basic fiber rather

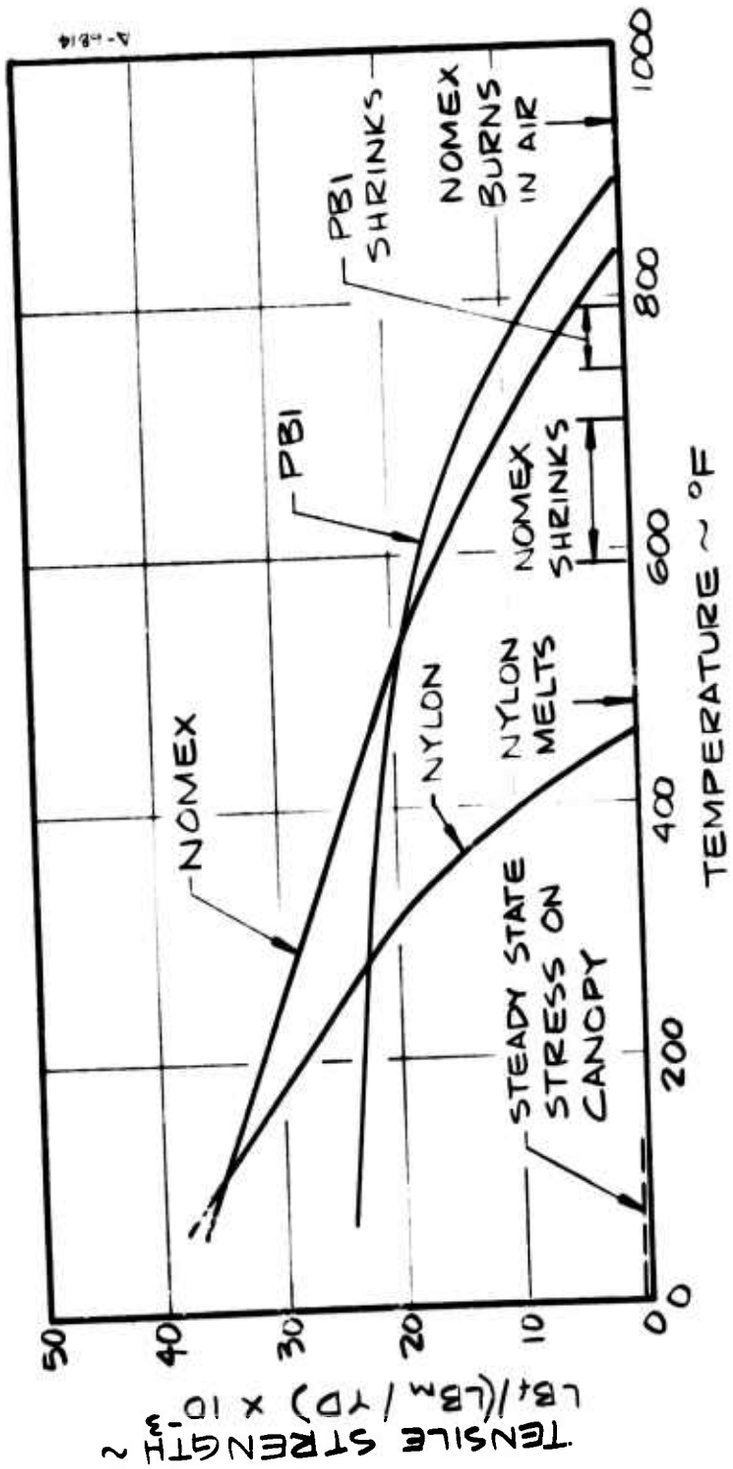

Figure 6. Comparative fabric tensile strength.

than configuration. The resultant correlation for Nylon, Nomex, and PBI is illustrated in Figure 6. Indicated in this figure are the temperature ranges where shrinkage has been observed for Nomex and PBI. If the steady-state load on a canopy in steady descent is expressed in these units it is observed that the load is very low (234 lb_f/lbm/yd) and that all candidate fabrics retain sufficient load carrying capability up to temperatures near which they totally lose all tensile strength. The potential for shrinkage, induced failure, and possible tearing resulting from shrinkage, have not been considered. In the latter case the only available data were obtained for a test configuration in which the fabric was restrained from shrinking and the resultant induced stresses were much larger than would be anticipated for a fully inflated canopy in steady descent.

The ultimate failure criterion selected for this study is the temperature at which the fabric strength (in units of strength/unit mass/unit length) is reduced to the steady-state load. The selection of this failure criterion neglects any factor of safety since deployment loading is not considered and the imposition of safety factor (on the order of 10 or less) would not alter the relative performance of the candidate fabrics. Utilization of a safety factor would simply reduce the fail temperature of all candidate fabrics and, since none of the current candidates are predicted to survive low altitude through-the-fire trajectories, would be an unwarranted conservatism for purposes of this study.

Fabric shrinkage is also considered a potential failure mechanism but it is not clear how shrinkage relates to failure (due to a lack of applicable data) and thus no attempt was made to include the effects. If shrinkage of any degree is to be considered a failure then the failure criterion can be altered to the respective temperatures at which shrinkage onset has been observed for the candidate fabrics. A summary of the significant threshold temperatures used in this study for the candidate fabrics is given in Table 9.

TABLE 9. FABRIC THRESHOLD TEMPERATURES

Fabric	Shrinkage		Failure		Melting		Burning	
	°F	°C	°F	°C	°F	°C	°F	°C
Nomex	590	310	835	446	---	---	938	503
PBI	740	393	890	477	---	---	---	---
Nylon	---	---	450	232	488	253	---	---

3.5 AFPARTS COMPUTER CODE DESCRIPTION

The AFPARTS (Aerotherm Fire Environment Parachute Thermal Simulation) computer program is a new code developed expressly for this study. It incorporates all of the analytical models describing the fire, its environment, and the fabric thermal response as detailed above. The AFPARTS code is a "user-oriented" program in that it utilizes NAMELIST input and the required inputs are kept to a minimum.

Almost all required operating data are stored within the program. For example, the properties of the fire combustion zone are stored as a function of fire base diameter. The only inputs required to describe the fire are the base diameter and the wind velocity. Specification of the initial x, y, z coordinates of the parachute allow the automatic calculation of the trajectory. The input of two angles determines the location of the area element on the canopy, defines the pressure distribution, and allows the calculation of the incident radiant environment. A code number input specifies the material (PBI, Nomex or Nylon) of interest for which all properties are stored. The fabric thermal response is calculated as a function of time utilizing the boundary conditions automatically determined according to the relation of the trajectory to the fire. Output includes fire definition, trajectory, incident radiant heating, convective coefficients, recovery temperature, flow velocities, and fabric density and temperature. Also included in the output are indicators of the relative position of the parachute with respect to the fire centerline and the fabric condition, namely, whether it is in its normal (virgin) state, charring, melting, burning, shrinking, or has failed.

Although all necessary data for the conditions and materials of interest in this study have been stored, the code is not limited to the constraints adopted for this study. All required operating data may be input by the user allowing the evaluation of any fabric and/or fire within the limitations imposed by the analytical models that are used. A more detailed description of the code is contained in the AFPARTS User's Manual [28].

SECTION 4

PARAMETRIC ANALYSIS

The parametric analysis had two primary objectives. First, specific candidate fabrics were to be evaluated to determine their relative survivability in a crash-fire thermal environment. The analytical models and the nominal thermal properties of Nylon, Nomex, and PBI fabrics are described in Section 3 of this report. It is noted there that the canopy fabric is the most critical component in a personnel parachute system from the standpoint of thermal survivability. Therefore, the analysis was limited to a comparison of three candidate canopy fabrics.

The second objective was to investigate the influence of various environmental parameters upon fabric thermal performance. Before discussing the results of the analysis the range of environmental parameters considered in the study will be defined.

4.1 FIRE PARAMETERS

As described in Section 2, the fire model developed in this study is tied to the characteristics of large open pool fires of JP-4 fuel. The characteristics of the base region (combustion zone) are dependent on the fire base diameter. Solution of the conservation equations with the constraint of local thermochemical equilibrium defines the base region variation of fire properties (temperature, velocity, radius, density, etc.,) with altitude. For purposes of simplicity, the nominal base region was defined to extend to the altitude where the stoichiometric air/fuel ratio is attained and the entire combustion zone was assumed to have uniform properties corresponding to the equilibrium composition at the stoichiometric temperature. The conservation equations define the diameter at the top of the combustion zone and the variation of the fire diameter with altitude is assumed to be linear in this region.

The plume definition requires the properties at the top of the combustion zone as an initial condition. As noted in the preceding discussion, specification of the fire base diameter is sufficient to define the conditions at the top of the combustion zone. Solution of the conservation equations

assuming frozen chemistry in the plume defines the variation of plume properties (temperature, density, radius, velocity, etc.) with altitude. Therefore, the only parameter that influences the fire profiles is the base diameter.

The range of fire base diameter considered in this analysis is from 50 feet to 200 feet (15m - 61m) and is considered representative of the majority of aircraft crash fires. Calculations were performed with the AFPARTS code to define nominal fires with base diameters of 50 feet (15.24m), 100 feet (30.48m), and 200 feet (60.96m). The results of the calculations are illustrated in Figures 7, 8, and 9 which show the variation of temperature, radius, and updraft velocity with altitude for the three base diameters considered. The plume is truncated at an altitude corresponding to a plume temperature of 120°F (49°C) since the decay rate of temperature with altitude is very slow and the environmental effects of the high altitude regions are not very significant. Several features of these fires should be noted. First, the current model indicates that the combustion zone temperature increases with fire base diameter. This effect is related to the surface area to volume ratio which impacts the radiation losses from the fire. As fire diameter increases, the surface area to volume ratio decreases with a resultant increase in combustion zone temperature. Also, the major portion of temperature decay occurs within two fire base diameters from the top of the combustion zone. Secondly, the radius of the fire decreases with altitude in the combustion zone reaching a minimum at the altitude corresponding to stoichiometric conditions. At higher altitudes the effects of entrainment increase the plume radius to almost twice that of the fire base. Therefore, it should be noted that at altitudes high above the combustion zone, the extent of the plume is such that although it may appear that a parachute is not within the geometric bounds of a fire, as judged from the ground, it may indeed be within a hot gas region. Third, the updraft velocities in the fire plume increase with fire base diameter and can reach values of 40 - 80 ft/sec (12 - 24 m/sec). Therefore, the parachute will have a net upward velocity relative to the ground equal to the difference of the updraft and descent velocities, 10 - 50 ft/sec (3 - 15 m/sec). In a wind-blown fire the effective updrafts are parallel to the fire centerline and the resultant vertical component is reduced by the cosine of the fire tilt angle.

The range of wind velocities considered in the analysis is from 0 - 30 knots (0 - 15 m/sec). The effect of wind upon the fire is to tilt the entire fire column in the direction of the wind vector. The tilt angle increases

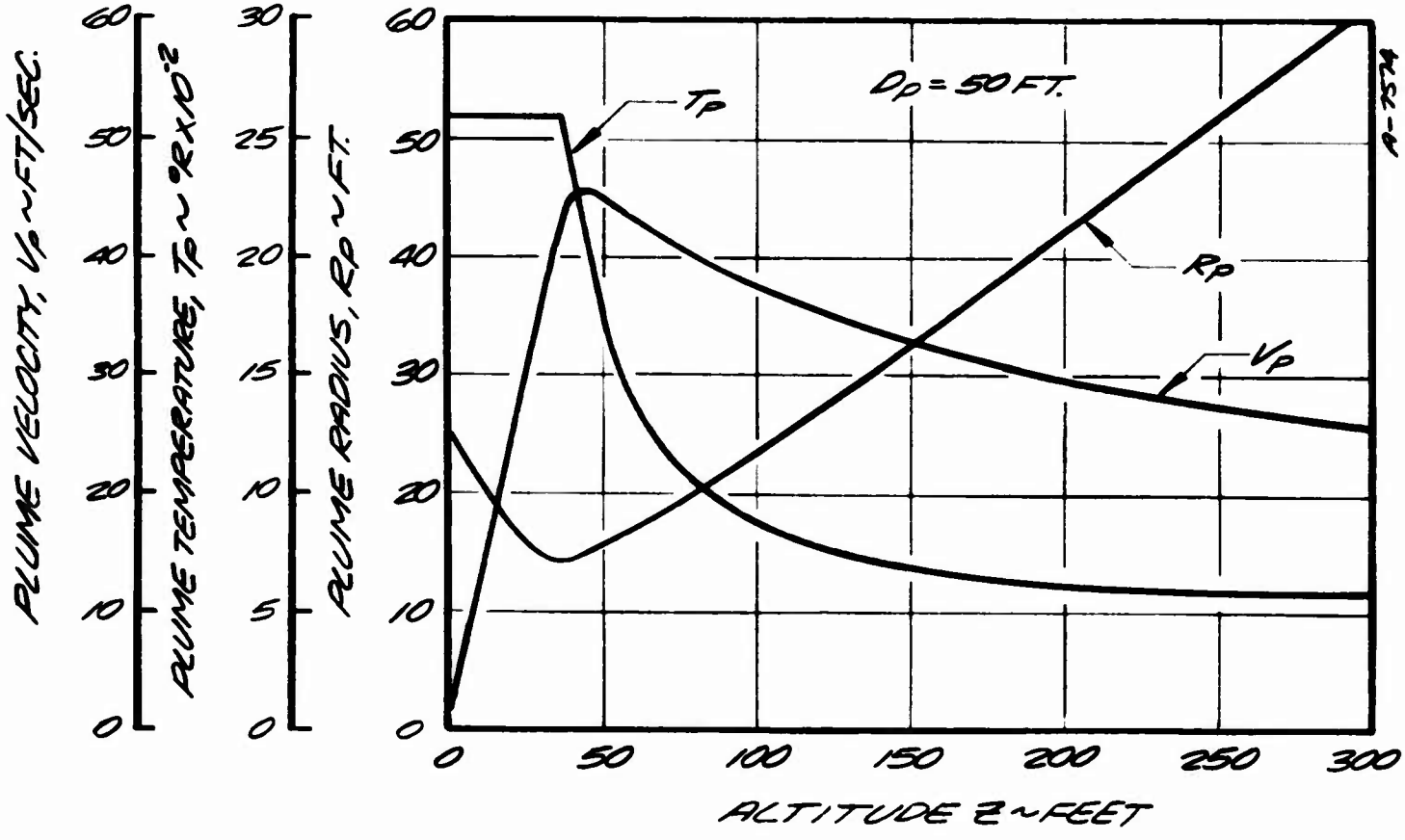

Figure 7. Vertical Profiles in a 50-foot (15 meter) base diameter fire.

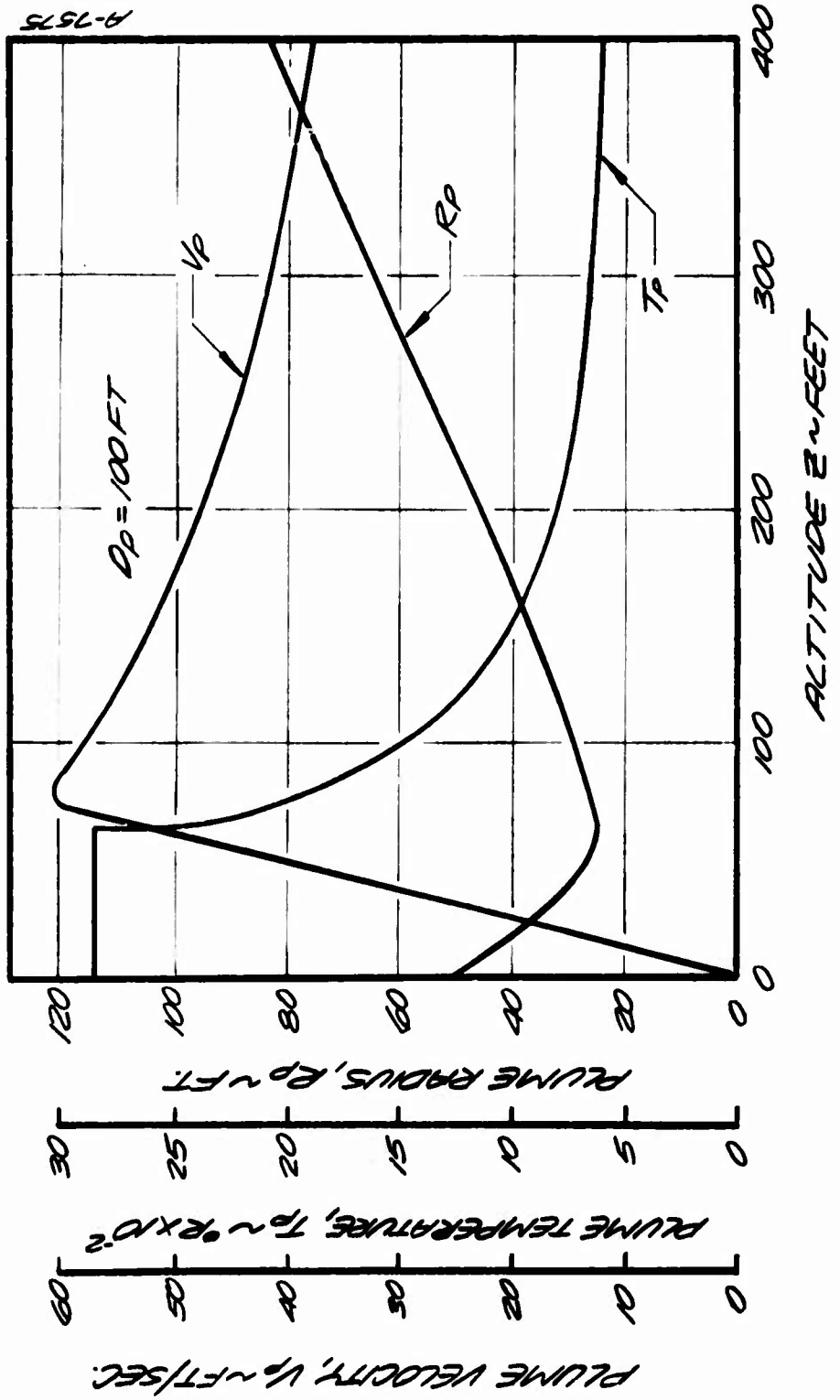

Figure 3. Vertical profiles in a 100-foot (30 meter) base diameter firc.

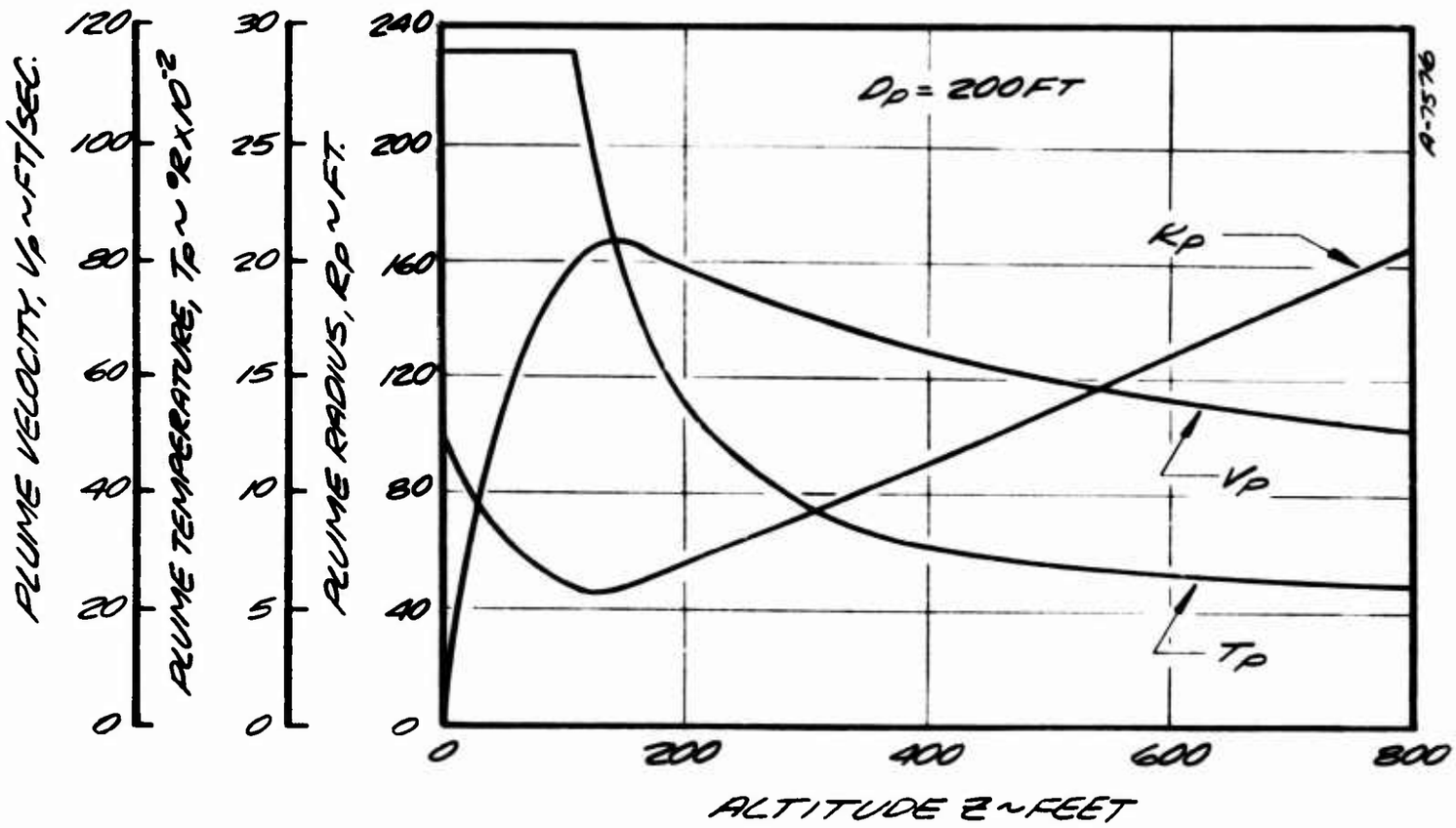

Figure 9. Vertical profiles in a 200-foot (61 meter) base diameter fire.

with wind velocity and decreases at larger fire diameters as would be expected. The results of AFPARTS calculations for wind-blown fire bending is shown in Figure 10.

4.2 TRAJECTORY PARAMETERS

The trajectory model described in Section 2 assumes that the parachute travels with the local velocity field. It should be noted that variations in load (man and equipment) and permeability (which affects the drag coefficient) leads to variations in steady descent velocity. The range of descent velocities was taken as 16 - 30 ft/sec, with 19 ft/sec as nominal. Calculations were performed for the upper and lower bounds of this range and it was shown that the results are insensitive to descent velocity. Thus, all the results shown in this report are based upon a 30 ft/sec descent velocity.

Once the fire is defined (including the wind velocity and the resultant tilting of the fire) the specification of the initial parachute coordinates is all the data necessary to define the parachute trajectory. To reduce the possible trajectory matrix to a manageable size, the initial altitude, z_{p_o}, was selected to be that altitude corresponding to a plume temperature of 140°F (60°C) for all cases. Since the vertical profiles within the fire get stretched out as fire diameter increases (Figures 7 - 9) the initial altitude of the parachute increases for larger fires.

Selection of the other two initial position coordinates, x_{p_o} and y_{p_o}, determines the altitude at which the parachute enters the fire. Worst case conditions are for trajectories in the plane of the fire centerline, i.e., $y_{p_o} = 0$. Trajectories which do not enter the fire, i.e., $y_{p_o} >> D_b$, were considered of minor interest. For windless conditions the initial position coordinates were chosen to obtain vertical descent trajectories very close to the fire boundary without entering the fire. Note, if there is no wind the current model would predict that a parachute in the fire would remain there indefinitely if the updraft velocity exceeded the normal descent velocity. The majority of trajectories were chosen to be in the plane of the fire centerline. Initial position coordinates were selected such that the parachute would enter the plume at altitudes corresponding to plume temperatures from 440°F (227°C) to 1140°F (615°C). The matrix of trajectories considered in this analysis is given in Table 10. Two selected trajectories (Cases 100.21 and 100.22) are shown in Figure 11. The environment consists of a 100 foot (30.48m) base diameter fire in a 20 knot (10 m/sec) wind. The initial altitude in both cases is 428 feet (130 m) and the trajectories are in the plane of the fire centerline, i.e., $y_{p_o} = 0$. For an initial position, x_{p_o}, 285 feet (87 m) upwind of the fire base center the trajectory enters the plume at an altitude of

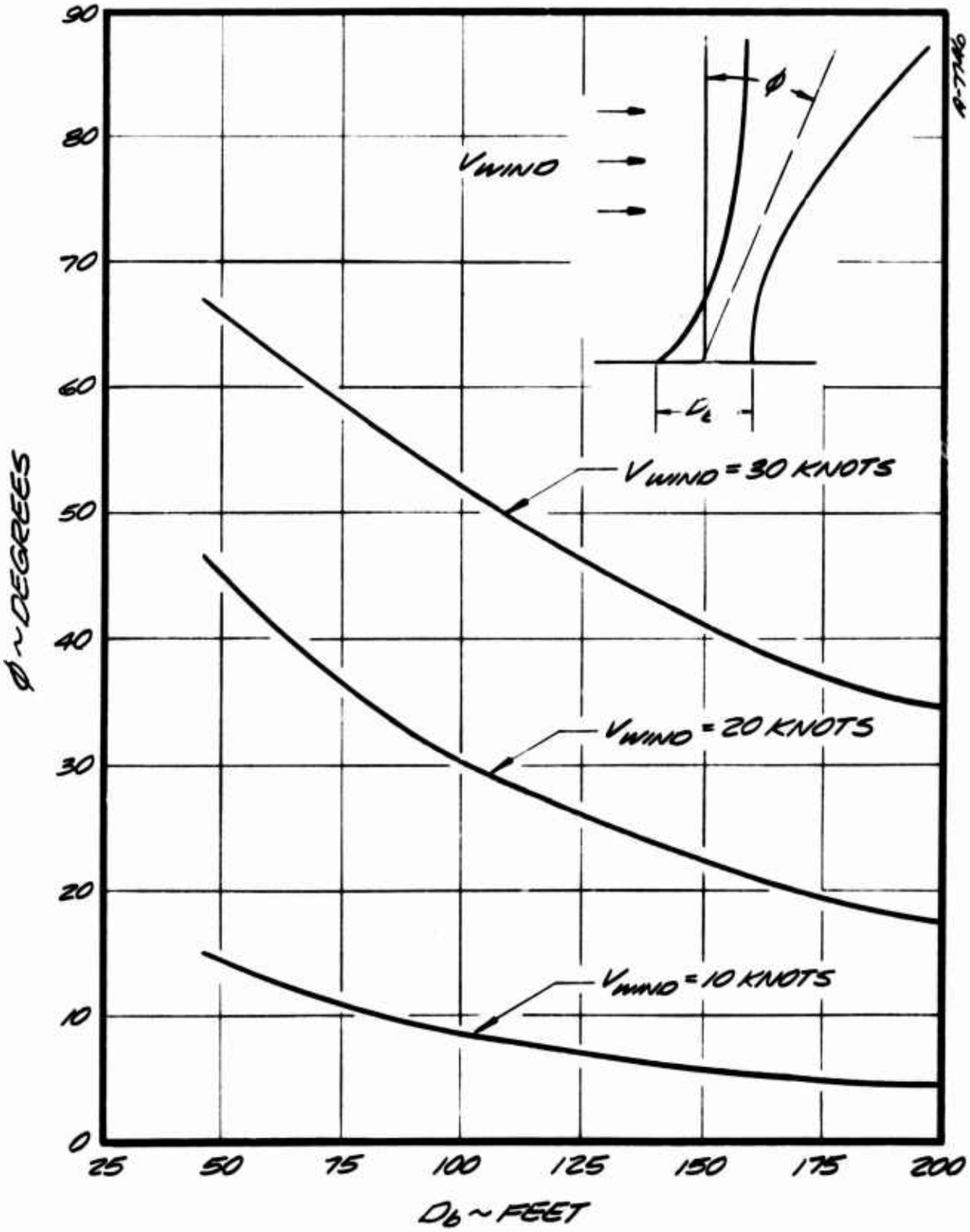

Figure 10. Bending of wind-blown fires.

TABLE 10. INITIAL TRAJECTORY AND FIRE PARAMETERS

Case	Fire Base Diameter (feet)	Wind Velocity (knots)	X_{p_o} (feet)	Y_{p_o} (feet)	Z_{p_o} (feet)	α (degrees)	δ (degrees)	Z_{p_e} (feet)	T_{p_e} (degrees R)
50.11	50.	10.	-100.	0.0	247.8	0.0	45.0	92.8	932.
50.12			-112.					80.5	1048.
50.13			-119.					58.5	1450.
50.21		20.	-148.					78.5	1074.
50.22			-176.					76.8	1095.
50.23			-193.					48.8	1800.
50.31		30.	-188.					71.5	1179.
50.32			-216.					63.8	1316.
50.33			-233.					58.5	1450.
100.11	100.	10.	-210.	0.0	428.8	0.0	45.0	142.8	1035.
100.12			-230.					98.8	1495.
100.13			-250.					66.8	2412.
100.21		20.	-285.					150.0	980.
100.22			-310.					135.0	1072.
100.23			-330.					127.8	1144.
100.24			-370.					99.5	1483.
100.31		30.	-345.					143.8	1018.
100.32			-420.					128.5	1131.
100.33			-475.					98.5	1482.
200.11	200.	10.	-435.	0.0	808.0	0.0	45.0	276.	1010.
200.12			-460.					219.	1260.
200.13			-470.					184.	1528.
200.21		20.	-640.					276.	1010.
200.22			-710.					247.	1115.
200.23			-755.					184.	1528.
200.31		30.	-865.					276.	1010.
200.32			-980.					219.	1260.
200.33			-1035.					184.	1528.
50.01	50.	0.0	-60.0	0.0	247.8	0.0	0.0	---	---
100.01	100.		-120.0		427.8			---	---
200.01	200.		-250.0		808.0			---	---
50.14	50.	10.	-140.	75.0	247.8	270.0	0.0	---	---
50.24		20.	-280.					---	---
50.34		30.	-420.					---	---
100.14	100.	10.	-230.	10.0	428.8	0.0	45.0	99.	1481.
100.15				20.0					

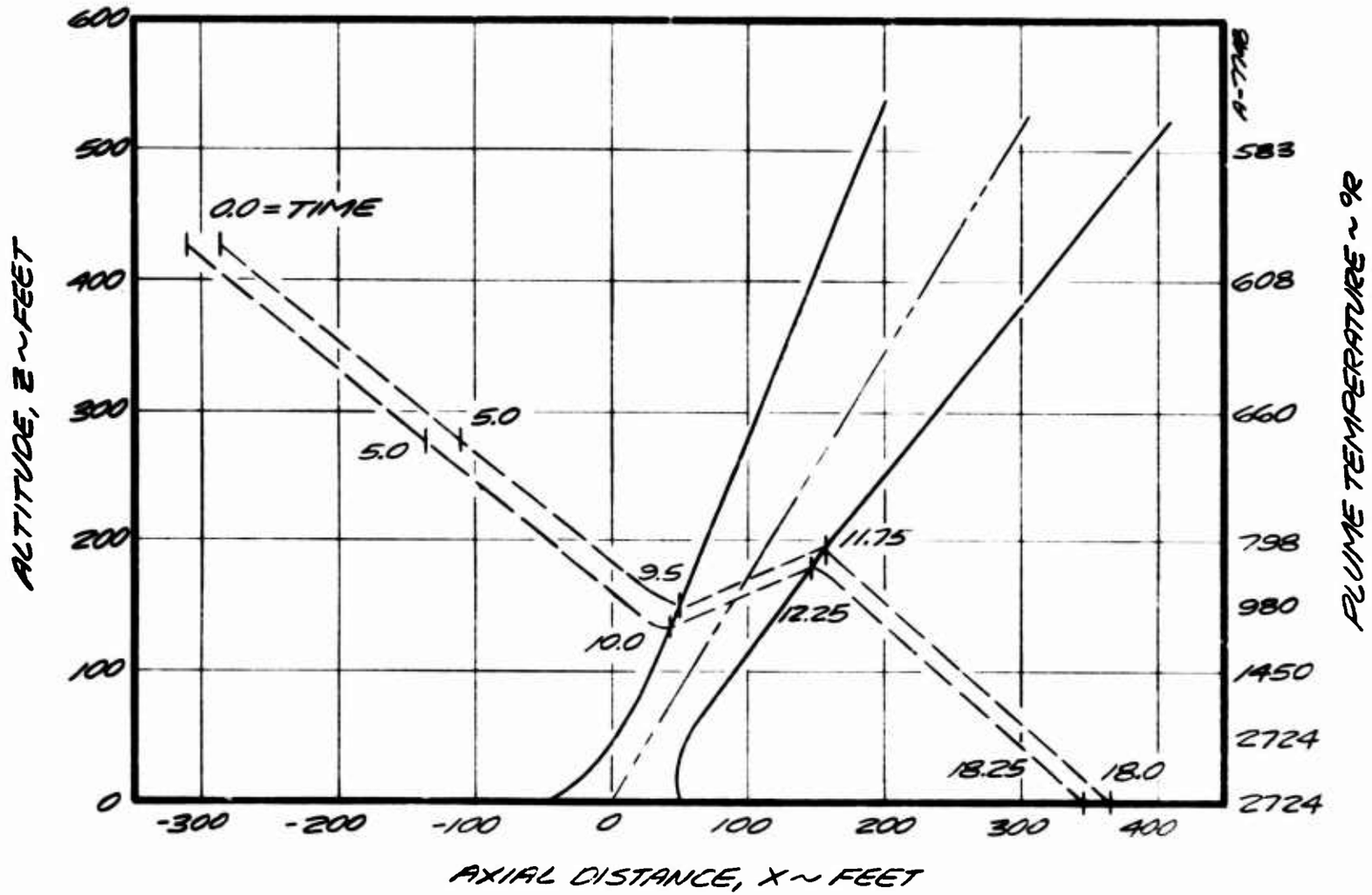

Figure 11. Parachute trajectories along fire centerline
100-foot base diameter, 20-knot wind

150 feet (46 m) and encounters an environment in which the surrounding gases are at a temperature of 520°F (271°C). If the initial position is 310 feet (94 m) upwind of the fire base center the parachute would enter the plume at an altitude of 135 feet (41 m) encountering plume gases at 612°F (322°C). The residence time in the plume for these selected cases is about 2.25 seconds. Note that the updrafts in the plume carry the parachute to higher altitudes. It is also observed that a difference of 25 feet (7 m) in the initial position coordinates results in a 92°F (57°C) difference in the ambient temperature encountered by the parachute canopy on plume entry.

4.3 CANOPY PARAMETERS

Other than the differences in the properties of the candidate canopy fabrics the only parameter requiring definition is the location on the canopy of the particular area element of interest. This selection influences the pressure gradient across the fabric and the radiation configuration factors to the fire. Determination of the location of the element that experiences the maximum thermal input for any given trajectory is not trivial. Recalling (Section 2.2) that the element location on the canopy is specified by two angles, α and δ, where α is the angle that the projection of the surface normal makes with the wind vector and δ is the angle between the surface normal and a plane parallel to the ground, the specification $\alpha = \delta = 0$ defines a canopy location that is irradiated on the outside surface only when the parachute is upwind of the fire and on a centerline trajectory. The specification $\alpha = 0°$ and $\delta = 45°$ defines a canopy location half way up and in the plane of the trajectory. This location was selected as nominal for all centerline trajectories through the fire, since it is irradiated on both sides and has the mean pressure gradient across the fabric. For windless conditions, the element $\alpha = \delta = 0$ was selected since this orientation will maximize the radiant input as the canopy descends to low altitudes.

4.4 RESULTS

A significant result of this study was the development of an integrated analysis procedure for the evaluation of parachute materials in aircraft crash fire thermal environments. This newly developed capability is in the form of a computer code, AFPARTS, which contains new analytical models for large crash fires, parachute descent trajectories as influenced by the fire, and fabric thermal response. The data used to model each part of this problem were collected primarily from the literature. No new property data were generated as a result of this program.

The results of this study will be discussed in terms of the analytical models that were developed and the evaluation of parachute performance as predicted by these models. The development of the analytical models was based on basic physical principles and the available data in the literature. The general results of the literature survey and their implications will be discussed first, followed by the specific results of the parametric analysis.

4.4.1 General Results

In developing the analytical models an investigation of the parameters of interest included the following major areas:

- JP-4 fuel fire thermal chemical environment
- Parachute descent trajectories as influenced by wind and fire
- Fabric thermal-optical-mechanical properties.

These investigations have led to some general results, independent of the parametric analysis, which are summarized below:

Fuel Fire Environment

In developing an analytical model for large open pool fires, characteristic of JP-4 aircraft crash fires, two significant factors became apparent from surveying the literature; first, no existing model for the thermochemical and geometrical characteristics of JP-4 fire plumes could be found, and second, the available data are limited to a very few measurements of the temperature profile in the combustion zone of small pool fires. No data could be found on the temperature profile in fire plumes.

The fire model developed for this study includes the only complete model for JP-4 fire plumes known. It must also be noted that the characteristics of the combustion zone, as modeled for large pool fires, necessitated an extrapolation based on the available data for small pool fires.

The results of modeling the fire have identified certain characteristics that have significant implications in relation to a parachute descending near the fire. The state of knowledge on fuel fires indicates that the combustion zone is fuel rich with accompanying large amounts of carbon particles (soot). This characteristic supports the assumption of an optically thick zone that radiates as a black body. The fire plume, above the combustion zone, is relatively inert which implies an absence of chemical interaction between the plume gases and the fabric until such fabric temperatures are achieved where fabric decomposition becomes significant.

The entrainment of air by the fire has a significant effect on the geometric characteristics of the fire plume. From mass and momentum considerations, air entrainment produces large updrafts in the fire which results in the plume extending several fire base diameters above the ground. The radial extent of the plume, which contains a hot mixture of combustion products and entrained air, increases continuously and can exceed that of the fire base. These characteristics have some implications relative to a parachute descending near a large crash fire. Due to the continual increase of plume radius with altitude, the probability of a descending parachute entering the plume increases at higher altitudes. It follows that, for trajectories that enter the fire, the transit time through the fire increases with altitude. As a result of the updrafts in the plume the parachute is lifted to higher altitudes in the plume where, due to the decay of fire temperature with altitude, it experiences a cooler ambient environment. Thus, for the range of fire size and descent velocities considered in this study, the highest temperature ambient environment experienced by a parachute entering a fire plume is associated with the temperature at the altitude of entry.

The effects of wind on the fire result in bending the entire fire column. Although it is assumed that the thermal and geometric characteristics of the fire are unaffected by tilting the fire, the overall result is in reducing the vertical component of the updraft velocity field and altering the geometric relationship for radiation from the fire to the parachute.

Parachute Descent Trajectories

In modeling the descent trajectory of a parachute near a large fuel fire the existing literature and accident reports were unable to contribute any quantitative information. This deficiency necessitated the use of the basic assumption that the parachute travels with the local velocity field. The implications resulting from this model are worth noting. The effects of air entrainment by the fire, although not large, results in a symmetric velocity field which continually draws a parachute toward the fire centerline. Under windless conditions, this field can be sufficient to draw a parachute into the fire if its descent trajectory passes within the order of one fire base radius of the plume. The presence of any wind imparts a horizontal velocity component to the parachute which results in a substantial decrease of the encounter times near the fire (of the order of seconds). As mentioned previously, the updrafts in the fire can lift the parachute to higher altitudes which prevents the parachute from descending into an increasingly severe thermal environment associated with the lower altitude regions of the fire.

Fabric Properties

In surveying the literature very little data were found on the thermal and optical properties of parachute materials. This necessitated extrapolating data for the same materials but of different construction and weight. An order of magnitude analysis based on the weight and thickness of the various parachute components shows that, on the basis of the thermal time constant, the canopy fabric is the most critical component in the C-9 parachute. Other parachute components are not critical to failure since their larger thermal capacity results in at least an order of magnitude slower thermal response compared to canopy fabrics.

It is apparent that the selected temperature dependent failure criteria are critical in evaluating failure thresholds for candidate materials. Again, no strength data for 1.1 oz/sq.yd. canopy fabrics were found. A correlation of available data on the basis of a strength-to-weight ratio provided a basis for selecting these criteria.

Mechanical failure has been identified as a potential failure mechanism due to the decay of fabric tensile strength at elevated temperatures (Figure 6). In this respect, both Nomex and PBI have significant additional thermal tolerance relative to Nylon due to their retention of strength to several hundred degrees (°F) above Nylon. No safety factor on the steady-state load was utilized in defining the strength failure criteria since no existing definition could be identified. It also should be noted that this failure

criterion is based upon tensile data taken at elevated temperatures where sufficient time is allowed for the fabric to reach an equilibrium with its surroundings. Such steady-state data may not be indicative of the ultimate strength limitations of a fabric when experiencing high temperatures over a very short time duration. Since fabric decomposition is a kinetic process, and strength may be related to the chemical nature of the fiber, time is likely to be an important consideration.

Fabric shrinkage has been identified as a possible failure mechanism since it can result in degraded aerodynamic performance of the parachute. The forms of Nomex and PBI studied both shrink significantly (30 to 40 percent) which may lead to failure before loss of strength. Nomex and PBI still exhibit improved thermal tolerance compared to Nylon even if shrinkage is taken to be the primary failure criterion. No specific criteria defining the allowable limits of shrinkage could be identified. Thus, the shrinkage failure criterion was defined as the temperature associated with the onset of shrinkage.

Burning and/or melting clearly represent states of failure. However, existing data indicate that candidate fabrics will shrink or lose mechanical strength prior to attaining conditions favorable for burning or melting.

4.4.2 Results of Parametric Analysis

AFPARTS calculations were performed for all of the fire/trajectory cases defined in Table X for canopy fabrics constructed of Nomex, PBI, and Nylon. The prime objective of the parametric study was to define the failure threshold of each of the candidate fabrics for the range of fire and trajectory conditions defined above.

One significant result is readily apparent. The thermal response of Nomex and PBI canopy fabrics is not sufficient to cause loss of mechanical strength for trajectories that do not enter the fire. For bypass trajectories, i.e., trajectories where the wind carries the parachute by the fire but where the offset from the fire is sufficient such that the canopy never enters the plume, the encounter time is so short that fabric thermal response is insignificant. Examination of the calculations indicates that the radiant energy absorbed by the canopy is offset by the convective cooling provided by the blow-through of cool ambient gases through the fabric.

Similar results are observed for the windless vertical descent trajectories. For these cases the encounter time extends over the entire descent. However, the radiation to the canopy only becomes significant at the lower altitudes since the emission from the cooler regions of the plume is small. The trajectories were chosen as close to the fire as possible without having the entrainment of air by the fire pull the parachute into it. The radiant emission from the fire increases with the size of the fire and incident radiant fluxes up to 11 Btu/sq.ft.-sec (12.5 watts/cm^2) were calculated at the lower altitudes to a parachute within 100 feet of a 200 foot diameter fire. As the fabric is heated the potential for convective cooling increases and the combined blow-by and blow-through cooling were found to be quite significant. For the smaller fires the time during which the radiant input is significant is small since the hottest region of the fire is contained within about one fire diameter above the ground. The fabric temperature rise for these cases was found to be small. For the largest fires the altitude range, and thus the encounter time, over which there is a significant radiant input to the fabric is extended. Significant fabric temperature response was noted for these cases, sufficient to induce fabric shrinkage for PBI and Nomex at altitudes less than 50 feet (15 m) and mechanical failure of Nylon fabric at 80 feet (24 m) above the ground. In general, it should be noted that the thermal capacity of canopy fabrics is so small, (~ .003 Btu/ft^2°F) that very low thermal inputs result in rapid fabric temperature rise.

As expected, through-the-fire trajectories were found to be critical for canopy fabrics. Whereas blow-by and blow-through of ambient gases provide substantial cooling of the fabric when outside of the fire, the same phenomena contribute substantial heating to the fabric when the environs consist of hot plume gases. The thermal response of canopy fabric in a through-the-fire trajectory is typified by the temperature history shown in Figure 12. The case illustrated (Case 100.21) is representative of an area element (α = 0°; δ = 45°) on a nylon canopy on a centerline trajectory through a 100 foot (30 m) base diameter fire in a 20 knot (10 m/sec) wind. The initial position coordinates (given in Table X) are such that the canopy enters the plume at an altitude of 150 feet (45.7 m) where the plume gas temperature is 520°F (271°C). The thermal response of the fabric is insignificant until the parachute is very close to the fire. As the parachute enters the fire the combined effects of radiant and convective heating result in a very rapid temperature rise. Due to the updrafts in the fire the canopy gains altitude and encounters an environment where the local plume gas temperature is decreasing. The fabric temperature continues to rise until is is equal

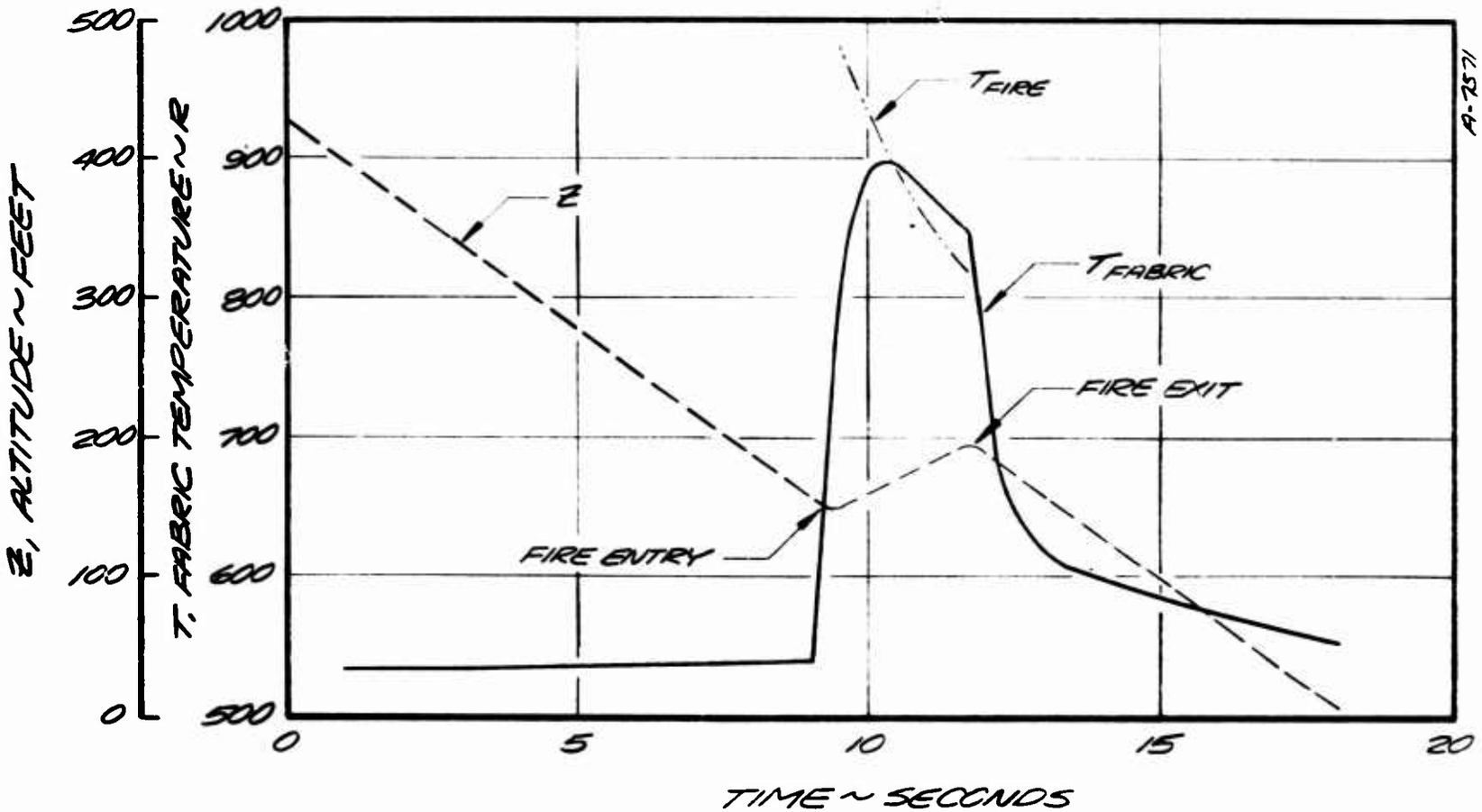

Figure 12. Typical thermal response of nylon canopy fabric in through-the-fire trajectories.

to the temperature of the local surroundings. Since the canopy continues to gain altitude and encounter even cooler ambient gases the convective effects begin to cool the fabric since the fabric is now at a higher temperature than the surroundings. As the canopy leaves the fire, on the downwind side, the cool ambient gases provide rapid convective cooling of the fabric. It should be noted that although the canopy is in the plume for about 2.25 seconds, peak fabric temperature is achieved in less than one second during which about 2/3 of the total fabric heating is due to blow-through convection. Since the peak nylon fabric temperature for this case of 435°F (224°C) is less than the assumed nylon fail temperature of 450°F (232°C) the canopy is predicted to survive this encounter. It is also of interest to note that the combination of temperature and time at temperature for this case is such that no fabric decomposition is predicted.

Examination of the results of all the through-the-fire cases considered indicated a strong dependency of maximum temperature attained by the canopy fabric on the plume temperature at the entry altitude. In correlating the results it was found that this maximum fabric temperature is a very weak function of fire diameter or wind velocity. It was possible to correlate maximum fabric temperature solely as a function of plume temperature at entry. The correlation for each of the candidate fabrics considered in this study is shown in Figure 13. Deviations due to the effects of wind and fire diameter would put ± 5 percent uncertainty bounds on the correlations. These correlations are valid even for through-the-fire trajectories that are offset from the fire centerline since encounter time does not fall off appreciably until the parachute is essentially "skirting" the fire. Using these correlations, the fail temperature of each candidate fabric can be related to a particular plume temperature at entry which, in turn, is associated with an entry altitude which varies with fire diameter. Therefore, it is possible to determine a minimum survival altitude for each candidate canopy fabric as a function of fire base diameter. These results are illustrated in Figure 14 for strength failure. Also shown are the altitudes at which failure is predicted to occur for Nomex and PBI fabrics if shrinkage is taken as the failure criterion.

It is apparent that the use of alternate materials in canopy fabrics show the potential for improved parachute survivability in encounters with JP-4 crash fires. It must be noted that the results depicted in Figure 14 represent worst case conditions, i.e., the parachute passing directly through a fully developed fuel fire. Under these conditions, for the C-9 parachute, the amount of improved performance, in terms of the difference in altitude of threshold failure, is from 20 to 100 feet depending upon material, fire diameter, and failure mode.

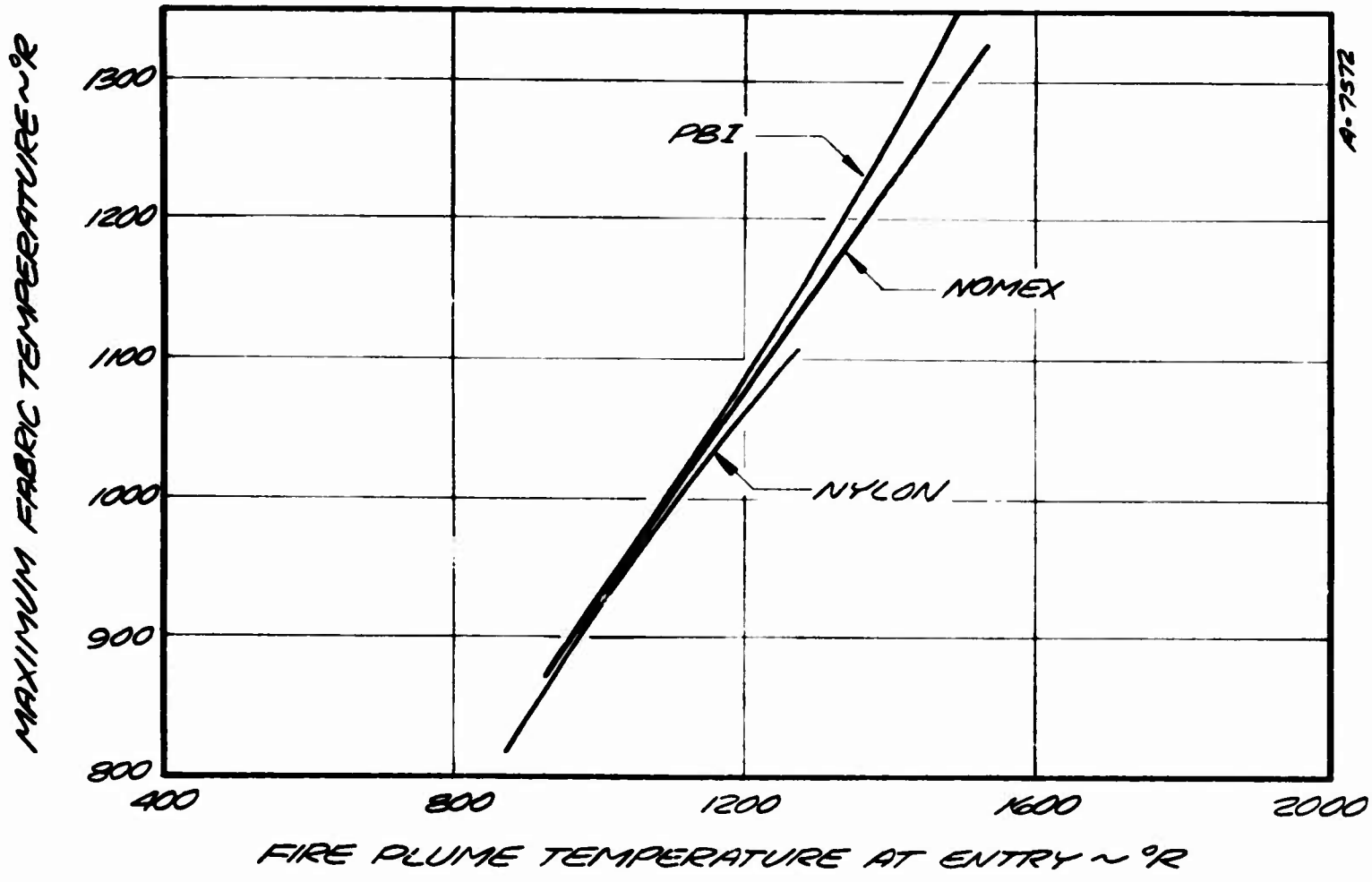

Figure 13. Maximum fabric temperature of candidate canopy fabrics for through-the-fire trajectories

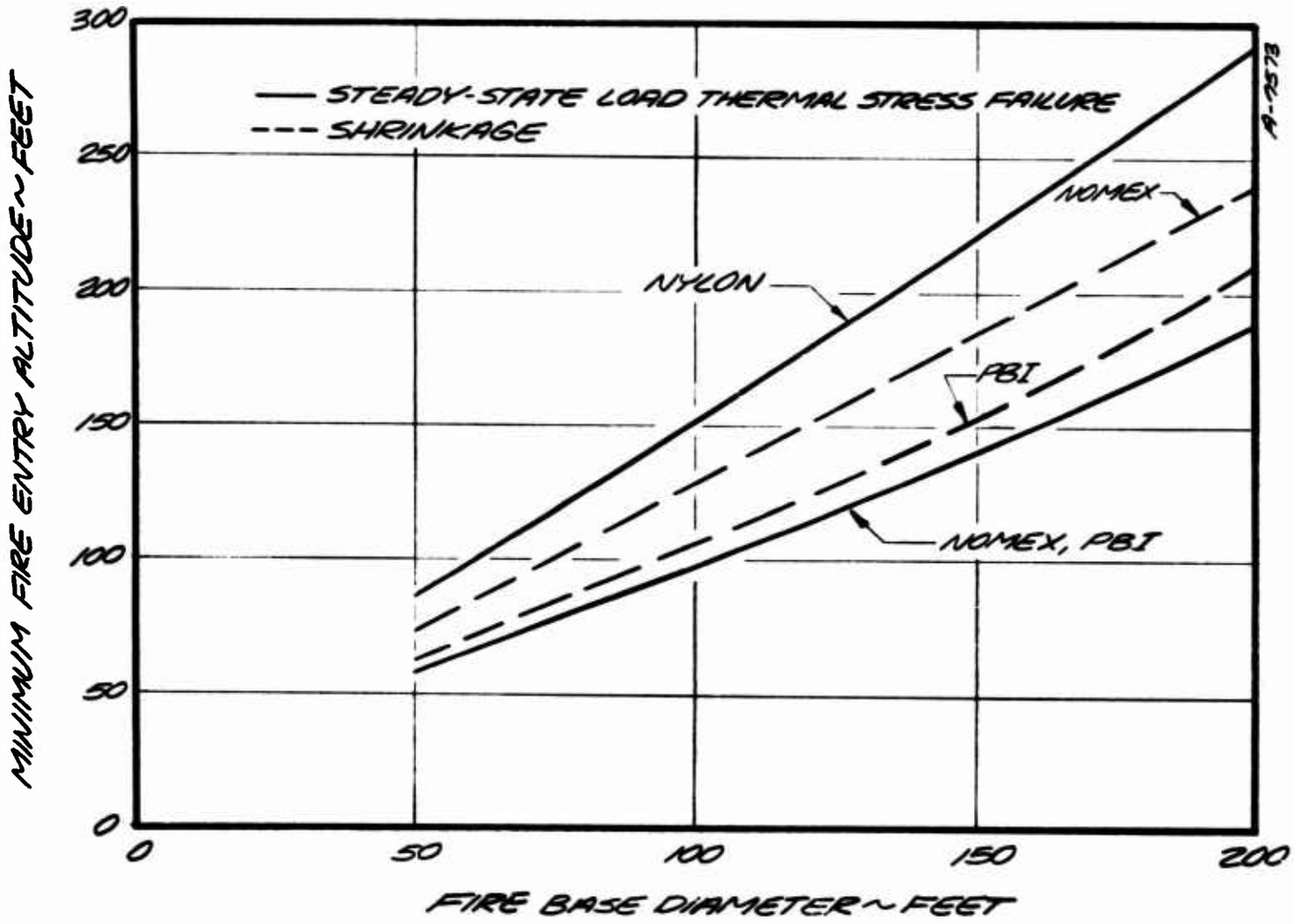

Figure 14. Minimum survival altitudes of candidate canopy fabrics for through-the-fire trajectories

The parametric analysis has identified some other important results. For C-9 canopy fabrics permeability is a critical property since the requirements result in a high blow-through convective heat transfer which dominates other modes of heat transfer. All other fabric thermal properties (specific heat, thermal conductivity, absorptance, etc.) are not critical for C-9 canopy fabrics due to the dominance of permeability and, in the more general case, the small variability of these among the candidate materials.

Strength failure of Nomex and PBI fabrics is predicted only for trajectories that pass through the fire whereas strength failure of Nylon canopy fabrics can occur for windless descent trajectories within one fire base radius of the periphery of large fires.

For through-the-fire trajectories the canopy fabric achieves its maximum temperature within approximately one second. Since the thermal time constant is so short, the maximum fabric temperature, and thus the various temperature-dependent failure mechanisms, can be directly related to the fire temperature at entry. Therefore, the vertical temperature profile of the fire is of primary importance in determining altitude thresholds of failure for candidate materials. The effects of fire diameter and wind velocity are only significant in so far as they influence the altitude at which the parachute enters the fire and the local gas temperature at that altitude. Their effects upon fabric thermal response is second-order.

It is important to note that, for conditions where the strength failure criterion is just exceeded, the combination of temperature and the time at this maximum temperature is such that no fabric decomposition is predicted.

The results of this study have identified three critical parameters affecting the survivability of C-9 parachutes; the temperature dependence of possible failure mechanisms, the blow-through convective heat transfer arising from the high permeability specification for Type I fabrics, and the vertical temperature profile in the fire plume. The uncertainties associated with the assumed failure criteria are significant. The use of steady-state tensile data to establish the strength failure criterion may be too conservative for the dynamic encounters under consideration. Similarly, it is known that the forms of Nomex and PBI under consideration exhibit significant shrinkage (30 to 40 percent) within a small temperature range. Shrinkage of canopy fabrics of this magnitude will result in degraded aerodynamic performance. However, there is some uncertainty as to how the effects of shrinkage relate to failure. These uncertainties can have a significant effect on the altitude of threshold failure.

In addition, no data exist to verify the fire model presented in this study. Due to the criticality of the fire temperature profile, this uncertainty relates directly to fabric survivability. Finally, this study, was limited to the C-9 parachute and three candidate materials, Nylon, Nomex, and PBI. The permeability of the Type I fabric used for the C-9 is a specification. However, the limitation imposed on this study on configuration, materials, and the use of worst case conditions restricts the applicability of the results. The ultimate improvements in the thermal survivability of personnel parachutes can be evaluated fully only by expanding the scope of considerations and decreasing the uncertainties by obtaining additional data.

SECTION 5

LABORATORY TEST APPARATUS FEASIBILITY STUDY

A systematic development program to improve the resistance of parachute canopy fabrics to fire exposure requires environmental testing of candidate fabric designs at various stages in the development. The scale, and cost, of testing would be expected to increase as the development progresses toward a final design. A reasonable approach to thermal testing would involve two stages: small scale laboratory testing and "full scale" testing similar to fire-pit tests. Laboratory testing would evaluate fabric samples under closely controlled conditions simulating the fire environment with one or a combination of heating sources. Full scale testing would evaluate a complete parachute, scaled down in size for better control, exposed to an actual fire.

A preliminary design study has been performed on the laboratory scale test apparatus. The purpose of the study was the following:

- Identify the parameters to be simulated
- Assess the feasibility of simulating and measuring the critical parameters and identify trade-offs to be considered
- Evaluate the major trade-offs
- Design the test apparatus, in a preliminary manner

The following sections will consider the preceding tasks in the order given.

5.1 APPARATUS REQUIREMENTS

5.1.1 Apparatus Function

The purpose of the parachute fabric fire simulation laboratory test apparatus is to 1) screen candidate parachute canopy fabrics, and 2) advance the state of knowledge concerning the basic mechanisms involved in parachute thermal failure. As a secondary requirement the apparatus should provide enough flexibility to be used with modification for flight suit thermal testing.

5.1.2 Parameters to be Simulated

In low level aircraft crashes, if the ejected personnel and their parachutes are exposed to the high temperature crash fire environment, the following conditions will exist:

1. The parachute descends at a steady rate of approximately 19 ft/sec, relative to the surrounding air or hot gas.
2. The heating rates to the fabric change with time as the chute descends toward higher temperatures and as the horizontal distance between chute and the hot environment changes.
3. The heating mechanisms which could destroy the chute with simultaneous nonfatal burn injury to personnel are: a) radiation to one or both sides of the fabric, primarily from the hot gas plume and secondarily from the more distant combustion zone of the fire, and b) convection due primarily to hot gas blown through the fabric while in the plume and secondarily to hot gas blown by.
4. Hot gas and radiation temperatures (since the gas can be considered a blackbody) in the combustion zone are 2100°F to 2500°F (1149°C to 1371°C). In the plume, temperatures decrease rapidly with increasing altitude, in the manner shown in Figures 7, 8, and 9.
5. Durations of exposure to significant heat flux levels are less than ten seconds.

A discussion follows of the preceding environmental conditions as applied in the test apparatus, giving consideration to the relative importance of the parameters and the feasibility of achieving them in testing.

5.1.3 Feasibility Considerations

5.1.3.1 Heating Modes

Proper simulation of the parachute fabric heating environment requires both radiation and convection. Radiation, ideally, will be imposed from both sides of the sample although it is acceptable and certainly much simpler to irradiate one side only. Due to the problem of reflected energy, pyrometric measurement of fabric temperature is not feasible from the irradiated side. The dominant convection mode results from hot gas passing up through the parachute canopy. Associated with this and less important is blow-by on the under surface of the canopy. Also of small influence is blow-by on the upper surface. Due to the

importance of blow-through, both in heating (or cooling the fabric) and in removal of products of decomposition, the test apparatus will simulate the impact of hot gas on the fabric from one direction, as in descent. Blow-by on that surface is simultaneously created. Simulation of blow-by on the opposite surface is not warranted.

5.1.3.2 Heating Profile

It became immediately evident in the study that simulation of the actual descent history of the parachute would not be practical mainly because of the rapid variation in heating rates and the difficulty in reproducing the same heating profile in multiple test runs. In addition, it is somewhat artificial to select one transient heating profile over the multitude of possibilities. Steady state heating at a predetermined level will be much less complex and more repeatable for screening-type tests. This applies to both radiant flux and hot gas temperature and velocity. Convection due to blow-through depends, of course, on the permeability of the test sample, which may change due to shrinkage in a test just as in reality.

The requirement for short, repeatable test durations indicates that a shutter system is required to provide essentially a square-pulse of radiant energy of predetermined duration. Water-cooling of the shutter is required. Opening and closing times on the order of 100 milliseconds should be achievable with air cylinder actuation. In the preliminary design discussion, it will be shown that the application of gas to the fabric simultaneously with the application of radiant energy may be achieved by means of either a shutter or an automatic valve. The shutter approach presents technical problems because it must include a gas-tight seal. As an off-the-shelf item, a gas-tight valve is more readily achievable. If the valve is located close to the gas inlet to the test chamber, the feed duct fill time and heat soak can be designed to be small.

5.1.3.3 Fire/Parachute Geometry

Although transient descent will not be attempted, apparatus versatility is increased by simulating in different tests, different view factors from the parachute to the hot gas. This may be done by dividing the radiant heat source into separately controlled zones. However it is necessary to water-cool the passive zones to prevent reradiation. Similarly the impinging gas temperature (and velocity) will be controllable to simulate varying plume altitudes (and descent rates).

5.1.3.4 Radiation Temperature and Spectrum

It is not necessary to simulate the combustion zone temperatures predicted in Section 4 of this document. Radiation from the plume is of greater importance because the plume is encountered first and failure occurs at an altitude higher than the top of the combustion zone. In addition, updraft in the plume prevents the parachute from descending down the plume into the combustion zone. Simulation of plume temperatures that can destroy the fabric is therefore the primary criteria. A balance is achieved between feasibility and the desire for a maximum attainable effective enclosure radiation temperature at the level of 1700°F (equivalent to 10.4 Btu/ft^{2}sec heat flux incident on an enclosed surface). Present generation, and undoubtedly future generation, parachute fabrics rapidly fail in this environment. A refractory metal wall furnace can achieve 1900°F when heated by Inconel sheathed, tubular Nichrome elements welded to the wall. The effects of wall emittance, non heated regions, and a small amount of shadowing at the fabric mount serve to reduce the overall effective blackbody temperature of the furnace to about 1700°F (927°C).

Consideration was given to the possibility of achieving 2000°F (1093°C) plume temperature. Possible alternate approaches to achieve higher temperatures and heat flux levels are a graphite furnace or a quartz lamp array. Graphite elements, used in furnaces operating at 4000 - 5000°F, would add considerable expense to gain a few hundred degrees.

The quartz lamp array would efficiently elevate the heat flux. The 10 kw quartz lamp facility used at Aerotherm for flight suit material testing and other fire environment tests achieves 15 Btu/ft^{2}sec at full voltage. However, the optical response of fabrics to lamp filament temperatures of 4500°F (2482°C) proves to be significantly different from the response to fire temperatures due to the different spectral distribution of the source. Fire simulation testing with a lamp system, particularly in combined radiant/convective heating, adds a major uncertainty to the results.

Considering the alternatives, the Nichrome element radiator is expected to provide the most accuracy for the least cost.

5.1.3.5 Gas Velocity, Temperature, and Composition

Gas velocities impacting on the fabric on the order of 20 ft/sec are readily achievable. If a higher velocity is required to simulate plume entrance, this can also be done. The peak velocity requirement will be refined early in the detailed study.

In convective heating, the fabric will fail under significantly lower gas temperatures than under radiant heating. Exposure of fabric to blow-through hot gas rapidly heats the material close to recovery temperature. Consequently, the maximum achievable gas temperature can be allowed to be less than the radiant temperature in the thermal test facility. Reference to Figure 6 shows that all present generation parachute fabrics fail at 900°F or below. Therefore, a maximum gas temperature of 1100°F is sufficient for test purposes and can be achieved in a clean, efficient manner by blowing the gas through an electric circulation heater.

If higher gas temperatures are desired in future testing of next generation fabrics, a combustion unit with temperature control by air dilution may be incorporated in the apparatus.

The results of Section 4 indicate that the use of products of combustion as the test gas is not required for faithful simulation of critical parameters. Heat transfer is the primary influence of combustion gases. Chemical reaction rates between fuel combustion products and fabric are quite limited at the fabric temperatures achieved. The use of air as a test gas greatly simplifies operation.

5.1.3.6 Fabric Sample Size

The test sample size is interrelated with various factors associated with the detailed configuration of the test apparatus. Since detailed design of the facility is not a part of this study, only an approximate sample size may be defined here. Detailed considerations will include flux uniformity, tension uniformity, gas impact velocity uniformity, and fabric temperature measurement errors. Related parameters are test chamber size and electrical power requirements. At this stage, a sample size in the range of seven to ten square inches seems to be a good compromise of all factors.

5.1.3.7 Fabric Tension

The fabric sample in the test apparatus will be stressed by means of the combined effects of a preload plus gas impact. The preload serves to provide a smooth, wrinkle-free test sample and to seal off gas leakage at the sample perimeter. Gas impact results in simulation of descent loads. Reference to Figure 6 shows that parachute fabric loading in steady state descent is a small fraction of the material tensile strength over most of the useful temperature range. However at the onset of shrinkage, tensile loading becomes critical because the amount of shrinkage is influenced by the load and, in turn, shrinkage tends to alter the load by altering air permeability. Therefore it must be concluded that proper simulation of descent loading is vital.

5.1.3.8 Summary

The basic parameters to be simulated in the parachute fabric fire simulation apparatus are summarized in Table 11.

TABLE 11. TEST APPARATUS ENVIRONMENTAL CONDITIONS

Parameter	Capability
Heating Mode	Combined radiation/convection
Heating Profile	Square pulse of variable duration
Radiation Temperature and Spectrum	Variable, up to 1700°F equivalent blackbody hemispherical source (10.4 Btu/ft^{2}sec incident radiation)
Test Gas Composition, Veclocity and Temperature	Air, up to 20 ft/sec and 1100°F
Fabric Sample Size Exposed	7 to 10 square inches
Fabric Tension	Similar to descent tension

5.1.4 Parameters to be Measured

Instrumentation of the apparatus serves two functions: measurement of the environment imposed on the test material and measurement of the material response. Primary environmental conditions are radiant heat flux at the test sample, radiation source temperature, gas impact velocity, gas temperature, and exposure duration. Although blow-through convection heating cannot be measured, it might be useful to measure blow-by convection. Natural convection heating of the test sample from the radiation source will be minimized in chamber design and a measurement of this heating mode in initial checkout, at least, would be useful to verify adequacy of design.

Since fabric response is difficult to quantify, post-test inspection will be a primary indicator of degradation. Observation of the sample under exposure can be provided for by means of an observation port and a port for a high speed movie camera. Besides providing a permanent record, the film will allow detailed inspection of the failure mechanisms. Measurement of the fabric temperature history is highly useful data when comparing fabric responses. A pyrometric technique previously used by Aerotherm in fabric research (Reference 5) is applicable in the parachute fire simulation apparatus. However the application in the apparatus considered here is more difficult because the heating source, as well as the test sample, will be emitting primarily in the infrared.

On preliminary examination, the accurate measurement of fabric tension history does not appear necessary or feasible. As was noted in Section 5.1.3, calculations show that tensile loading in steady descent does not approach fabric tensile limits until just prior to thermal failure. Therefore, tensile failure will be an abrupt occurrence and will coincide very closely with observable responses such as shrinkage, discoloration, and melting or charring.

Looking at feasibility, the proposed testing technique will expose only a portion of the fabric sample to heating and therefore the tensile load imposed by the holding fixture is partially supported by undegraded material. As a result, changes in loading in the exposed region due to gas impact, shrinkage, or elongation are not easily discernable.

The preliminary design proposes to impose a static preload in the fabric by means of a simple pulley/weight system. Dynamic effects resulting from exposure of the sample to the environment will alter the loading condition somewhat. Further investigation in the detailed design will evaluate dynamic and mounting effects and modify the design if necessary.

In summary, Table 12 identifies the quantities to be measured in the parachute fire simulation apparatus and the proposed measuring devices.

TABLE 12. TEST APPARATUS INSTRUMENTATION

Parameter	Measuring Device
Radiant heat flux	Radiometer
Radiator temperature	Thermocouples
Blow-by convective heat flux	Calorimeter
Gas total and static pressures	Pitot probe
Gas temperature	Thermocouple
Fabric response history	High speed motion picture camera
Fabric temperature history	Pyrometer
Fabric static loading	Counter weights

5.2 APPARATUS PRELIMINARY DESIGN

An overall elevation view of the parachute fabric test apparatus preliminary design is shown in Figure 15. To identify scale, the inside diameter of the test chamber, on the left side of the figure, is approximately 1 foot. So, not including a control panel and the power supply equipment, which are not shown, the laboratory floor area required is roughly 10 square feet.

The most critical component in the system is the test chamber. In support of the test chamber are the instrumentation, the air handling equipment, the controls, and power, water and compressed air supplies. The following discussion will consider each of the above subsystems. It should be emphasized that because the design is preliminary, it is subject to possible changes in a detailed design. It is expected that those changes would not influence the basic concepts.

5.2.1 Test Chamber

The test chamber consists of an insulated enclosure in which the fabric sample is exposed to the heating environment for a controlled duration. Two views of the test chamber are seen in Figures 16 and 17. Included in the chamber system are the following components:

- Electric radiant heating panels
- Water-cooled cold plates
- Water-cooled pneumatic-actuated shutter
- Fabric support and tension system
- Hot gas supply and exhaust ports
- Chamber ports for observation
- Chamber access system
- Insulation

Prior to consideration of each component, it is worthwhile to examine the basic reasons supporting the selected chamber arrangement.

5.2.1.1 Chamber Configuration Trade-Offs

Various alternate configurations were considered for the relative arrangement of the radiant/convective heating modes. A cylindrical test chamber was selected primarily to make the most efficient use of the radiant heating surfaces. At the designed radiant panel temperatures, convection heat transfer is roughly equivalent to radiation. So the radiant panels must be located above

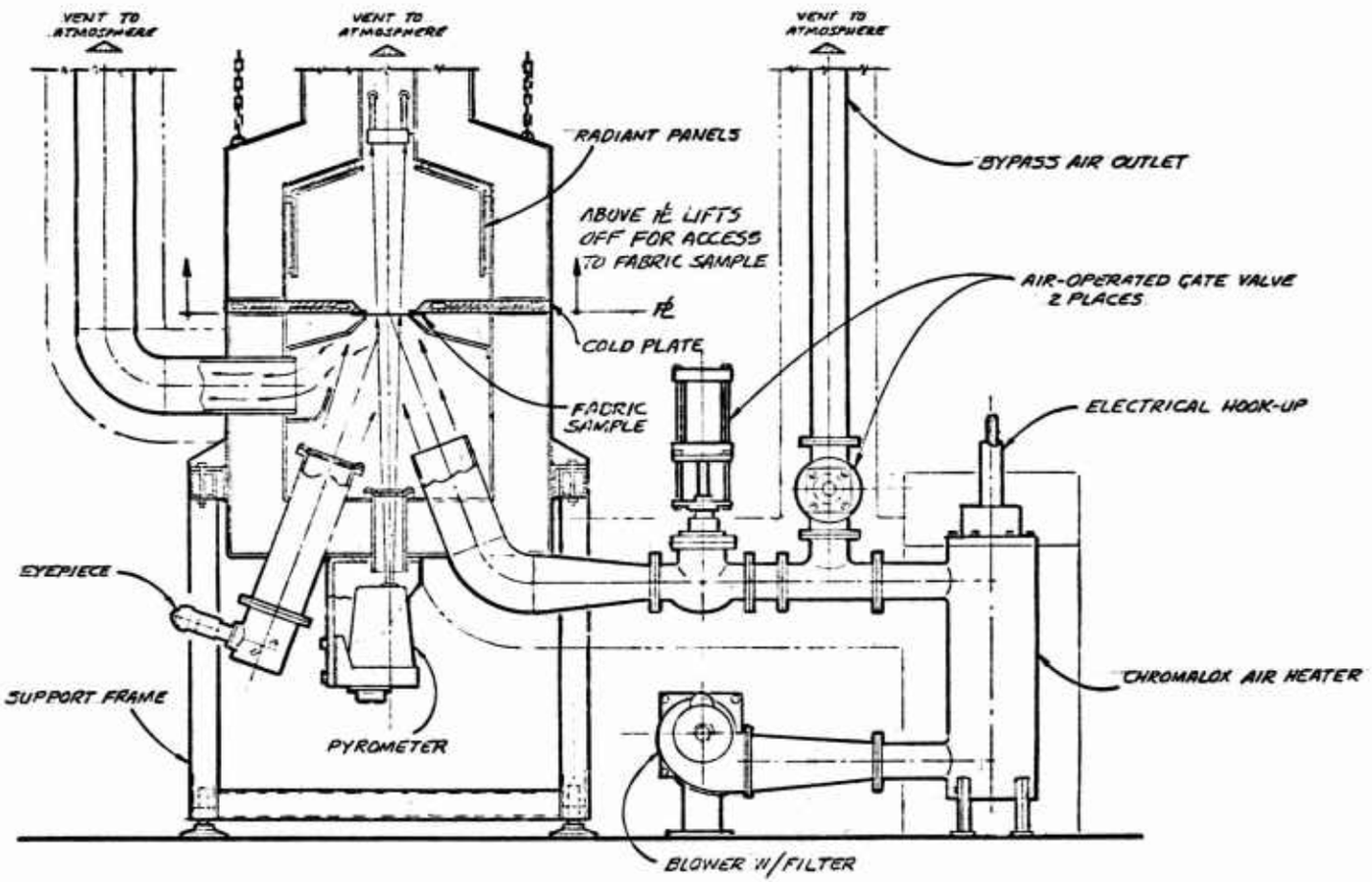

ELEVATION & SECTION AT Y-Y AXIS

Figure 15. Parachute fabric fire simulation laboratory test apparatus.

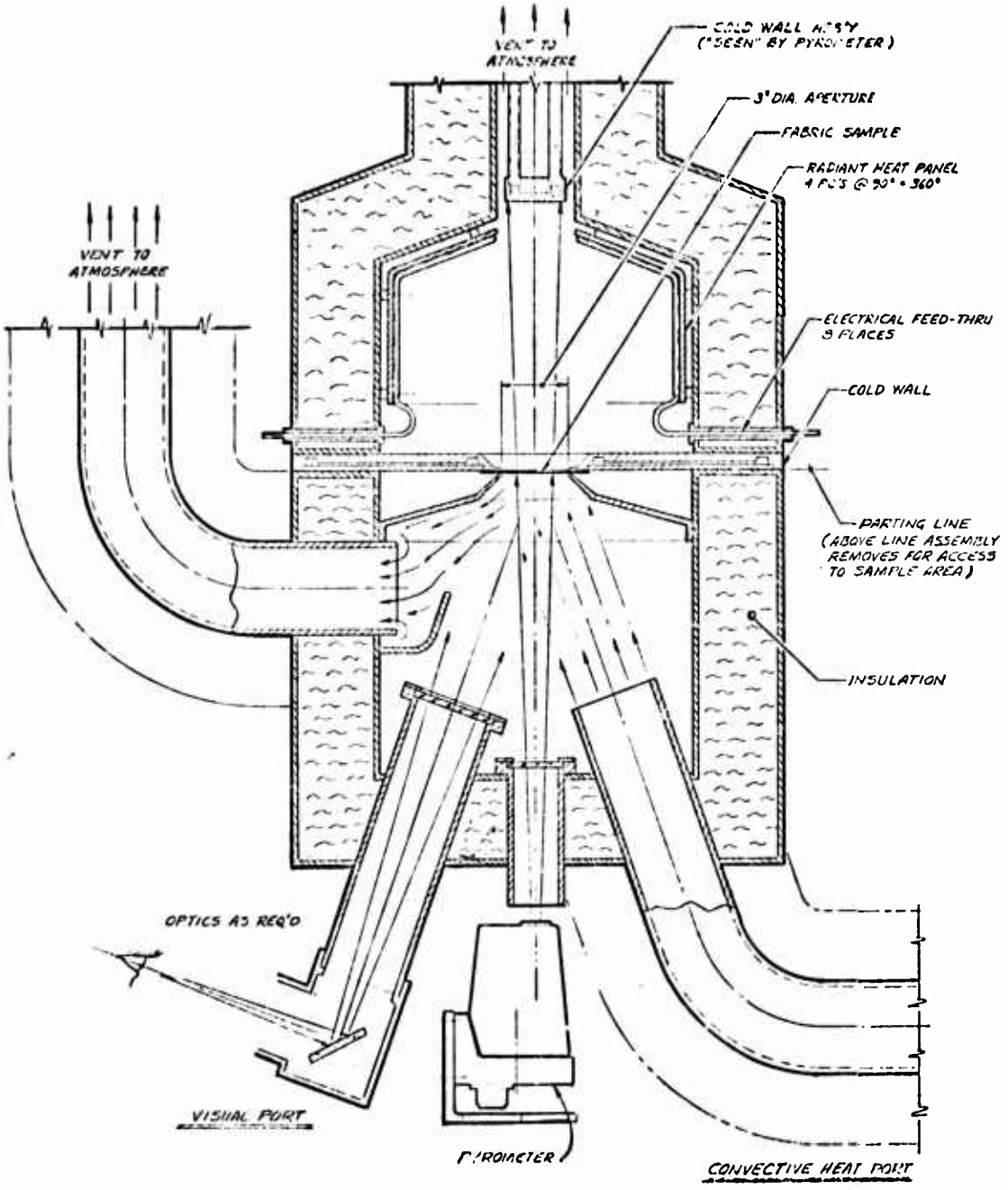

Figure 16. Test chamber, section at Y-Y axis.

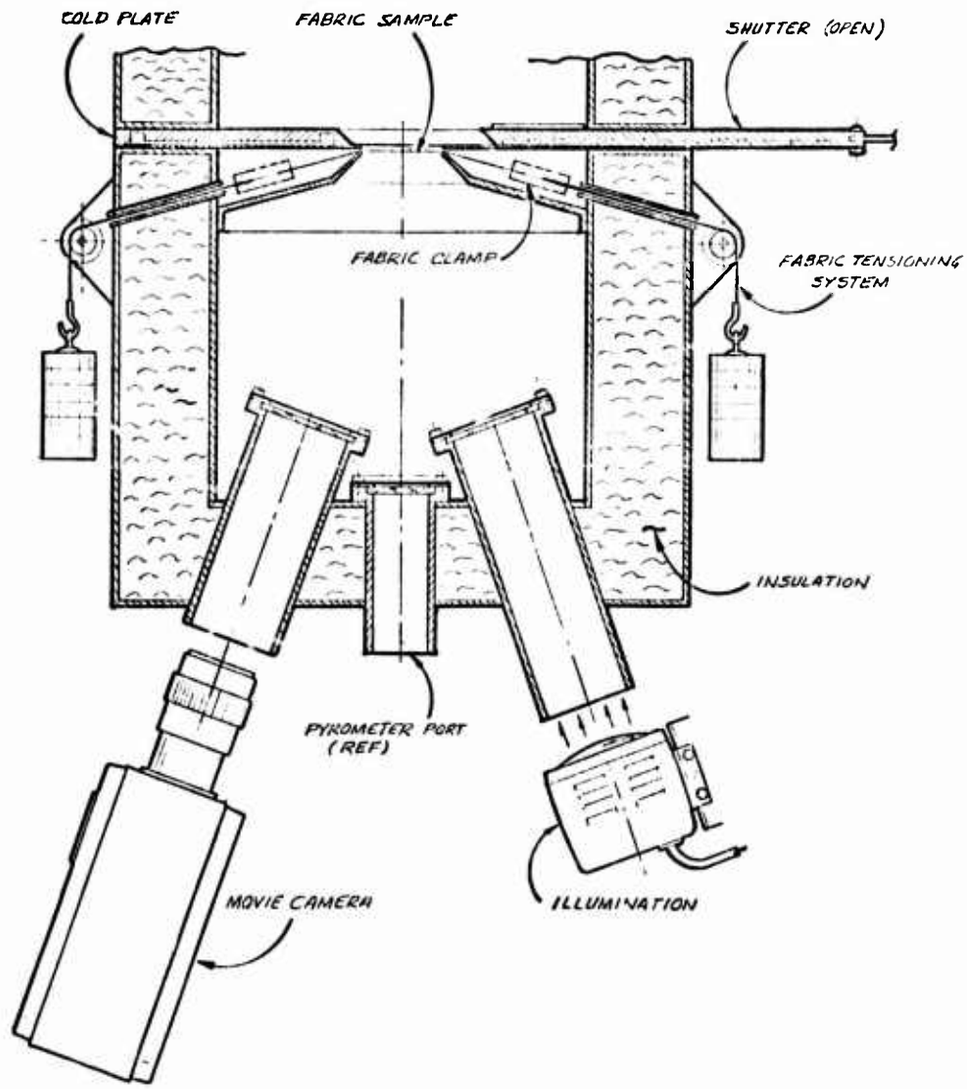

Figure 17. Test chamber, section at X-X axis.

the test sample to minimize the influence of natural convection from the panels. This is a strong argument against attempting to radiatively heat from both sides of the fabric. In addition, spacing the radiant panels further from the sample (resulting in a larger chamber and greater electrical power) reduces the chance for unwanted convection from the panels. The chamber size trade-off requires further study in the detailed design.

Control of the hot gas activation is a major factor in chamber design. If a gas-tight shutter were feasible, then the heated gas could be introduced above the fabric and a single shutter would control both heating modes. Steady state gas flow would be established prior to exposing the fabric with a bypass either internal or external to the chamber. However the drawbacks in this system include not only the shutter technical problem but also panel radiation blockage by the gas duct and the possible need for a high temperature induced draft fan to draw the gas out the chamber bottom.

Another concept, and the selected one, involves injection of hot gas from below, eliminating the radiation blockage and the extra fan problems. However gas activation must be controlled accurately and since the sealed shutter is difficult, the valving technique was selected. At an exit velocity of 20 ft/sec, gas flow in a two foot long duct between the activation valve and the chamber inlet will become established on the same time scale as the radiant shutter opening time. Another concern is gas temperature drop and recovery time if hot gas is introduced into a cold duct. Calculation for a thin walled duct two feet long with complete mixing shows that the gas temperature will drop less than 100°F and will recover in about 0.25 seconds. With a large enough duct, gas temperature in the core region, impinging on the fabric, should not be influenced by cooling at the edge of the stream. Further investigation is warranted here. Possible determination that gas activation transients are unacceptable leads to a potential alternate design which incorporates two shutters, above and below the fabric. The lower one may not have to be water-cooled. The shutters would be synchronized to open slightly later than gas valve activation. The low shutter would provide a "gas-tight" seal.

5.2.1.2 Radiant Panels

The radiant panels consist of four Inconel or stainless steel plates to which are welded Inconel-sheathed resistance elements as shown in Figure 18. The plates are replaceable in case one fails. Electrical power to the panels will be controlled by one or more manual auto-transformers. If the panels were individually controlled, any combination could be operated to simulate a reduced view factor from the fabric to the high temperature source. However the passive panels would heat and reradiate at an intermediate temperature between the

NOTE : 4 PANELS COMPRISE A SET

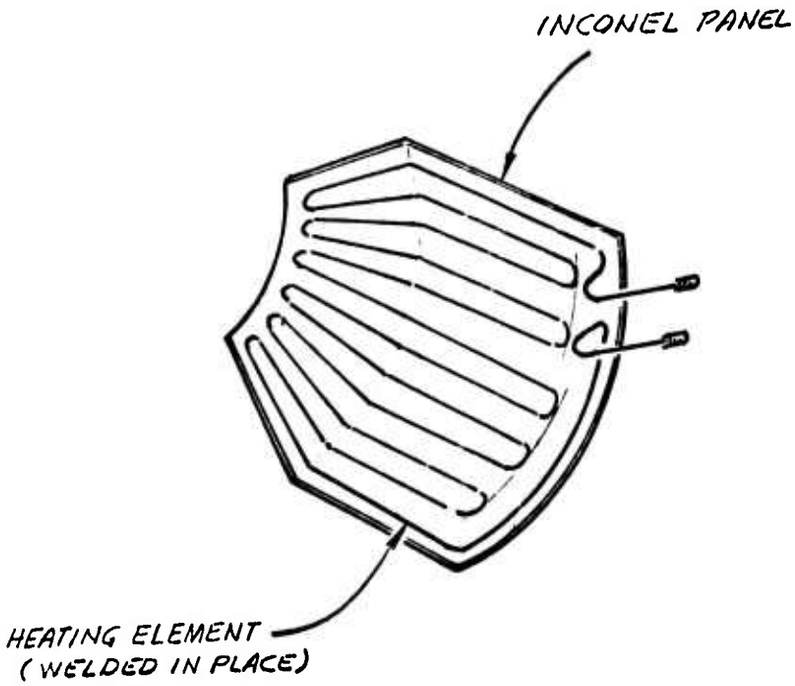

Figure 18. Radiant heating panel.

radiant source and the cold plate. Thus no obvious benefit is achieved by heating individual panels unless water cooling is provided for the passive panels. The water passages which could be attached to the rear of the radiant panel, would be drained when not in use. This technique should be examined in the detailed design.

Optical data on Inconel shows that oxidation at high temperature produces an emittance at 2000°F that exceeds 0.8, resulting in an efficient emitter. Since the heater element sheath has an upper temperature limit of 2000°F, the panel design will be based on a drop of 100°F from sheath to average panel temperature, resulting in a 1900°F panel temperature, at full power.

The maximum power requirement for the radiator panels, combined, is 10 - 20 kw, depending on chamber size. Initial calibration of the auto transformer settings to heat flux and panel temperature will allow simple set point adjustment in subsequent runs.

5.2.1.3 Cold Plates

The test chamber will have three separate water-cooled plates, one of which is the radiant shutter. The cold plate at the chamber midsection serves to 1) provide a radiant aperture for fabric exposure, 2) protect the instruments and chamber below from the radiant source, 3) provide a guideway for the shutter and 4) supply a heat sink for rapid cool-down of the test chamber. The preliminary concept of the midsection cold plate appears in Figure 19. Since the plate is cooled at all times, aluminum is a potential material. Aluminum can achieve a low absorptance when kept clean and has the desired high thermal conductivity. Calculation of the water cooling capacity indicates that a 12 inch diameter plate will absorb roughly 3 kw at peak chamber temperature. Translated into water flow rate this amounts to 0.3 gpm with a 50°F temperature rise. The velocity in a passage equivalent to 1/4 inch diameter is 2.6 ft/sec.

A second cold plate is located at the top of the chamber and is used to provide a cold background against which the pyrometer can measure fabric temperature. Since the pyrometer operates around 11 microns wavelength and optical data collected on flight suit fabrics (much thicker than parachute canopy material) indicates very little transmission beyond 6 microns (Reference 5), the cold plate background may be unnecessary. It is included here for completeness.

5.2.1.4 Shutter

The water-cooled radiant shutter is depicted in Figure 20. The supply and return water tubes are external to the test chamber at all times, simplifying

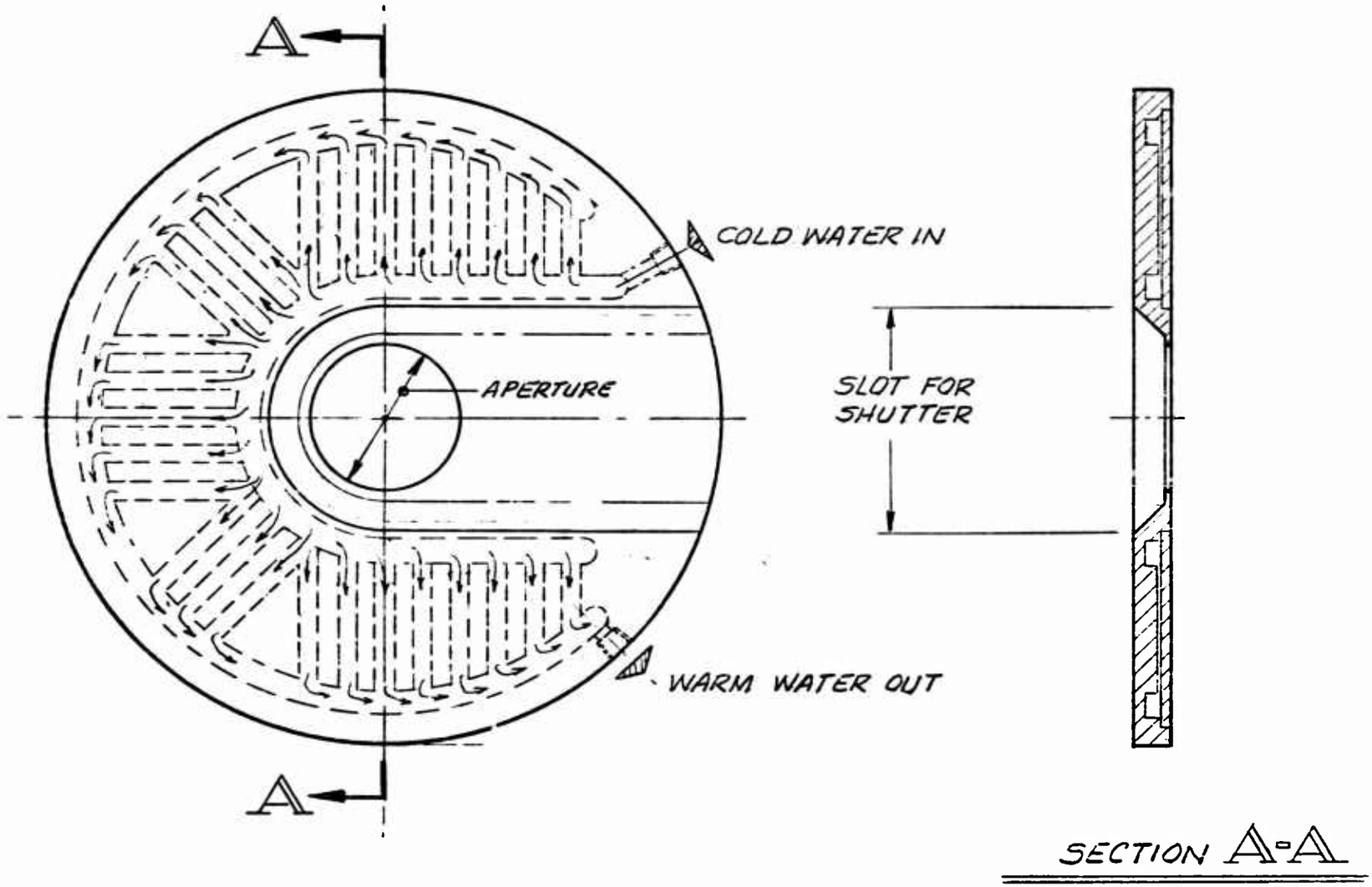

Figure 19. Cold plate.

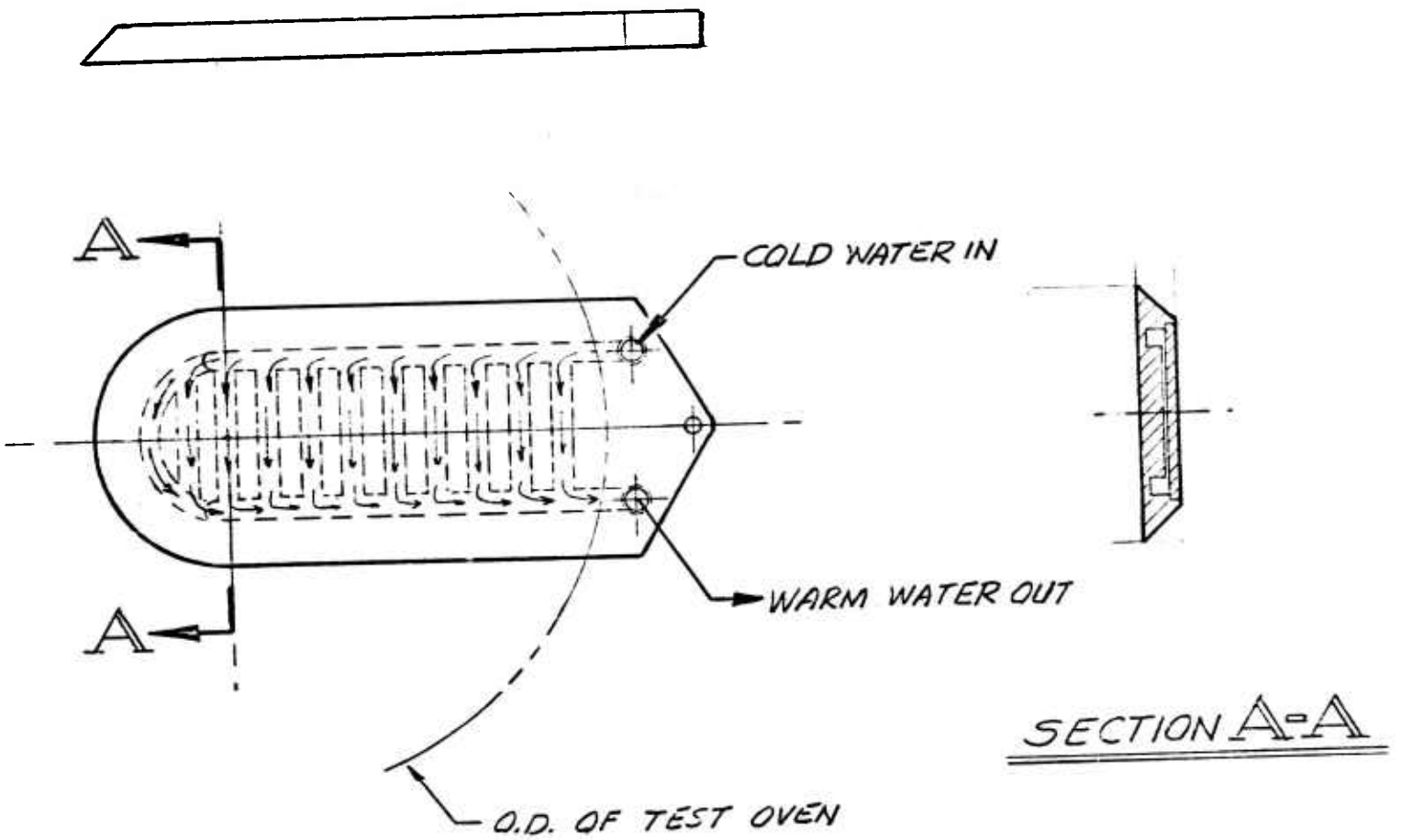

Figure 20. Water-cooled shutter.

the connection. The shutter is activated by a double-acting air cylinder. The laboratory compressed air supply to the piston is controlled by solenoid valves activated by a switch and an electric timer. Shutter opening would be activated by the test operator using the switch. Shutter closing would be automatic, as preset on the timer.

5.2.1.5 Fabric Sample Support Assembly

Experience with the Aerotherm 10 kw radiant lamp test facility has shown that, if the fabric is preloaded on only one axis, an aperture is required to expose only a portion of the fabric sample. If this were not done, the unsupported edges would curl as the fabric shrinks and the heating would become very nonuniform over the sample. The concept of the parachute fabric test apparatus therefore employs tension in one axis with an aperture. The alternate approach of providing tension in multiple axes runs into trouble when the fabric begins to shrink, drawing the fabric clamps inward to possibly bind against each other.

The fabric in the clamp system is shown in Figure 21. Detail of a proposed concept of the clamp is given in Figure 22. The fabric is pinned to a clamp at each end of the sample, which may be 5 inches wide by 6 to 8 inches long (the exposed area is a 3 inch diameter spot at the center). The clamps are attached on a bench and the assembly is then installed in the chamber by hooking to the tensioning cables which connect to weights on pulleys outside the chamber. The total system is seen in Figure 17. Pretension in the fabric is similar to parachute descent loading, which is calculated to be about 0.75 lb/inch at 20 ft/sec descent rate.

The fabric is drawn over what amounts to a hot gas aperture, a smooth-edged opening, the same diameter as the radiant aperture above. This aperture is necessary because the hot gas, if allowed to heat the fabric edges that are not supported, will cause them to curl. The aperture approach is presently untested and some bench experiments are required in the detailed effort to verify it.

As hot gas strikes the fabric the exposed region will bow upward, tending to lift off the aperture. Pretension must be enough to just prevent lift-off because the gas will then blow to the edges, causing curl. It should be noted that in this dynamic situation the tension in the fabric is essentially the same as the static mode, as is desired.

5.2.1.6 Hot Gas Supply and Exhaust

Referring back to Figures 15 and 16, the hot gas is directed at the test sample at a nearly normal angle. The inlet duct is larger than the test aperture

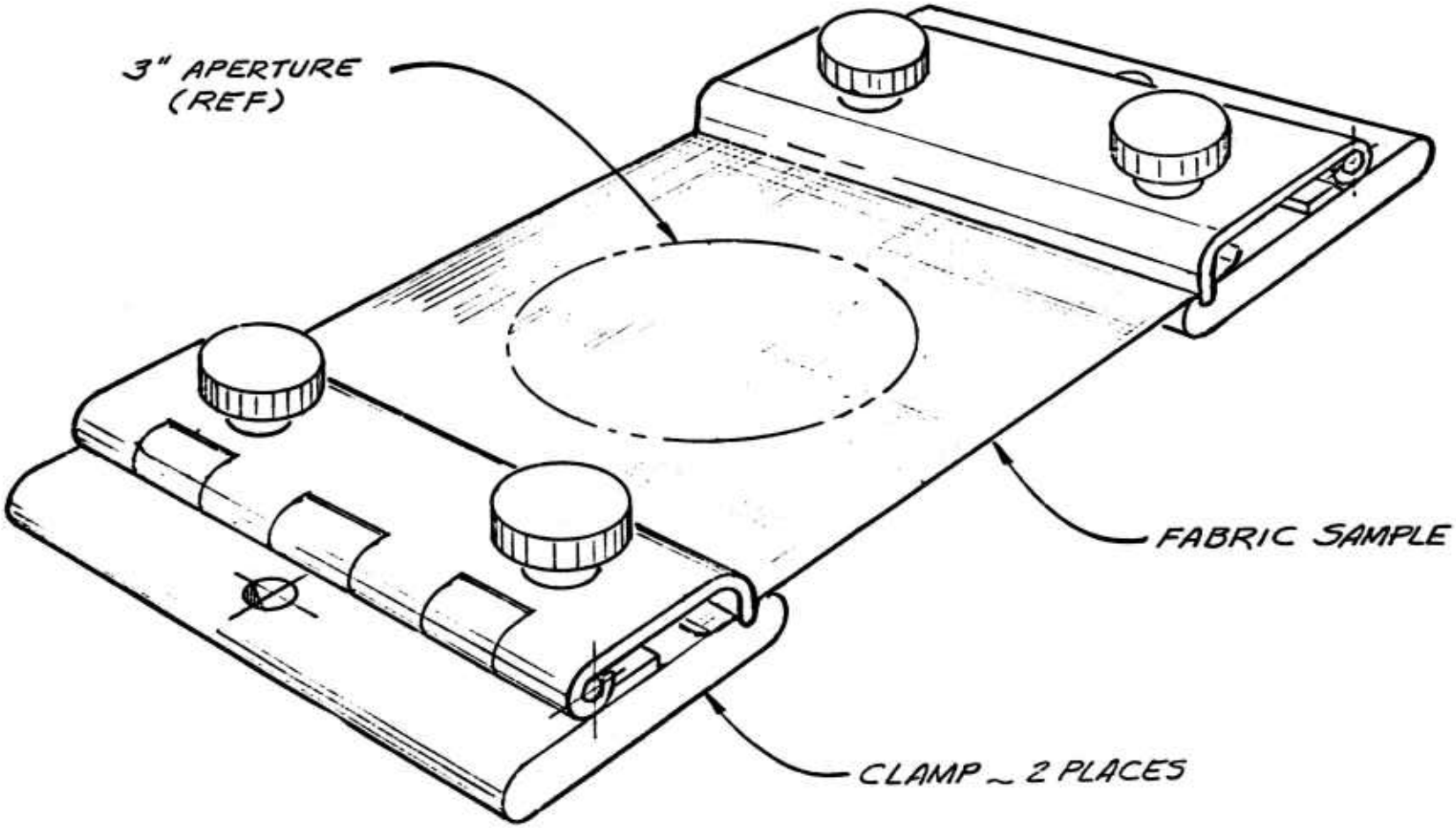

Figure 21. Fabric and clamp assembly.

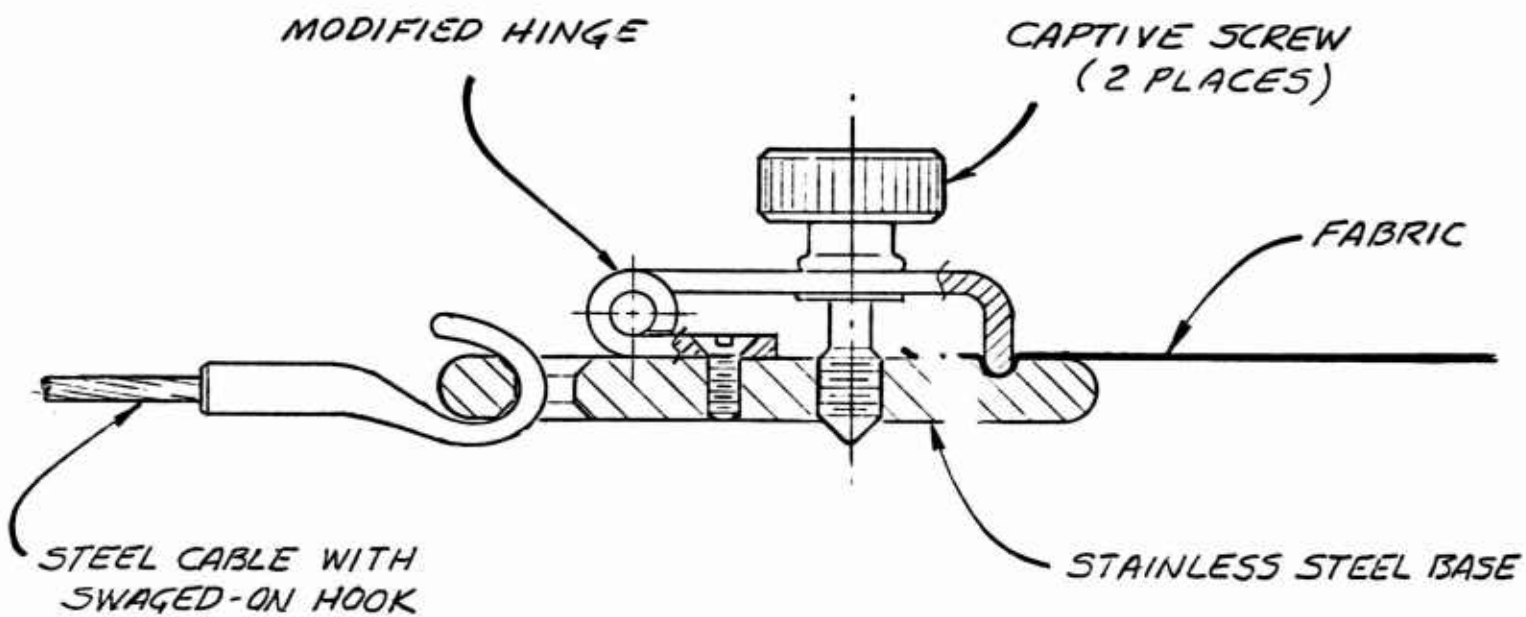

Figure 22. Fabric clamp.

to ensure uniform blowing through the fabric. Spill-over is vented out a duct on the side of the chamber. An exhaust duct is also provided at the top of the chamber. To minimize radiation from the hot supply duct to the fabric and also allow unobstructed views with the optical instrumentation, the duct must be offset below the sample by 8 to 12 inches.

5.2.1.7 Chamber Ports

Besides the hot gas opening, the bottom of the test chamber is penetrated by four ports. These ports provide access for 1) visual observation of the test, 2) pyrometer operation for fabric temperature measurement, 3) camera operation, and 4) illumination for the observer and the camera. Windows are necessary on the ports to prevent escape of hot gas. The pyrometer window must be an infrared window at 11 microns, such as Irtran-2.

5.2.1.8 Insulation

High temperature insulation is required to enclose the test chamber and the ducting to prevent injury to personnel, and damage to instrumentation as well as to reduce power requirements.

The insulation thickness requirement was calculated for the chamber upper section using an aluminum silicate fibrous insulation such as Johns-Manville Cerafelt (Figure 23). The calculation was made for a 12 inch cylindrical enclosure. A larger diameter will require more insulation for the same exterior temperature. A trade-off is required here to determine the optimum choice between an unwieldy design and a safe surface temperature. It is possible that a guard screen could be stood-off from the insulation on the upper segment to augment an insulation thickness of 4 inches. The problem is not nearly as severe in the bottom segment of the chamber because temperatures are lower and gas flow is intermittant.

5.2.1.9 Chamber Access

Access to the midsection cold plate between tests is achived by unclamping the two sections and lifting the upper section on a pully system. Technician contact with the hot upper section is not necessary, so multiple tests could be run without cool-down delays.

5.2.2 Instrumentation

The instrumentation requirements are summarized in Section 5.1.4. All items are essentially off the shelf. Of particular note is the pyrometer proposed which is the Barnes Thermalmaster IT4-A or IT4-B with a 2° field of view

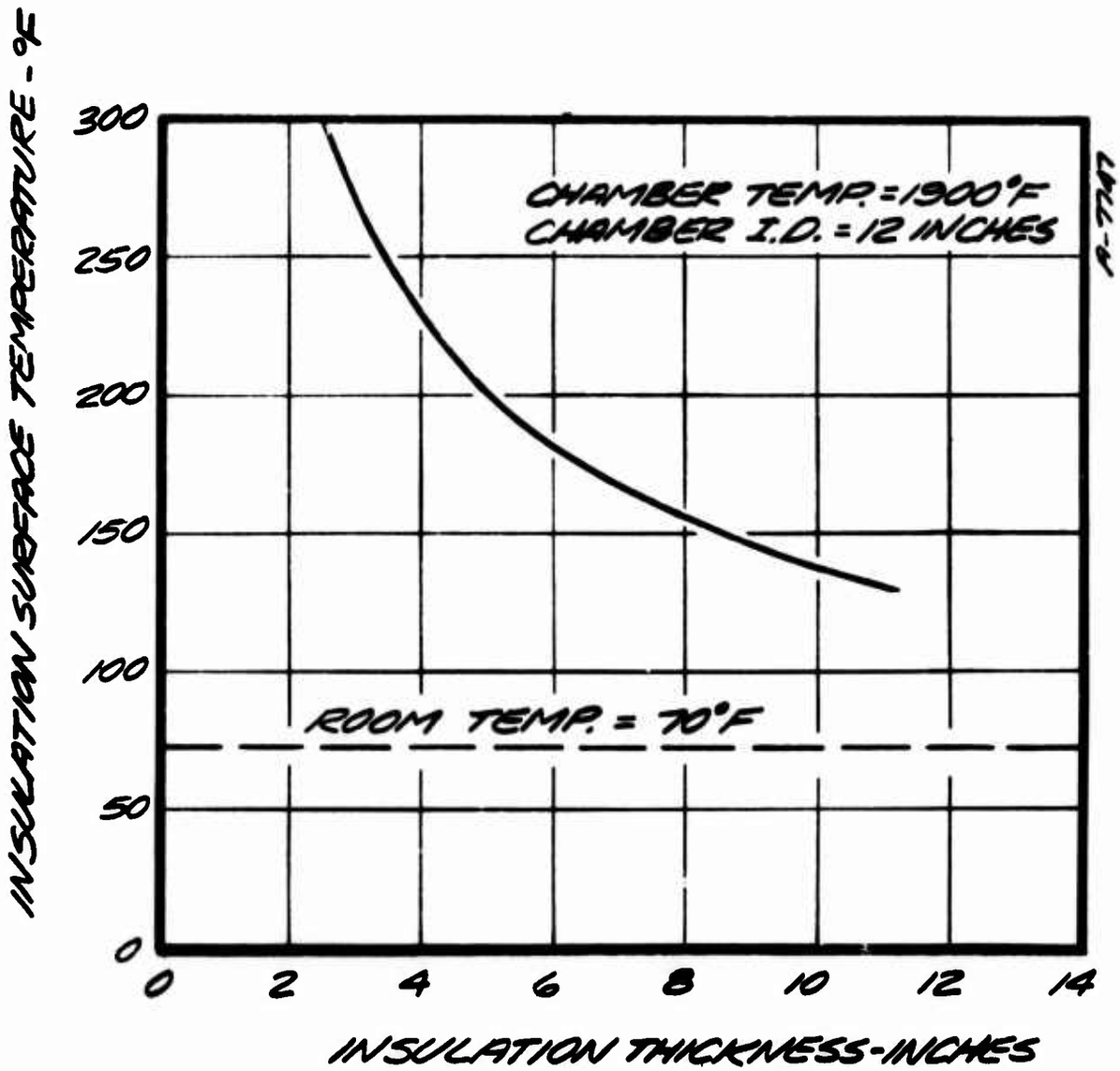

Figure 23. Test chamber insulation requirement in the high temperature region

lens. Both models are centered on 11 microns; the IT4-A has a band width of 55 percent while the IT4-B has a band width of 20 percent. The latter model may be more adaptable to available port window materials. Calibration of the pyrometer viewing a blackbody source through the window will be necessary.

5.2.3 Air Handling System

Figure 15, the elevation view of the test apparatus, shows the air handling equipment consisting of a blower, an electric circulation heater, two air-operated gate valves and connecting ducting, all operating at near-ambient pressure. Insulation on the ducting and heater is important to minimize energy losses. The specified 1100°F maximum test gas temperature is operating the heater right at its upper limit. In typical operation, the air handling system will be activated prior to the test run with the bypass valve open and the valve to the test chamber closed. The blower speed will be manually controlled by using an orifice meter in the ducting. The heater will heat the air to specified set point as determined by a downstream thermocouple. An SCR controller on the heater would be a worthwhile investment to simplify control. When set point is achieved and the test chamber is ready, the operator will activate the shutter "open" switch which also operates the air system valves, opening to the test chamber and closing the bypass. The reverse happens simultaneously with shutter closing. It may be necessary to immediately purge the test chamber with room air to prevent residual heating of the test sample.

The power requirement for the air heater is approximately 1.5 kw.

5.2.4 Controls

The control panel for the parachute fabric test apparatus will include the following items:

1. Radiant panel on-off switches
2. Radiant panel auto transformer manual controls
3. Radiant panel voltmeters
4. Radiant panel thermocouple meters
5. Heat flux radiometer meter
6. Blower on-off switch
7. Blower speed control
8. Orifice Δp meter
9. Air heater on-off switch

10. Air heater SCR controller

11. Air heater outlet temperature meter

12. Cooling water flow meters

13. Cold plate water inlet/outlet temperature meters

14. Shutter open switch

15. Shutter timer dial

16. Air valve position indicator lights

Transient test data that must be recorded through the exposure are the following:

1. Gas pitot pressures

2. Gas temperature

3. Pyrometer signal

4. Blow-by calorimeter

A strip chart recorder or oscillograph will be necessary to record the transient data.

The high speed camera will probably be operated off the shutter open-close signals.

5.2.5 Utilities

The heaters will require 110 volt or 220 volt AC power. City water will be required. Water flow is low enough to not warrant recirculation. Laboratory air at 100 psi is required for valve and shutter actuation.

5.3 APPLICATION TO FLIGHT SUIT TESTING

The primary purpose of the test apparatus is for testing of parachute fabrics. As a secondary purpose the apparatus should be flexible enough to be used with modification for flight suit testing in simulated JP-4 fuel fire conditions. The intent is to simulate the fire blackbody radiant temperature as well as gas blow-through on a fabric sample mounted on a simulated arm.

A major difficulty in converting the apparatus to the flight suit tests defined is that the facility imposes radiation energy and convection gas from opposite sides of the sample. This restriction is imposed for specific reasons, namely that the radiant source must be above the test sample due to natural convection, that the hot gas should pass upward, and that the gas duct should not interfere with the radiant panels.

With no alterations, the facility may be used in radiant-only testing of flight suit materials. It may also be used, without the simulated arm, at very low blow-through velocities based on calculated predictions or measurements in other types of tests.

To impose radiant energy and gas from the same side of the fabric requires a reconfiguration of the test apparatus, introducing the gas in the chamber upper section.

The simulated arm (actually a half shell of an arm) would replace the aperture in the present design. Gas would therefore not gain access to the chamber lower section and must be vented from the upper section. A new upper section would be built to replace the presently proposed one and gas ducting would be valved into existing ducting.

An interesting feature of the flight suit testing configuration is that pyrometric temperature measurements could be made of the fabric with the pyrometer in its present location. An infrared window would be installed in the simulated arm so that the fabric is visible to the pyrometer.

The change-over would not be simple but presently appears feasible.

SECTION 6

CONCLUSIONS AND RECOMMENDATIONS

The analysis effort performed has considered in detail the thermal response of personnel parachute components when exposed to the thermal environment from aircraft crash fires. The development of an integrated analysis capability, which contains new analytical models for large aircraft fires, parachute descent trajectories, and fabric thermal response, has resulted in the identification of those parameters that are critical to parachute survivability in these severe thermal environments.

6.1 CONCLUSIONS

The results of this study have led to the following important conclusions:

- The canopy fabric is the most critical component in the parachute system due to its very low thermal capacity (thin and lightweight) and its high permeability.
- The three most critical parameters identified are the vertical temperature profile in the fire plume, the temperature dependence of possible failure mechanisms, and the high permeability requirements for canopy fabrics.
- Permeability is a key property since the C-9 requirement results in a high blow-through convective heat transfer which dominates other modes of heat transfer.
- All other fabric thermal properties (specific heat, thermal conductivity, etc.) are not critical for C-9 canopy fabrics due to 1) the dominance of permeability, and 2) the small variability of these properties among the candidate materials. Optical properties, which are not critical for the C-9 canopy fabrics, might be significant for other configurations.

- The vertical temperature profile in the fire is of primary importance in determining the altitude of threshold failure due to the small thermal time constant of canopy materials. In this study the plume model was developed analytically from physical principles and assumptions. No data were found to verify this model.
- Three possible failure modes were considered: excessive shrinkage, loss of mechanical strength, and burning. No established failure criteria exist for any of these modes. For the purposes of this study the temperature range and amount of shrinkage are noted to indicate potential failure; loss of strength below the steady-state descent loads (i.e., no safety factor) is considered mechanical failure; and any evidence of burning is considered a failure.
- Failure temperatures for each of the failure modes and for Nylon, Nomex and PBI are as indicated

	Shrinkage (maximum amount)	Mechanical Strength	Burning
Nylon	not determined	450°F	488°F (melts)
Nomex	590 - 710°F (30% linear)	835°F	935°F
PBI	750 - 790°F (40% linear)	890°F	not observed

Nylon loses strength at a temperature well below any form of failure in Nomex or PBI. Both Nomex and PBI undergo significant amounts of shrinkage at temperatures well below those for mechanical failure. Whereas the latter mode represents certain failure, no data were found or generated which equate the shrinkage with failure. Burning or melting does not occur at temperatures below the mechanical failure temperatures for any of these materials, and thus is not a failure mode of concern.

- The failure altitudes for the three candidate fabrics are shown in Figure 14 for fires with base diameters from 50 to 200 feet. These results are based upon:
  - Worst case fully developed fires

- Worst case trajectories - passing directly through fire/plume center
- Failure temperatures - criteria as shown above

For example, a nylon canopy entering a 100 foot diameter fire below an altitude of 150 feet is predicted to fail mechanically. For this same fire size Nomex begins to shrink at 130 feet entry altitude and PBI at 110 feet. Both Nomex and PBI fail mechanically at entry altitudes of 100 feet or less. For the smaller diameter fires, these altitude differences are in the range of 10 to 30 feet whereas for a 200 foot diameter fire, differences of 50 to 100 feet are predicted.

Uncertainties in the fire model, undeveloped fires, uncertainties in the failure temperatures and modes of failure all have an effect on the absolute level and relative differences in level for these three materials.

- Strength failure of Nomex and PBI fabrics is predicted only for through-the-fire trajectories. Nylon is predicted to fail under windless conditions for descent within one fire base radius of the periphery of large fires.

The need for experimental data in a simulated fire environment was addressed in this study. A laboratory test apparatus which can provide end-use simulation is shown to be feasible and a preliminary design concept is presented. Such an apparatus can be used to verify the analytical results and to screen candidate fabrics.

6.2 RECOMMENDATIONS

This study has shown that improvements in the thermal survivability of personnel parachutes on exposure to aircraft crash fires is attainable through the use of improved fabrics for the parachute canopy. In addition, the vertical temperature profile in the fire, the temperature dependence of possible failure modes and, in particular, the permeability requirements of the C-9 configuration have been identified as the most critical parameters influencing parachute thermal survivability. It must be recognized that the uncertainties associated with the first two parameters and the limited scope of this study (which did not consider alternate configurations, other improved fabrics, and only addressed worst case conditions) does not allow an accurate evaluation of the ultimate improvements in parachute thermal survivability that can be realized. The following recommendations are provided to define additional tasks that should be performed in order to improve the developed capabilities and permit an evaluation of the achievable improvements in parachute thermal performance.

- Consider configurations other than the C-9. Other canopy designs, such as a ribbon chute, can utilize less permeable materials. By reducing the convective heating any improvements in thermal and optical properties would result in improved thermal tolerance.
- Consider other improved fabrics. Whereas Nomex and PBI exhibit significant improvements in performance relative to Nylon on the basis of a strength failure the possible failure due to shrinkage restricts the achievable improvements utilizing these materials. Materials with improved dimensional stability, such as Nomex II and Stabilized PBI, should be investigated.
- Obtain data on actual candidate fabrics. Such data is obviously required to verify the analysis, the failure criteria, and candidate designs. In addition to basic property data, the need for a well-simulated test to evaluate materials under actual end-use conditions is clearly indicated.
- Construct a laboratory test apparatus for accurate end-use simulation testing of candidate materials. The facility concept presented as part of this study indicates the desirability of a well-controlled environment and a means to monitor fabric temperature.

  In the event it is not possible to contruct this apparatus, several other existing facilities should be considered as potential substitutes. These include wind tunnels, the shrinkage test apparatus used in the previous study of flight suit fabrics, and the JP-4 burner constructed by the Air Force Materials Laboratory. The feasibility of using one of these facilities for simulation testing, including possible modifications, would require investigation by the Air Force and Aerotherm.
- Obtain a better understanding of the fire environment. The uncertainties associated with the vertical temperature variation within the fire plume must be resolved to allow an accurate evaluation of failure thresholds. A test program at the Natick fire pit in which the geometrical characteristics of large open pool fires can be verified through photographs and the temperature distribution in the plume can be measured would provide much needed data with which the analytical model can be correlated and updated.

APPENDIX A

DEVELOPMENT OF THE FIRE MODEL

LIST OF SYMBOLS

A_p	projected area of fire column normal to wind vector
C_f	fire column drag coefficient, Equation (8)
C_{p_a}	frozen specific heat of ambient air
$C_{p_{cp}}$	frozen specific heat of combustion products at top of combustion zone
d_b	base diameter of fire
E_p	entrainment coefficient
F_D	drag force on fire column due to wind
Fr	Froude number, $V_w^2/g\ d_{ave}$
g	gravitational constant
g_c	gravitational acceleration
h_a	sensible specific enthalpy of air at fire temperature
h_{a_o}	sensible, or total (sensible + chemical) specific enthalpy of air at ambient conditions
h_{cp}	total (sensible + chemical) specific enthalpy of combustion products in combustion zone or plume, or sensible enthalpy of combustion products at top of combustion zone at local plume temperature
h_p	sensible specific enthalpy of plume gas mixture, Equation (15)
K_D	drag coefficient correlation constant, Equation (9)
$\dot{m}_a$	mass flowrate of air along fire axis
$\dot{m}_{cp}$	mass flowrate of combustion products along fire axis
$\dot{m}_f$	mass flowrate for fuel vaporization at fuel surface

M_a	molecular weight of ambient air
M_{cp}	molecular weight of combustion products at top of combustion zone
p	ambient pressure (1 atm)
p_a	partial pressure of air in plume gas mixture
p_{cp}	partial pressure of top-of-combustion-zone combustion products in plume gas mixture
q	nondimensional temperature, Equation (49)
r_{cp}	radius of fire column in combustion zone or plume
r_p	radius of fire column in plume
Re	Reynolds number, $\rho_{a_o} V_w d_{ave}/\mu_{a_o}$
R_u	universal gas constant
t	time
T_m	flame temperature
T_{cp}	average fire temperature in combustion zone or plume
T_p	average fire temperature in plume
V_a	velocity of entrained air at fire periphery
V_{cp}	vertical component of velocity in combustion zone or plume
V_p	vertical component of velocity in plume
V_w	wind velocity

LIST OF SYMBOLS (concluded)

y	vertical coordinate
ε_{cp}	effective emissivity of gases at periphery of combustion zone or plume
ε_{p}	effective emissivity of gases at periphery of plume
θ	fire column tilt angle
ρ_{a}	density of air at local conditions in plume
ρ_{a_o}	density of ambient air
ρ_{cp}	density of combustion products in combustion zone or plume, or density of combustion products at top of combustion zone at local plume conditions
ρ_{f}	density of fuel vapor at normal boiling point
ρ_{p}	density of plume gas mixture, Equation (13)
σ	Stefan-Boltzmann constant

I. COMBUSTION ZONE AND PLUME - CHEMICAL EQUILIBRIUM

Figure A-1 depicts the fire geometry and differential control volume used to derive the set of governing equations applicable to both the combustion zone and the plume, under windless and wind conditions. The wind vector is assumed to be parallel to the ground plane and to cause elemental disks in the fire parallel to the ground to slip relative to one another. Thus, at a given elevation fire properties are assumed to be uniform in a plane parallel to the ground. Furthermore, fire properties as a function of altitude are assumed to be independent of wind. If, in addition, air entrainment and fuel burning rate are assumed to be negligibly affected by wind[7], then a single set of governing equations is valid both with and without wind. Essentially, wind serves to alter only the configuration of the fire by tilting it. Note, however, that although fire properties as a function of altitude are assumed independent of wind, the gradients of these properties along the axis of the fire will change with the presence of wind.

The tilt model used here differs from that introduced by Welker and Sliepcevich[8], who assume the fire column remains cylindrical in shape with the presence of wind. They considered only small pool fires ($d_b \leq 2'$) and assumed the entire fire column to be thermochemically uniform. Use of their tilt assumption here would result in a tilting of the plane of uniform fire properties relative to the ground plane. This assumption is felt to be invalid for the large fires of interest here.

As mentioned above, the advantage of decoupling the effects of wind is that a single set of conservation equations can be used for both tilting and nontilting fires. These equations can be solved ignoring information regarding the wind. Then, a posthoc solution of the tangential momentum equation gives the plume tilt angle as a function of wind velocity.

The derivation of the continuity equation is carried out in detail to illustrate the method. Referring to the elemental control volume in Figure A-1:

$$\text{mass rate into bottom of c.v.} = \rho_{cp} V_{cp} \pi r_{cp}^2$$

$$\text{mass rate into side of c.v.} = \rho_{a_o} V_a 2\pi r_{cp} \delta y$$

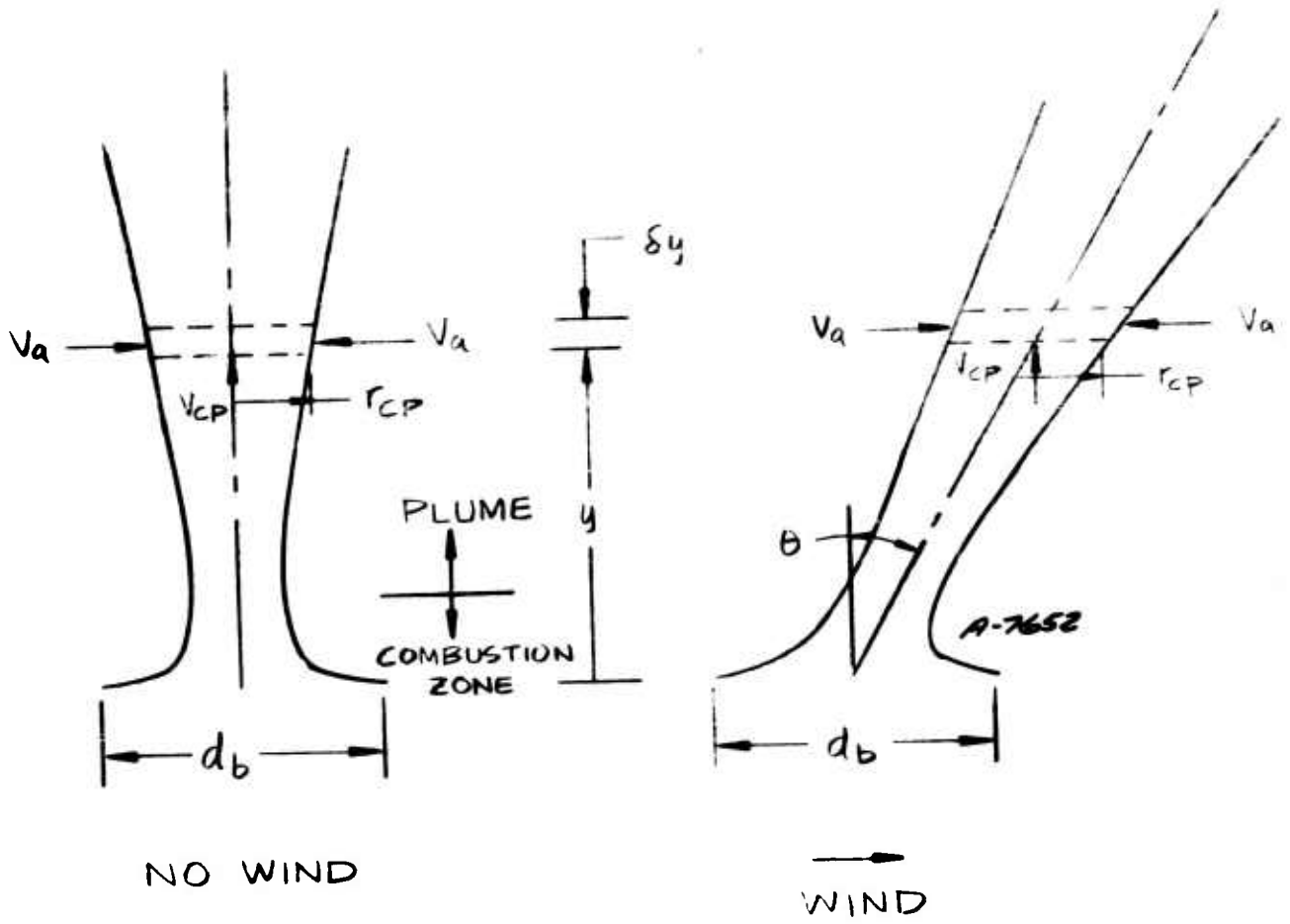

Figure A-1. Fire configuration and elemental control volume used to derive governing equations

mass rate out of top of c.v. $= \rho_{cp} V_{cp} \pi r_{cp}^2 + \frac{d}{dy} (\rho_{cp} V_{cp} \pi r_{cp}^2) \delta y$

Under steady-state conditions (no accumulation of mass in the control volume) these quantities can be combined to give

$$\frac{d}{dy} (\rho_{cp} V_{cp} r_{cp}^2) = 2\rho_{a_o} V_a r_{cp} \qquad \text{(A-1)}$$

For a strongly-buoyant fire plume, a correlation relating the entrained air velocity V_a to the vertical component of the combustion products velocity V_{cp} has been developed[3]:

$$V_a = E_p \left(\frac{\rho_{cp}}{\rho_{a_o}} \right)^{1/2} V_{cp} \qquad \text{(A-2)}$$

where E_p is an entrainment parameter or coefficient. Combining Equations (1) and (2) gives the desired form of the continuity equation:

$$\frac{d}{dy} (\rho_{cp} V_{cp} r_{cp}^2) = 2E_p \left(\rho_{a_o} \rho_{cp} \right)^{1/2} V_{cp} r_{cp} \qquad \text{(A-3)}$$

Equation (3) is a global or total continuity equation. A second "species" continuity equation can be written for the air entrainment mass rate:

$$\frac{d\dot{m}_a}{dy} = 2\pi E_p \left(\rho_{a_o} \rho_{cp} \right)^{1/2} V_{cp} r_{cp} \qquad \text{(A-4)}$$

Equations (3) and (4) together state that the mass rate of combustion products, $\dot{m}_{cp} = \rho_{cp} V_{cp} \pi r_{cp}^2$, changes solely by virtue of the addition of entrained air at each elevation in the fire. In other words, no other mass is created or lost in the fire column. Note that "instant mixing" of the entrained air is implied in this formulation.

A vertical momentum equation can be derived by equating the vertical buoyancy force on the elemental control volume to the excess of outgoing over incoming vertical momentum flux:

$$\frac{d}{dy}\left(\rho_{cp}V_{cp}^2 r_{cp}^2\right) = g\left(\rho_{a_o} - \rho_{cp}\right) r_{cp}^2 \qquad \text{(A-5)}$$

Since the ambient air is assumed to move only in planes parallel to the ground, due either to entrainment or wind, it does not contribute to the vertical momentum equation.

The global energy equation is derived by assuming the only energy loss mechanism to be radiation out the side of the elemental control volume. Radiation transport in the vertical direction is taken to be negligible, a valid assumption whenever the combustion gases are optically thick. Calculations were carried out which indicated conduction heat transfer in the vertical direction in the fire and convection heat transfer at the fire periphery are generally negligible compared to the transverse radiation losses. Although the fire is highly turbulent, it is assumed to radiate at a mean temperature which is constant throughout the fire at a fixed elevation but varies as a function of elevation. The remaining energy transfer modes are convection of energy into and out of the differential control volume from the entrained air and upward flowing combustion gases. The resulting energy equation is

$$\frac{d}{dy}\left(\rho_{cp}V_{cp}r_{cp}^2 h_{cp}\right) = 2r_{cp}\left[E_p\left(\rho_{a_o}\rho_{cp}\right)^{1/2} V_{cp}h_{a_o} - \sigma\varepsilon_{cp}T_{cp}^4\right] \qquad \text{(A-6)}$$

Equation (3), (4), (5), and (6) comprise the set of governing equations for the combustion zone and plume, with or without wind. The corresponding unknowns are T_{cp}, V_{cp}, r_{cp}, and $\dot{m}_a$. The density ρ_{cp} and enthalpy h_{cp} of the combustion products are calculated from equilibrium chemistry, knowing the fuel chemical composition and burning rate $\dot{m}_f$, the local air/fuel ratio $\dot{m}_a/\dot{m}_f$, and local temperature T_{cp} (the total pressure in the fire is assumed to be 1 atm).

Once the variables T_{cp}, V_{cp}, r_{cp}, and $\dot{m}_a$ have been calculated from the ground level up to an altitude where T_{cp} approaches the ambient temperature, the tilt angle can be computed for any specified wind velocity. The tilt angle θ is computed by solving the horizontal momentum equation, which requires that the total drag force on the fire column due to the presence of wind equal the excess of outgoing over incoming tangential momentum flux:

$$g_c F_D = \left[\rho_{cp}V_{cp}^2 \pi r_{cp}^2\right]_{\substack{\text{plume}\\ \text{top}}} \tan\theta \qquad \text{(A-7)}$$

The plume top can be arbitrarily defined as that point at which T_{cp} is within 50°F of the ambient temperature. A more precise definition is not necessary, since the calculated tilt angle has been found to be relatively insensitive to the plume cutoff assumption. The drag force is calculated from the definition of the plume drag coefficient:

$$C_f = \frac{g_c F_D}{\left(\frac{1}{2}\rho_{a_o} V_w^2\right)\left(A_p\right)} \tag{A-8}$$

where A_p is the projected area of the fire column normal to the wind vector. Originally, the flame drag coefficient of Welker and Sliepcevich[8] was considered:

$$C_f = K_D \left(\frac{\rho_{a_o}}{\rho_f}\right)^{0.88} \left(\mathrm{ReFr}\right)^{-0.015} \tag{A-9}$$

For the small flames studied in their work, $d_b \leq 2.0$ ft (0.61 meters), the leading constant value of $K_D = 16.4$ was found to best correlate the data. However, use of this value for the much larger fires of interest in this study, while giving the proper trends, predicted excessive tilt angles for moderate to high wind velocities (up to 30 knots (15.4 m/sec)). Therefore, in order to provide more plausible tilt angles the fire tilt data of Alger, et al.[7], were used in conjunction with the model developed here to back out the optimum value of K_D. This value was found to be $K_D = 2.122$.

II. PLUME - FROZEN

The frozen plume model assumes that the plume gases are made up of two "species": an entrained air "specie", and a combustion product "specie" which has the thermochemical properties of the combustion zone. Therefore, at any position above the combustion zone the partial pressures of the two components are given by

$$p_{cp} = \frac{\rho_{cp} R_u T_p}{M_{cp}} \tag{A-10}$$

$$p_a = \frac{\rho_a R_u T_p}{M_a} \tag{A-11}$$

where

$$p_a + p_{cp} = p = 1 \text{ atm} \tag{A-12}$$

and

$$\rho_{cp} + \rho_a = \rho_p \tag{A-13}$$

Equations (10), (11), and (12) can be combined to give

$$\frac{\rho_{cp}}{M_{cp}} + \frac{\rho_a}{M_a} = \frac{p}{R_u T_p} \tag{A-14}$$

The plume mixture enthalpy is defined as

$$\rho_p h_p = \rho_{cp} h_{cp} + \rho_a h_a \tag{A-15}$$

where

$$h_{cp} = C_{p_{cp}} T_p \tag{A-16}$$

$$h_a = C_{p_a} T_p \tag{A-17}$$

since the component specific heats are assumed to be constant.

The global continuity, vertical momentum, and energy equations of the frozen plume have the same form as the corresponding equations for the chemically-reacting plume:

$$\frac{d}{dy}\left(\rho_p V_p r_p^2\right) = 2E_p\left(\rho_{a_o}\rho_p\right)^{1/2} V_p r_p \tag{A-18}$$

$$\frac{d}{dy}\left(\rho_p V_p^2 r_p^2\right) = g\left(\rho_{a_o} - \rho_p\right) r_p^2 \tag{A-19}$$

$$\frac{d}{dy}\left(\rho_p V_p r_p^2 h_p\right) = 2r_p\left[E_p\left(\rho_{a_o}\rho_p\right)^{1/2} V_p h_{a_o} - \sigma\varepsilon_p T_p^4\right] \tag{A-20}$$

The "species" continuity equation for the frozen plume differs from its chemically-reacting analog:

$$\dot{m}_{cp} = \rho_{cp} V_p \pi r_p^2 \qquad \text{(A-21)}$$

Equation (21) simply states that the mass flux of the combustion products "species" is constant throughout the plume, being equal to its value at the top of the combustion zone.

The six unknowns in the frozen plume are ρ_p, ρ_{cp}, ρ_a, T_p, V_p, and r_p. The six governing equations are Equations (13), (14), (18), (19), (20), and (21). Equations (15, (16), and (17) are used in the energy equation (Equation (20)), to replace h_p with T_p.

Once the properties of the entire frozen plume have been computed, the tilt angle can be determined utilizing the same approach as was used in the chemically-reacting case. Hence,

$$g_c F_D = \left[\rho_p V_p^2 \pi r_p^2\right]_{\substack{\text{plume} \\ \text{top}}} \tan\theta \qquad \text{(A-22)}$$

III. SOLUTION TECHNIQUES

Numerical solution techniques were required for both the chemically-reacting combustion zone/plume model and the frozen plume model. Closed-form solutions to the relatively simple governing equations of the frozen plume were unattainable due to nonlinearities resulting from the nonlinear form of the entrainment equation (Equation (2)) and the inclusion of a radiation term in the energy equation. Of course, consideration of numerous chemical species in the chemically-reacting formulation rendered closed-form solutions unfeasible for that model.

III.1 Combustion Zone and Plume-Chemical Equilibrium

Several manipulations of Equations (3), (4), (5), and (6) were carried out prior to casting them into finite-difference form. First, the continuity equation was used to simplify both the momentum and energy equations. The resulting simplified set of equations is

$$\frac{d}{dy}\left(\rho_{cp} V_{cp} r_{cp}^2\right) = 2E_p \left(\rho_a \rho_{cp}\right)^{1/2} V_{cp} r_{cp} = t_1 \qquad \text{(A-23)}$$

$$\frac{dV_{cp}}{dy} = (\rho_{cp} V_{cp} r_{cp})^{-1} \left[g\left(\rho_{a_o} - \rho_{cp}\right) r_{cp}^2 - V_{cp}\, t_1 \right] = t_2 \qquad \text{(A-24)}$$

$$\frac{dh_{cp}}{dy} = (\rho_{cp} V_{cp} r_{cp}^2)^{-1} \left[t_1 \left(h_{a_o} - h_{cp}\right) - 2 r_{cp} \sigma \varepsilon_{cp} T_{cp}^4 \right] = t_3 \qquad \text{(A-25)}$$

$$\frac{d\dot{m}_a}{dy} = \pi t_1 = t_4 \qquad \text{(A-26)}$$

Next, the functional dependence of ρ_{cp} and h_{cp} on T_{cp} and $\dot{m}_a$, under the constraint of chemical equilibrium, is explicitly considered:

$$\rho_{cp} = \rho_{cp}\ (T_{cp},\ \dot{m}_a/\dot{m}_f) \equiv \rho_{cp}(T_{cp},\ \dot{m}_a) \qquad \text{(A-27)}$$

$$h_{cp} = h_{cp}\ (T_{cp},\ \dot{m}_a/\dot{m}_f) = h_{cp}(T_{cp},\ \dot{m}_a) \qquad \text{(A-28)}$$

since $\dot{m}_f$ is a specified constant for a given fire base diameter. Then,

$$\frac{d\rho_{cp}}{dy} = \frac{\partial \rho_{cp}}{\partial T_{cp}} \frac{dT_{cp}}{dy} + \frac{\partial \rho_{cp}}{\partial \dot{m}_a} \frac{d\dot{m}_a}{dy} \qquad \text{(A-29)}$$

$$\frac{dh_{cp}}{dy} = \frac{\partial h_{cp}}{\partial T_{cp}} \frac{dT_{cp}}{dy} + \frac{\partial h_{cp}}{\partial \dot{m}_a} \frac{d\dot{m}_a}{dy} \qquad \text{(A-30)}$$

Using Equations (29) and (30), the derivative on the left-hand side of Equation (23) can be expanded, and the enthalpy gradient in Equation (25) can be transformed into a temperature gradient. The final form of the governing equations is then

$$\frac{dr_{cp}}{dy} = (2 r_{cp} V_{cp})^{-1} \left\{ \rho_{cp}^{-1} \left[t_1 - V_{cp} r_{cp}^2 \left(\frac{\partial \rho_{cp}}{\partial \dot{m}_a} t_4 + \frac{\partial \rho_{cp}}{\partial T_{cp}} t_3' \right) \right] - r_{cp}^2 t_2 \right\} = t_1' \qquad \text{(A-31)}$$

$$\frac{dV_{cp}}{dy} = t_2 \qquad \text{(A-32)}$$

$$\frac{dT_{cp}}{dy} = \left(\frac{\partial h_{cp}}{\partial T_{cp}}\right)^{-1}\left(t_3 - \frac{\partial h_{cp}}{\partial \dot{m}_a}\, t_4\right) = t_3' \qquad \text{(A-33)}$$

$$\frac{d\dot{m}_a}{dy} = t_4 \qquad \text{(A-34)}$$

In functional form, the right-hand sides of the above equations are

$$t_1' = t_1' \,(T_{cp},\ V_{cp},\ r_{cp},\ \dot{m}_a) \qquad \text{(A-35)}$$

$$t_2 = t_2 \,(T_{cp},\ V_{cp},\ r_{cp},\ \dot{m}_a) \qquad \text{(A-36)}$$

$$t_3' = t_3' \,(T_{cp},\ V_{cp},\ r_{cp},\ \dot{m}_a) \qquad \text{(A-37)}$$

$$t_4 = t_4 \,(T_{cp},\ V_{cp},\ r_{cp},\ \dot{m}_a) \qquad \text{(A-38)}$$

The thermodynamic quantities in these equations, such as ρ_{cp}, h_{cp}, $\partial\rho_{cp}/\partial T_{cp}$, $\partial\rho_{cp}/\partial\dot{m}_a$, $\partial h_{cp}/\partial T_{cp}$, and $\partial h_{cp}/\partial\dot{m}_a$ are computed by the Aerotherm Chemical Equilibrium[9] (ACE) computer program (as functions of T_{cp} and $\dot{m}_a$, at one atmosphere).

Equations (31), (32), (33), and (34) are simultaneously integrated using a second-order Runge-Kutta numerical scheme. The algorithm for this scheme is illustrated by the following general pair of first order ordinary differential equations and their finite difference representations:

$$\frac{dy}{dx} = f[y(x),\ z(x)]$$

$$\frac{dz}{dx} = g[y(x),\ z(x)]$$

$$\begin{aligned} y_{i+1} &= y_i + \frac{h}{2}\left[f(y_i,\ z_i) + f(\bar{y}_{i+1},\ \bar{z}_{i+1})\right] \\ z_{i+1} &= z_i + \frac{h}{2}\left[g(y_i,\ z_i) + g(\bar{y}_{i+1},\ \bar{z}_{i+1})\right] \\ \bar{y}_{i+1} &= y_i + hf(y_i,\ z_i) \end{aligned} \qquad \text{(A-39)}$$

$$\bar{z}_{i+1} = z_i + hg(y_i, zi)$$

In Equations (39) h is the finite difference step size of the independent variable.

A computer routine has been written which solves Equations (31), (32), (33), and (34) using the algorithm of Equation (39). As already mentioned, the ACE program is used as a subroutine to determine the equilibrium chemical composition and other thermodynamic quantities of the fuel/air mixture at each step in the marching solution. A set of thermochemical data (enthalpy of formation, specific heat, standard state entropy) is input for each of the candidate chemical species, enabling the appropriate equilibrium constants to be computed. The JANAF[10] thermochemical base state is used: zero heat of formation for the elements in their most natural state at 298°K and 1 atm. The solution is initiated at the fuel surface. Required input information are the following:

1. Fuel vaporization flux and temperature and vapor density at the normal boiling point
2. Fire base diameter
3. Ambient air density, viscosity, and total enthalpy
4. Effective emissivity of combustion products
5. Entrainment coefficient
6. Wind velocity
7. Initial step size and step size increment criteria

III.2 PLUME - FROZEN

Equations (13), (14), (18), (19), (20), and (21) govern the frozen plume. The differential equations, Equations (18), (19), and (20) were solved with the simple Eulerian finite difference scheme. For the pair of differential equations in Equation (39), this difference approach gives simply:

$$y_{i+1} = y_i + hf(y_i, z_i)$$
$$z_{i+1} = z_i + hg(y_i, z_i) \qquad \text{(A-40)}$$

Equation (20) was manipulated to the following form, utilizing Equations (15), (16), (17), (18) and (21):

$$\left(\dot{m}_{cp}C_{p_{cp}} + \rho_a V_p \pi r_p^2 C_{p_a}\right)\frac{dT_p}{dy} = 2\pi r_p\left[E_p\left(\rho_{a_o}\rho_p\right)^{1/2} V_p\left(h_{a_o} - C_{p_a}T_p\right) - \sigma\varepsilon_p T_p^4\right] \qquad \text{(A-41)}$$

Then, using the finite difference algorithm of Equation (40) the global continuity, vertical momentum, and energy equations, Equations (18), (19), and (40), take the following form:

$$\rho_{p_{i+1}} V_{p_{i+1}}\left(r_{p_{i+1}}\right)^2 = C_1\left(\rho_{p_i}, V_{p_i}, r_{p_i}\right) \qquad \text{(A-42)}$$

$$\rho_{p_{i+1}}\left(V_{p_{i+1}}\right)^2\left(r_{p_{i+1}}\right)^2 = C_2\left(\rho_{p_i}, V_{p_i}, r_{p_i}\right) \qquad \text{(A-43)}$$

$$T_{p_{i+1}} = C_3\left(\rho_{a_i}, \rho_{p_i}, V_{p_i}, r_{p_i}, T_{p_i}\right) \qquad \text{(A-44)}$$

In addition, the algebraic Equations (13), (14), and (21) take the forms:

$$\rho_{p_{i+1}} = \rho_{cp_{i+1}} + \rho_{a_{i+1}} \qquad \text{(A-45)}$$

$$\frac{\rho_{cp_{i+1}}}{M_{cp}} + \frac{\rho_{a_{i+1}}}{M_a} = \frac{p}{R_u T_{p_{i+1}}} \qquad \text{(A-46)}$$

$$\rho_{cp_{i+1}} V_{p_{i+1}} \pi\left(r_{p_{i+1}}\right)^2 = \dot{m}_{cp} \qquad \text{(A-47)}$$

At each step, Equations (42), (43), (44), (45), (46), and (47) are solved for the six unknowns $\rho_{cp_{i+1}}$, $\rho_{a_{i+1}}$, $\rho_{p_{i+1}}$, $T_{p_{i+1}}$, $V_{p_{i+1}}$, $r_{p_{i+1}}$.

Note that, relative to the chemical equilibrium version of the governing equations, the frozen plume finite difference equations are solved much more expediently since the ACE program is not required as a subroutine. Because the frozen plume solution proceeds so rapidly, there is relatively little advantage to using the maximum step size permissible under stability constraints. Thus, a constant step size is used throughout the entire marching solution.

Input data required by the frozen plume routine include the following:

1. Conditions at the top of the combustion zone:
   a. Temperature
   b. Air/fuel ratio

c. Density

d. Combustion products molecular weight and frozen specific heat

2. Fuel vaporization flux and vapor density at the normal boiling point
3. Diameter at fire base and diameter and height at top of combustion zone
4. Effective plume emissivity
5. Ambient air temperature, molecular weight, frozen specific heat, and viscosity
6. Entrainment coefficient
7. Wind velocity
8. Step size

APPENDIX B

DEVELOPMENT OF THE FIRE RADIANT ENVIRONMENT

Due to the nonisothermal nature of the hot gas region, the plume is subdivided into N horizontal, isothermal zones. Each zone is geometrically represented as a right circular cylinder of radius $\bar{R}_j$ and temperature $\bar{T}_j$, where $\bar{R}_j$ is the arithmetic mean of the radii at the top and bottom of the zone and $\bar{T}_j$ is the mean temperature. The radiant energy per unit time incident on one side of a differential area of a parachute component is obtained by numerical integration over the N zones; i.e.

$$Q = \sum_{j=1}^{N} A_{f_j} F_{f_j \to t} i_{b_j} \tag{B-1}$$

where

Q = total radiant energy per unit time incident on one side of the target

A_{f_j} = surface area of the j^{th} cylindrical zone

$F_{f_j \to t}$ = geometric configuration factor from the j^{th} cylindrical zone to the target

i_{b_j} = blackbody total intensity from the j^{th} cylindrical zone = $\sigma \bar{T}_j^4$

It can be shown that

$$A_{f_j} F_{f_j \to t} = A_t F_{t \to f_j} \tag{B-2}$$

which allows Equation (B-1) to be rewritten as

$$Q = \sum_{j=1}^{N} A_t F_{t \to f_j} i_{b_j} \tag{B-3}$$

The geometry for the configuration factor between a differential area element, dA_1, representative of a particular location on a parachute component, and a differential area element, dA_2, representative of a section of a cylindrical isothermal zone is shown in Figure B-1, and is calculated from

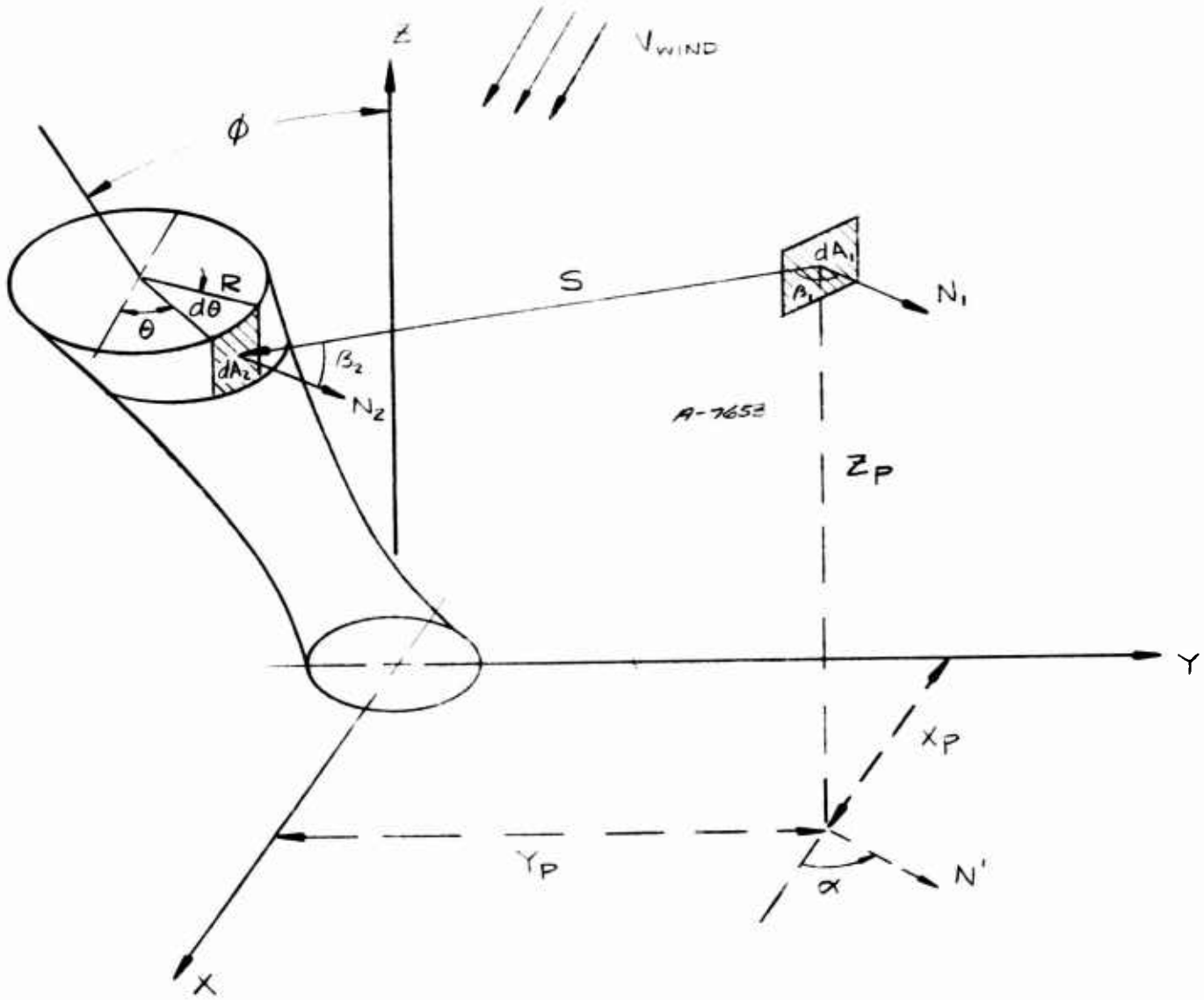

Figure B-1. Geometry between differential parachute element and wind-blown fire.

$$F_{dA_1 \to dA_2} = \frac{\cos \phi_1 \cos \phi_2 \, dA_2}{\pi S^2} \tag{B-4}$$

where

ϕ_1 = angle between N_1 and S

ϕ_2 = angle between N_2 and S

N_1 = unit normal vector to differential area dA_1

N_2 = unit normal vector to differential area dA_2

S = distance vector from dA_1 to dA_2

dA_2 = area of a differential section of cylindrical zone = $Rd\theta dz$

θ = angle from x-axis to center of dA_2

R = radius of cylindrical zone

dz = height of cylindrical zone

Noting that

$$\vec{N}_1 \cdot \vec{S} = |S| \cos \phi_1 \tag{B-5}$$

and

$$-\vec{N}_2 \cdot \vec{S} = |S| \cos \phi_2 \tag{B-6}$$

allows Equation (B-4) to be rewritten as:

$$F_{dA_1 \to dA_2} = \frac{\left(\vec{N}_1 \cdot \vec{S}\right)\left(-\vec{N}_2 \cdot \vec{S}\right) Rd\theta dz}{\pi S^4} \tag{B-7}$$

The unit normals can be represented by their components in a cartesian system as:

$$\vec{N}_2 = \cos \alpha \cos \delta \vec{I} + \sin \alpha \cos \delta \vec{J} + \sin \delta \vec{K} \tag{B-8}$$

and

$$\vec{N}_2 = \cos \theta \vec{I} + \sin \theta \vec{J} \tag{B-9}$$

where

α = angle from the x-axis to the projection of $\vec{N}_1$ on the x-y plane

δ = angle that $\vec{N}_1$ makes with the x-y plane

$\vec{i}$ = unit vector in the x-direction

$\vec{j}$ = unit vector in the y-direction

$\vec{k}$ = unit vector in the z-direction

The distance vector $\vec{S}$ can be represented by its components in a cartesian system as:

$$\vec{S} = (x - x_p)\vec{i} + (y - y_p)\vec{j} + (z - z_p)\vec{k} \tag{B-10}$$

where

x,y,z = coordinates of the center of differential area dA_2

x_p,y_p,z_p = coordinates of the center of differential area dA_1

The coordinates of differential area dA_2 are affected by tilting of the plume due to wind. From Figure B-1 it is seen that the coordinates of the center of dA_2 can be written as:

$$\begin{aligned} x &= z_j \tan \phi + R \cos \theta \\ y &= R \sin \theta \\ z &= z_j \end{aligned} \tag{B-11}$$

where ϕ is the wind-blown tilt angle of the plume. The configuration factor from dA_1 to the cylindrical surface A_{2_j} is obtained by numerical integration with respect to θ, or:

$$F_{t \to f_j} = F_{dA_1 \to A_{2_j}} = \sum_{k=1}^{M} \frac{\left(\vec{N}_1 \cdot \vec{S}_k\right)\left(-\vec{N}_{2_k} \cdot \vec{S}_k\right) R_j \Delta z_j \Delta\theta_k}{\pi S^4} \tag{B-12}$$

using Equations (B-8), (B-9), (B-10), and (B-11). Substituting Equation (B-12) into Equation (B-3) and noting that Q/A_t is the total radiant flux incident on one side of the target one obtains

$$\dot{q} = Q/A_t = \sum_{j=1}^{N} \sum_{k=1}^{M} \frac{\left(\vec{N}_1 \cdot \vec{S}_k\right)\left(-\vec{N}_{2_k} \cdot \vec{S}_k\right) \Delta\theta_k \sigma \bar{R}_j \bar{T}_j^4 \Delta z_j}{\pi S_k^4} \qquad \text{(B-13)}$$

Under some conditions both sides of a canopy element can be irradiated. To evaluate the incident radiant flux to the other side of the target requires the integrations given by Equation (B-13) with the direction of $\vec{N}_1$ reversed.

APPENDIX C

TENSILE STRENGTH OF CANDIDATE MATERIALS

I. FABRIC TENSILE STRENGTH DATA REDUCTION

A lack of data on the tensile strength of 1.1 oz/sq.yd. Nomex and PBI canopy fabrics necessitated the use of available tensile strength information to form the data base. The existing data were gathered from tests of webbings,[16] thicker canopy fabrics,[17] and tapes.[18] The data is presented as the quasi-static rupture load as a function of temperature.

Due to the variation in configuration, density, and thickness of the fabrics tested, an attempt was made to find a parameter common to all fabrics which can account for the above mentioned variations. This parameter should be related to mass, i.e., a comparison of fabrics of similar density and with the same mass/unit length implies that their cross-sectional areas should, on the average, be the same. Thus, what should be considered is the strength a fabric has per pound mass per unit length, which is analogous to the common tensile strength rating of materials given in pounds force per unit area.*

The original data for Nylon, Nomex, and PBI webbings[16] are given in Table C-I; the data for 2.0 oz/sq.yd. canopy fabrics[17] is given in Table C-II; and the data for tapes[18] is given in Table C-III. Also shown in these tables is the reduction of the quasi-static rupture load to a strength-to-weight ratio in units of $(lbs_f)/(lbs_m/yd)$. The strength-to-weight data are illustrated as a function of temperature for Nylon, Nomex, and PBI fabrics in Figure C-1. The relatively good correlation of this strength-to-weight ratio for fabrics with the same basic fiber but a variety of configurations suggests that, for purposes of this study, the tensile strength of a fabric is primarily a function of the basic fiber. The solid lines in Figure C-1 indicate the variation of the average tensile strength of Nylon, Nomex, and PBI fabrics with temperature.

II. CANOPY STRESSES IN STEADY DESCENT

The ultimate failure criterion considered in this study is the rupture of a canopy fabric due to the decay of the tensile strength of the fabric at

*Note that for materials which are solid such a measure is precise; however for fabrics which may have varying configurations, different weaves, and different numbers of yarns, this comparison is not precise, but is used here to provide a reasonable estimate for an untested configuration and weight.

TABLE C-1. WEBBING TENSILE STRENGTH DATA

Material	Width (inches)	Thickness (inches)	Unit Weight (yds/lb_m)	Temperature (°F)	Rupture Load (lbs_f)	Strength/Weight (lbs_f)/(lbs_m/yd)	Source
Nylon	1-13/16	0.100	7.3	70. 250.	4670. 3750.	34091. 27375.	Ref. 16
Nomex	1-13/16	0.120	5.8	70. 250.	5260. 4650.	30508. 26970.	
PBI	1-3/4	0.165	4.7	70. 250.	4860. 4980.	22842. 23406.	

TABLE C-2. CANOPY FABRIC TENSILE STRENGTH DATA

Material	Construction	Weave Pattern	Weight (oz/sq.yd.)	Unit Weight ($yds/lb_m/in\text{-}width$)	Temperature (°F)	Rupture Load ($lbs_f/in\text{-}width$)	Strength/Weight ($(lbs_f)/(lbs_m/yd)$)	Source
Nylon	100/34/6Z	MIL-C-7350-I	2.0	288.	70. 200. 300. 400. 450.	106. 79. 59. 21. 2.	30528. 22752. 16992. 6048. 576.	Ref. 17
Nomex	100/50/4Z		2.0	288.	70. 200. 300. 400. 500. 600. 700. 750.	104. 93. 81. 67. 54. 40. 23. 15.	29952. 26784. 23328. 19296. 15552. 11520. 6624. 4320.	
PBI	100/25/3Z warp 100/25/2Z filling		2.1	274.28	70. 200. 400. 600. 700. 800.	70. 65. 58. 44. 35. 10.	19200. 17828. 15908. 12068. 9600. 2742.	

TABLE C-3. TAPE TENSILE STRENGTH DATA

Material	Construction	Width (inches)	Unit Weight (yds/lb_m)	Temperature (°F)	Rupture Load (lbs_f)	Strength/Weight (lbs_f)/(lbs_m/yd)	Source
Nylon	840/136/0.5Z	9/16	69.6	70.	631.	43917.	Ref. 18
				400.	331.	23038.	
				465.	73.	5081.	
Nomex	200/100/0		79.9	70.	424.	33878.	
				550.	197.	15740.	
				800.	39.	3116.	
PBI	200/50/0		76.3	70.	304.	23195.	
				700.	160.	12208.	
				850.	39.	2975.	

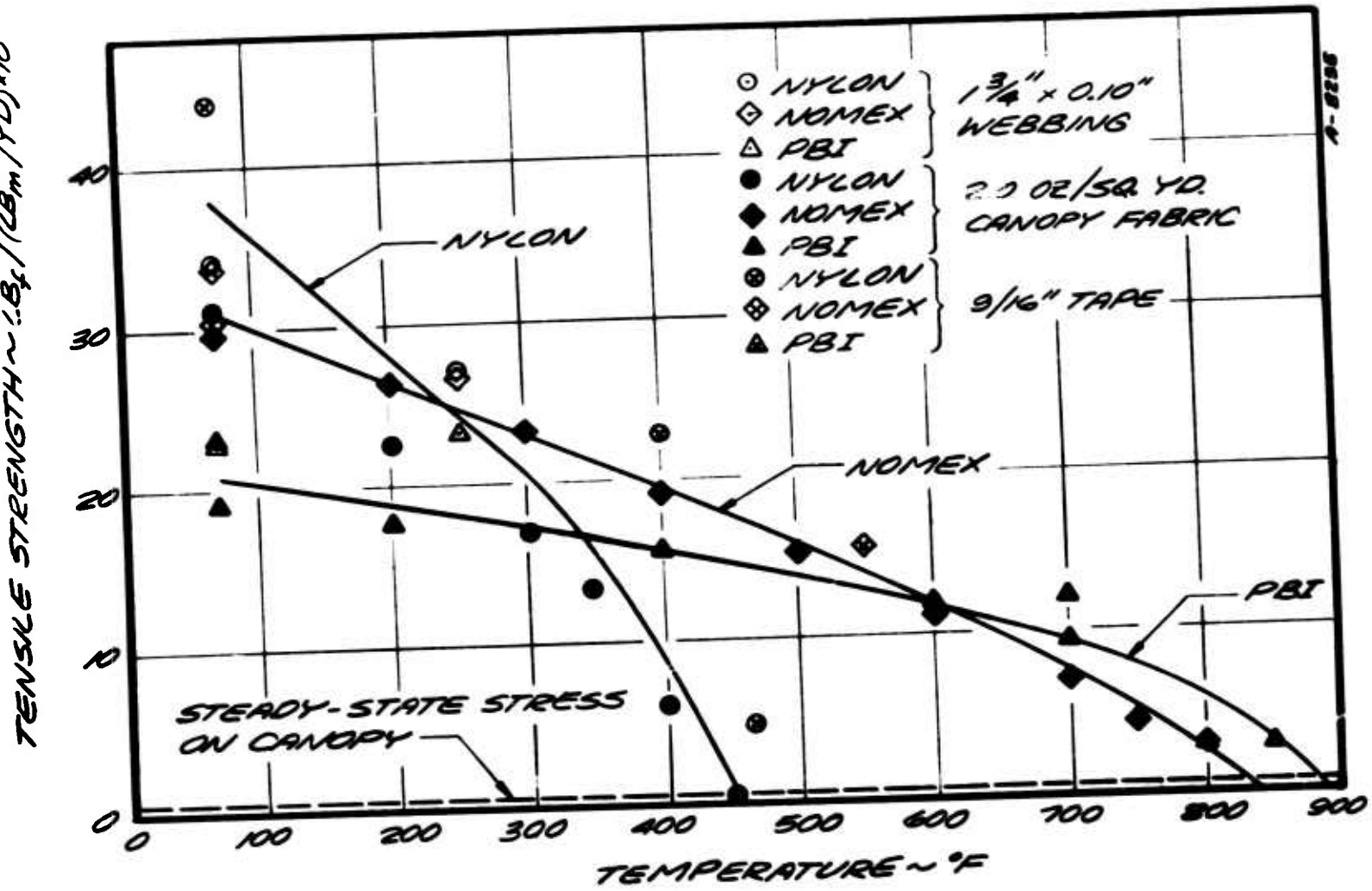

Figure C-1. Fabric tensile strength data.

elevated temperatures. To evaluate the temperature limit of the candidate materials the tensile stress on a canopy in steady descent is required.

In steady descent, a force balance on the circumference of the fully inflated canopy gives

$$F = \pi D f \qquad \text{(C-1)}$$

where

F = load on the canopy

D = diameter of the fully-inflated canopy

f = tensile force/unit circumferential width

If the fully inflated canopy is assumed to be a hemisphere then

$$D = \frac{2}{\pi} D_o \qquad \text{(C-2)}$$

where

D_o = diameter of flat-circular canopy (uninflated)

Assuming that the maximum meridional stress on a canopy is 1.5 times the circumferential stress allows the evaluation of the maximum tensile stress per unit mass per unit length for a canopy fabric in steady descent. Utilizing the properties of the Air Force C-9 canopies and assuming a load of 200 lbs, i.e.,

$F = 200\ \text{lbs}_f$

$D_o = 28$ feet

$W = 1.1$ oz/sq.yd. $= 0.0019\ \text{lbs}_m/\text{yd(length)} \cdot \text{in(width)}$

$$\text{Tensile Strength} = f_{max}/W = \frac{1.5\ F}{2 D_o W} \qquad \text{(C-3)}$$

$$= \frac{1.5 * 200\ \text{lbs}_f}{2 * 28\ \text{feet} * 12\text{in/ft} * 0.0019\ (\text{lbs}_m/\text{in}\cdot\text{yd})}$$

$$= 234\ (\text{lbs}_f)/(\text{lbs}_m/\text{yd})$$

This value is shown in Figure C-1 and the intersection with the curves for each candidate fabric determines their respective fail temperatures. Thus Nylon fabrics are predicted to fail at 450°F whereas Nomex fabrics provide improved thermal survivability to at least 800°F and PBI fabrics to at least 850°F.*

*Temperatures at highest reported test condition

In this study, no attempt has been made to apply a safety factor to this steady state load failure criterion as this would require an arbitrary definition. It is noted, however, that if a higher failure loading were specified, failure temperatures would decrease with Nomex and PBI remaining superior to Nylon above approximately 300 to 350°F equivalent to loads about 80 times greater than the steady state descent load.

REFERENCES

1. Taylor, G. I., "Fire Under Influence of Natural Convection," International Symposium on the Use of Models in Fire Research, NAS-NRC Publication 786, 1961, pp. 10-31.

2. Smith, R. K., "Radiation Effect on Large Fire Plumes," Eleventh Symposium (International) on Combustion, August 14 to 20, 1966, pp. 507-515.

3. Morton, R. E., "Modeling Fire Plumes," Tenth Symposium (International) on Combustion, August 17 to 21, 1964, pp. 973-982.

4. Albright, J. D., Knox, F. S., III, DuBois, D. R. and Keiser, G. M. "The Testing of Thermal Protective Clothing in a Reproducible Fuel Fire Environment, A Feasibility Study," USAARL Report No. 71-24, U. S. Army Aeromedical Research Laboratory, Fort Rucker, Alabama, June 1971.

5. Morse, H. L., Thompson, J. G., Clark, K. J., Green, K. A., and Moyer, C. B., "Analysis of the Thermal Response of Protective Fabrics," Technical Report AFML-TR-73-17, Air Force Materials Laboratory, Air Force Systems Command, Wright-Patterson Air Force Base, Ohio, January 1973

6. Nielsen, H. J. and Tao, L. N., "The Fire Plume Above a Large Free-Burning Fire," Tenth Symposium (International) on Combustion, August 17 to 21, 1964, pp. 965-972.

7. Alger, R. S., and Capener, E. L., "Aircraft Ground Fire Suppression and Rescue Systems - Basic Relationships in Military Fires, Phases I and II," AGFSRS-72-1, Tri-Service System Program Office for Aircraft Ground Fire Suppression and Rescue, SMF, Wright-Patterson Air Force Base, Ohio, April 1972.

8. Welker, J. R., and Sliepcevich, C. M., "Bending of Wind-Blown Flames from Liquid Pools," Fire Technology, Vol. 2, 1966, pp. 127-135.

9. Powars, C. A. and Kendall, R. M., "User's Manual, Aerotherm Chemical Equilibrium (ACE) Computer Program, May 1969.

10. JANAF Thermochemical Tables, The Dow Chemical Co., Midland, Michigan.

11. Bader, B. E., "Heat Transfer in Liquid Hydrocarbon Fuel Fires," Chemical Engineering Progress Symposium Series, Vol. 61, No. 56, 1965, pp. 78-90.

12. "Performance and Design Criteria for Deployable Aerodynamic Decelerators," Aeronautical Systems Division, ASD-TR-61-579, December 1963.

13. Goldstein, H. E., "Pyrolysis Kinetics of Nylon 6-6, Phenolic Resin and Their Composites," Paper Presented at the San Francisco Meeting of the American Chemical Society, Division of Organic Coating and Plastics Chemistry, Volume 28, Number 1, April 1968.

14. Moyer, C. B., Suchsland, K. E., and Bartlett, E. P.,"Thermochemical Ablation of Aromatic/Heterocyclic Polymeric Composites, Part I, Composition Effects on Recession Rate and Surface Temperature," AFML-TR-72-179, Part I, October 1972.

15. Engholm, G., Lis, S. J., and Baschiere, R. J., " Thermal Transport and Radiative Properties of Fibrous Structural Materials," ASD-TDR-62-810, November 1962, p. 85.

16. Freeston, W. D., Jr., and Johnstone, D. S., "High Temperature, Abrasion-Resistant Parachute Riser Materials," AFML-TR-67-323, Air Force Materials Laboratory, Air Force Systems Command, Wright-Patterson Air Force Base, Ohio, October 1967.

17. Schulman, S. and Johnstone, D. S., "Tensile Properties of Fibrous Materials at Standard Conditions and Vacuum at Elevated Temperatures," AIAA Paper No. 68-954, September 1968.

18. Opt, P. C. and Coskren, R., "Tensile Impact Behavior at Elevated Temperatures of Webbings, Tapes, and Ribbons for Decelerators," AIAA Paper No. 68-952, September 1968.

19. Moyer, C. B., Suchsland, K. E., and Morse, H. L., "User's Manual for the ASTER Code, Aerotherm Skin Thermal Response Computer Program for the Prediction of Fabric and Skin Thermal Response to Fire Exposures," Aerotherm Report UM-73-33, Aerotherm Acurex Corporation, Mountain View, Ca., April 1973.

20. Abbett, M. J. and Davis, J. E., "Aerothermal Environment Prediction Techniques for Ablating Nosetips; PANT Series B Post Test Analysis Report," Aerotherm Project 7040, May 1973, pp. 3-28.

21. Kays, W. M., "Convective Heat and Mass Transfer," McGraw Hill Book Company, New York, 1966, pg. 211

22. Military Specification, Cloth, Parachute, Nylon, MIL-C-7020F, 26 March 1969.

23. Military Specification, Cloth, Parachute, Nylon, MIL-C-7020F, Amendment 1, 17 July 1970.

24. Military Specification, Cord, Nylon, MIL-C-5040E, 27 February 1969.

25. Military Specification, Webbing, Textile, Woven Nylon, MIL-W-4088G, 23 September 1971.

26. Military Specification, Cloth, Duck, Nylon, MIL-C-7219D, 12 November 1971.

27. Military Specification, Cloth, Duck, Nylon, MIL-C-7219D, Amendment 1, 20 October 1972.

28. Laub, B., "User's Manual for the AFPARTS Code, Aerotherm Fire Environment - Parachute Thermal Simulation Program," Aerotherm Report UM-74-44, Aerotherm Acurex Corporation, Mountain View, Ca., February 1974.

☆U.S.Government Printing Office: 1974 — 657-015/258